Meta stable excitations in conjugated organic systems

Carsten Rothe

Abstract

This thesis reports the properties of meta stable excitations such as triplet excitons occurring in light emitting conjugated polymers by means of subnanosecond time-resolved luminescence and transient absorption investigations.

Triplet diffusion and energy relaxation within a prototypical conjugated polymer has been studied by observing the bimolecular annihilation delayed fluorescence dependent on temperature, excitation dose and concentration. The results are analyzed employing the concept of dispersive hopping in a Gaussian distribution of states. After pulsed excitation the triplet migration is initially dispersive accompanied by a rapid energy relaxation. The subsequent classical regime is described by a time-independent diffusion constant and a invariable average triplet energy. Further, it is clearly found that triplet hopping in conjugated polymers is both an intra- and interchain process.

Both the singlet-to-triplet generation branching ratio and the recombination layer thickness in a working polyspirobifluorene device are determined by a relative comparison of the singlet and triplet densities after electrical and optical excitation. The singlet generation rate is a field independent universal constant, the value of which agrees with the quantum-statistical 1:3 limit. Evidence is provided that the charge carrier recombination does not occur homogeneously throughout the device. Instead a certain exciton generation layer exists which, for polyspirobifluorene, is about 6 nm thick. Also singlet excitons are quenched by charge carriers. The latter might be formed after triplet-triplet annihilation in a sequential process, which involves the formation of an intermediate geminate pair prior to the full charge carrier dissociation.

Finally, a new type of intramolecular delayed fluorescence is observed in the nanosecond time domain in luminescent polymers and also found to occur in a large number of conjugated organic systems. This luminescence is isoenergetic to the prompt fluorescence and shows the same excitation energy dependence, but rapidly decays with an algebraic law. In dilute solutions the overall emission quantum yield is a fraction of a percent only. Since all potential origins, including geminate pairs and triplet-triplet-annihilation, cannot describe the experimental results, the existence of a novel type of indirect singlet excitation is proposed.

Meta stable Excitations in Conjugated Organic Systems

By

Carsten Rothe

A thesis submitted to the Faculty of Science, at the University of Durham, for the Degree of Doctor of Philosophy

University of Durham
Department of Physics
November 2004

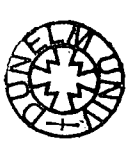

Declaration

The material in this thesis has not been submitted for examination for any other degree, or part thereof, at Durham University or any other institution. The material in this thesis is the work of the author except where formally acknowledged by reference.

Acknowledgements

Among the numerous people who supported me during this thesis my warmest thanks must go to my supervisor Prof. Andy Monkman. I consider him a stroke of luck for a young researcher for he is encouraging in scientific and enjoyable in non-scientific matters. Although there are many other points that certainly deserve attention, I would like to specially thank him for patiently proof reading this and other work in spite of his never-ending time constraints.

During this work a fruitful cooperation between the Philips Research Laboratories in Eindhoven and the Durham OEM group has been established. For this study ultra sensitive experiments were performed that critically rely on the quality and purity of the investigated samples. In this context many of the findings would have not been obtained without the ongoing and generous supply of high-quality, sealed devices and pure materials from Eindhoven. Special thanks are due to Dr. Klemens Brunner for many rewarding discussions, which additionally triggered three joint publications. Moreover, on a financial level this work was supported by means of a Royal Philips CASE Studentship.

Big thanks go to all current and past members of the Durham OEM group for their great support not only in science, especially for their help in relocating bits and pieces. Similar gratitude must also be expressed to the every time friendly and mostly helpful numerous Departmental staff, in particular to Phil and Norman.

I would also like to thank Prof. Hugh Burrows for his repeatedly very helpful and stimulating scientific advice but even more for his warm welcome in Portugal, which we will never forget.

Greatest thanks are bestowed upon Susi for her patience with me and for keeping the little Schlumpf out of my way during the writing. Finally, thanks are due to my family for their various support to reach this stage.

Table of Contents

Table of Figures

1. Introduction

The past century saw a revolutionary increase of the use of polymers for applications to all our benefit, which these days are implemented both in highly specialized technological applications but also in mass-produced everyday products. Mainly, this progress has been made possible by the matured level of chemical synthesis that now allows tailoring the mechanical and chemical properties of polymers within an amazing range to suit almost every application. At the same time, the production based on polymers is often more economical when compared to alternative, non-polymeric materials.

For a long time the most valued electrical property of polymers was considered their intrinsic ability to prevent conduction, which made them the ideal insulating material. On the other hand, some members of a certain class of polymers, namely conjugated polymers, exhibit substantial electrical conductance properties. In this context, three pioneering researchers were recently rewarded with the Noble Prize in Chemistry. Over the past 30 years intensive research efforts have been made to further improve the properties of these conducting polymers. However, the initial goal of a metallic polymer of commercial value as a low-cost alternative to current metal wires will most likely not be reached within the near future. As a consequence research activities in this field, including those of the OEM group of the University of Durham, were reduced.

Since the early 1990's light emitting conjugated polymers experience a considerable renaissance as their ability to convert electric current into light is subject to intensive research efforts. One of the goals for the near future is to revolutionize the multi billion dollar display market with thin, self-emitting organic displays featuring superior brightness and viewing angles compared to current technologies. Other strategies implement materials in laminar illumination schemes or polymeric solar cells. All these applications seek to marry inexpensive production with the high flexibility of polymers, which might again open up revolutionary synergetic effects.

At the moment insufficient lifetime and stability still prevent the advance of the polymer display technology into the consumer market. Progress is often constrained by the mutual interplay of synthesis, purification and device fabrication. In the early years many experimental findings were explained as genuine polymer properties but were in fact signs of backbone oxidation. Advances in chemical synthesis in conjunction with a better fundamental understanding have enabled us to avoid or at least account for these defect

sites. In a way one could say that organic semiconductors have to pass through a similar history of purification development as compared to inorganic semiconductors. The amorphous structure of polymers as compared to their inorganic counterparts further adds to the complexity of the problem as it renders the description of the energetic structure as well as of transport phenomena more difficult. In this context the early characterization of these materials as one-dimensional semiconductors with a large excitation delocalization and wave-like motion failed to predict many basic properties of light emitting conjugated polymers. Instead nowadays a more chemical point of view is generally adopted as excitations in these materials are considered localized and in such migration proceeds via discrete hopping.

Many different techniques have been successfully employed in order to study the rich photophysics of conjugated polymers. One specialized research area examines the very weak delayed photoluminescence of organic systems, which mainly consists of phosphorescence and delayed fluorescence. Here, after pulsed optical excitation, the strong prompt fluorescence is omitted by means of some sort of time-gated shutter, which then allows using very sensitive detectors for the observation of the long lived emissions. The first experiments that employed the latter technique started in the late 1950's with measurements in the milli- and microsecond time domain by using flash lamps or simple shutters for pulsed excitation. In that time, research activities mainly comprised the detection and characterization of phosphorescence and delayed fluorescence of small molecules and organic crystals. Over the years the time resolution of these experiments has continuously been improved thereby closely following the development of pulsed laser excitation sources, which now extend to the nanosecond time scale.

Using gated luminescence detection techniques, the first light-emitting conjugated polymers were investigated in the late 1990's. As with their small organic counterparts, initially the main goal was to directly measure the triplet exciton energy by observing phosphorescence spectra. This approach constitutes the only convincing possibility to gain insight into the otherwise non-emissive triplet exciton. Initial experiments verified a large singlet-to-triplet splitting in these materials and in such substantially supported the excitonic model as opposed to the band model. Furthermore, it was soon realized that the also observed delayed fluorescence provides a powerful tool in order to gain information about the nature of conjugated polymers - maybe even more than the

phosphorescence. Since then this delayed emission has been extensively studied and will also be the main focus point of this study.
For the investigation of metastable particles both the time-resolution and the sensitivity of the experimental set-up constrain the accessible time domain and in such the quality of the prospective experimental data. For the present investigation a time-resolved spectrometer is employed that has a subnanosecond time resolution combined with single photon sensitivity. To the author's best knowledge, this is the only spectrometer of its kind for research in light emitting polymers and in fact contributed a wealth of novel results in this field for example the first observation of genuine electrophosphorescence.

Following the introduction, the present thesis starts with a short theory chapter, which is mainly meant to introduce the basic concepts regarding the photophysics of conjugated organic systems, including, for example, the concept of conjugation and excitons.
Subsequently, the work focuses on three stand-alone experimental studies, which are closely linked. In following scientific publications, each experimental chapter comprises a brief introduction and a separate specialized theory section. Ahead of the data presentation the unique time-resolved spectrometer is introduced in detail in chapter 3.
The phenomenon of triplet exciton migration and bimolecular annihilation in a prototypical polyfluorene derivative after optical excitation is investigated in chapter 4. Here, the analysis of the experimental data within a theory that relies on hopping-like motion in a Gaussian distribution of localized states yields the first consistent picture of triplet exciton migration in solid-state light emitting polymers. This part is also considered to be an essential precursor to the understanding of the following two experimental chapters.
Electroluminescence certainly is the most promising technological application of light emitting conjugated polymers. A prime object in this field of research is the excitonic singlet-to-triplet branching ratio after charge carrier recombination. In chapter 5 several recent attempts to determine this ratio are discussed in view of the findings of the previous chapter. Subsequently, a superior experimental arrangement, which is based on relative measurements of the singlet and triplet yields after electrical and optical excitation, is introduced and applied on polyspirobifluorene devices. From these experiments obtained are the branching ratio and the recombination layer thickness. Also studied are the interactions of the triplet exciton with an applied electric field. The findings will have implications on the rules to design electroluminescent devices.

Chapter 6 presents experimental results regarding an optically excited delayed fluorescence that decays in the nanosecond time domain. This intrachain emission, which is generically observed in all kinds of conjugated organic systems, can neither by explained within the frameworks of established theories nor has it been described in the literature before. The observation of this luminescence on the one hand proves the excellence of the time-resolved spectrometer used but on the other hand also shows how incomplete the understanding of conjugated systems on a very basic level still is.
Finally, general conclusions are given in the last chapter.

2. Theory

2.1. Molecular Structure of conjugated polymers

The element carbon forms the backbone of the whole organic chemistry including, of course, conjugated polymers. Albeit an isolated carbon atom possesses the electron configuration $1s^2 2s^2 2p^2$ the difference in energy between the $2s$ and $2p$ orbitals is small and during a chemical reaction so-called hybrid orbitals are formed from linear combinations of the former $2s$ and $2p$ orbitals. Depending on reaction conditions sp^3, sp^2 and sp hybrid orbitals may be created. In the latter two cases the remaining unhybridised electrons are accommodated in the original p orbitals, which are oriented normally to the direction of the sp^x orbitals. Two sp hybrid orbitals of neighbouring carbon atoms now overlap and form a strong σ bond, which mainly determines the geometry of the molecule. Overlap means the sp orbitals are linearly combined to form bonding (σ) and anti-bonding (σ^*) molecular orbitals and the two electrons are accommodated in the energetically lower σ orbital. In the case of a sp^2 hybridisation the two leftover p orbitals form a π bond, where the two electrons fill the weakly bonding π orbital leaving the corresponding anti-bonding π^* orbital empty. A simple example of a molecule containing σ (H-C and C-C) and π (C-C) bonds is ethylene, shown in Figure 2-1.

In some organic compounds, mainly aromatic ring systems, several π bonds overlap to create extended molecular orbitals lying above and below parallel to the plane of the ring molecule. Consequently, an electron accommodated in such a π orbital is highly delocalised. Furthermore, if several of such identical aromatic units from a polymer backbone, then the electron delocalization in principle extends over the whole conjugated polymer. However, conjugation interruptions due to saturated bonds (for example if nitrogen is part of the repeat unit), twist angles between the monomer units and ulterior distortions lead to a finite *effective* conjugation length, clearly shorter than the polymer chain length. Typical values for the delocalisation of an optically excited electron are of the order of four repeat units.

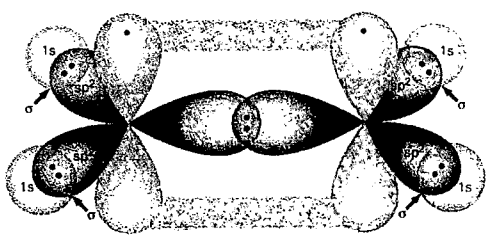

Figure 2-1 Chemical structure of ethylene, taken from Murowitz, REF 1

Regarding the correct description of the excited states in conjugated polymers, the strong localization contradicts the one dimensional semiconductor model, which initially has been proposed by Su, Schrieffer and Heeger.[2] Alternatively, experimental results have been explained - no different to small

organic molecules - in terms of an excitonic model according to Bässler and co workers.[3] The key parameter to distinguish between both models is the binding energy of an excited electron and its correlated hole. A small value (<< 0.1 eV) implies a free, wave-like electron such as employed for inorganic semiconductors. On the other hand, strongly bound and localized electron-hole pairs with a binding energy of several hundreds of meV need to be described by an excitonic model. Nowadays there is an overwhelming amount of various experimental proof that excited electrons are indeed strongly bound to their corresponding hole. This, for example, can be inferred from photoluminescence studies under applied electric field. Here strong bias fields are indeed required in order to dissociate the electron-hole pair, and thus quench the luminescence.[4] Consequently, this thesis will only apply the excitonic model.

2.2. Electronic Transitions between molecular orbitals

2.2.1. Absorption and allowed transitions

A material irradiated by an electromagnetic wave will absorb energy, provided the energies of the excitation wave match optically allowed transitions. The Beer Lambert Law often adequately describes the fraction of light of a certain frequency transmitted through a substance

$$I(x) = I(0)\exp(-\alpha x)$$

Equation 2-1

where *I* denotes the light intensity, *x* the depth of material through which the light beam has passed and α is a frequency dependent absorption coefficient. By their nature, transitions in polymers are rather broad and extend over typically 1 eV. Then it is useful to integrate the absorption coefficient over the frequency range where the transition appears:

$$f = 6.25\times10^{25}\int_{\nu_1}^{\nu_2}\alpha(\nu)d\nu$$

Equation 2-2

The dimensionless number *f* denotes the oscillator strength, which allows one to compare the strength of different optical transitions. A value of $f = 1$ is related to a strong (*allowed*) and $f = 0$ a very weak (*forbidden*) transition. The absolute number of *f* and hence the intensity of the associated absorption band is dependent on various factors, but in most cases simple selection rules adequately account for the strength of electronic transitions. The basic idea is that the system-describing Hamiltonian can be separated into decoupled Sub-Hamiltonians. Then for a strong electronic transition the associated solution must independently be an eigenfunction of all of these Sub-Hamiltonians. The selection rules for polyatomic molecules can be

summarized in relation to the oscillator strength f_a of a fully allowed $\pi \rightarrow \pi^*$ transition by the equation

$$f = p_s p_o p_p f_a$$

Equation 2-3

where the terms p_s, p_o, and p_p are probability factors, which represent electron spin, orbital symmetry, and parity, respectively. These factors are briefly discussed below.

- *Electron spin p_s*

A change in electron spin during the excitation is strongly forbidden. Consequently transitions between singlet and triplet states exhibit low oscillator strength and p_s is of order 10^{-5} only.

However, this selection rule breaks down if the transition occurs in the proximity of a heavy or paramagnetic atom. In this case the Sub-Hamiltonians are no longer independent of each other and so-called spin flips become more probable.

- *Orbital symmetry p_o*

For an allowed transition the two involved orbitals must simultaneously possess large amplitudes in the same region. If this is not fulfilled the transition is called overlap forbidden. From this point of view transitions between π and π^* are allowed since their orbitals lie in the same plane and have a high degree of spatial overlap. The most important example for a space forbidden transition is $n \leftrightarrow \pi^*$ where the n orbital accommodates non-bonding electrons (i.e. occurring if nitrogen is part of the aromatic ring molecule). This non-bonding orbital occupies a different plane than the π^* and therefore this transition becomes overlap forbidden with p_o roughly 10^{-2}.

- *Parity p_p*

In general, molecules exhibit some kind of symmetry. If for example a wave function changes sign at a centre of symmetry it is called ungerade (u) and termed gerade (g) otherwise. Allowed transitions take place between g and u, parity forbidden are g $\leftrightarrow$ g and u $\leftrightarrow$ u with p_p being reduced to 10^{-1}.

In an unsaturated carbon linkage two p_z orbitals of different carbon atoms form a symmetrical bonding π orbital and an anti-symmetrical non- bonding π^* orbital. Thus, for conjugated polymers $\pi \leftrightarrow \pi^*$ transitions are strongly parity allowed.

2.2.2. The Franck-Condon principle

Considering $\pi \leftrightarrow \pi^*$ transitions, the electrons in the ground state are accommodated in a bonding orbital. During excitation one of these electrons is promoted into an anti bonding molecular orbital, compare Figure 2-1. Consequently, the equilibrium distance between neighbouring carbon atoms will increase if the molecule is excited. Thus, the potential energy curves vary for different electronic configurations. For the purpose of illustration, the potential curves of the ground and first excited electronic state together with a

selection of vibrational modes for a diatomic molecule are shown in Figure 2-2.

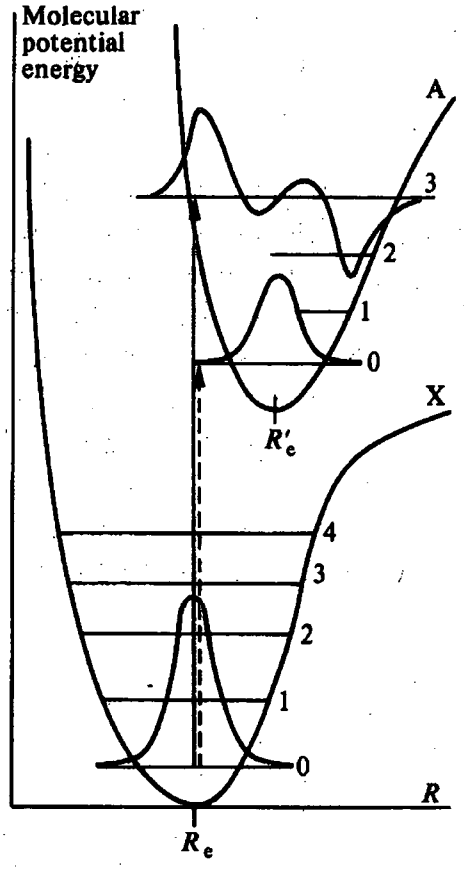

Figure 2-2 Illustration of the Frank-Condon principle for a diatomic molecule (taken from REF [5]. Here the most likely transition occupies the third vibrational mode of the excited state.

The time required for an electronic transition is very short (10^{-15} s) compared to the time of rearranging the equilibrium distance for an excited bond. Consequently the Franck-Condon principle follows, which states that the intermolecular separation is fixed during the absorption of light and therefore any transition is represented by a vertical line in a potential / distance diagram (compare Figure 2-2). The excited electron then occupies that vibrational mode with the greatest overlap with the wave function of the original state.

2.2.3. The Jablonski diagram and the vibrational structure of emission and absorption spectra

With the help of the so-called Jablonski diagram shown in Figure 2-3, one is now able to understand the general structure of absorption and emission spectra. At first the absorption starts from the singlet ground state at v = 0 (S_0^0) and ends in the first excited singlet state with v' ≥ 0 ($S_1^{v'}$). In an extremely short time period of only 10^{-13} s there is a radiationless transition from these higher excited vibrational levels and the system is deactivated to the lowest excited singlet state S_1^0. In the next several hundred picoseconds the excited singlet might decay to the ground state $S_0^v \leftarrow S_1^0$ either radiatively or radiationless. The latter case is termed *internal conversion* (IC). Radiation emitted between states of the same multiplicity is called *fluorescence* and between states of different multiplicity *phosphorescence*. Following optical excitation the triplet manifold of the polymer is usually populated via *inter-system-crossing* (ISC) from the S_1 state ($S_1 \rightarrow T_1$) and again the vibrational excess energy is lost rapidly. The depopulation of the triplet state takes place via IC or phosphorescence

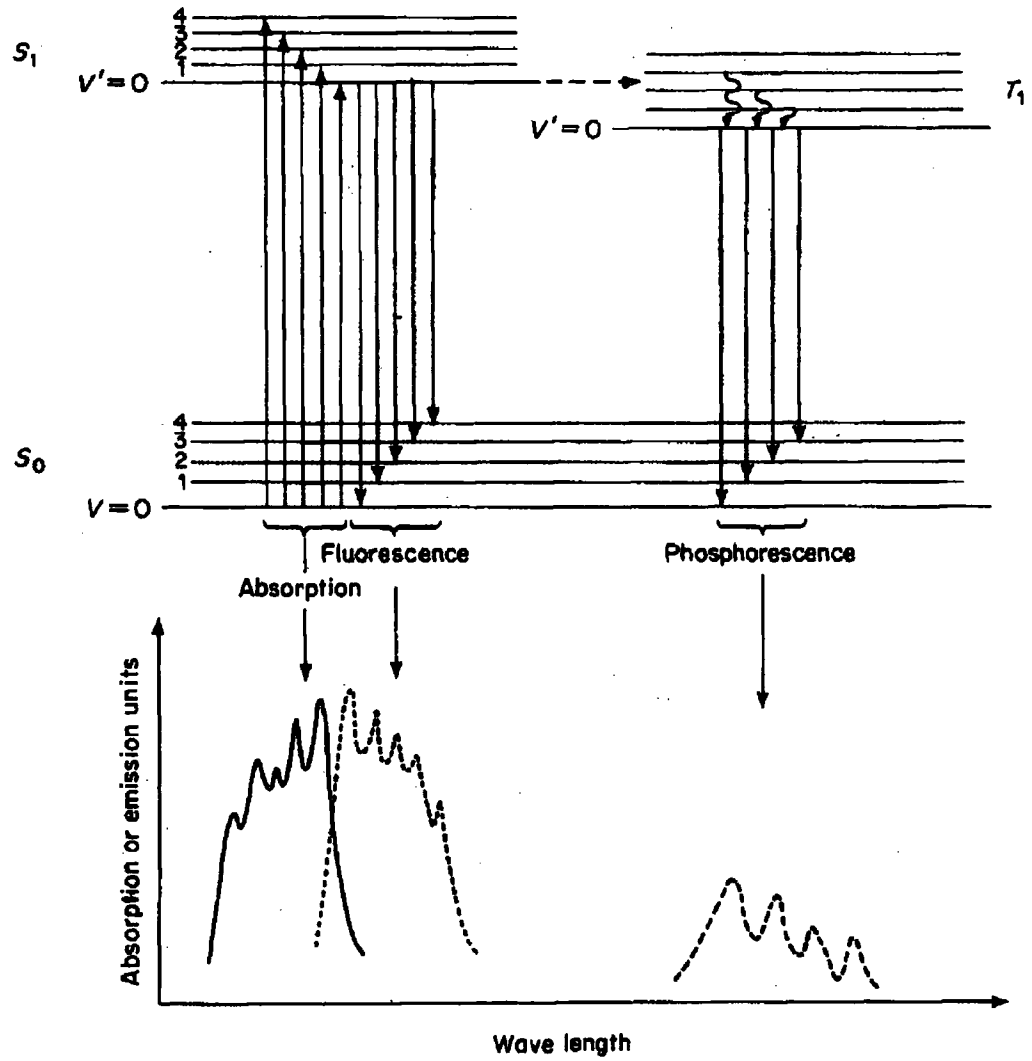

Figure 2-3 Jablonski diagram including absorption and emission for an polyatomic molecule taken from REF 6.

emission. For conjugated polymers the lifetime of the latter process is of the order of one second.

As shown in Figure 2-3 the fluorescence emission spectra are mirror symmetric to the absorption spectra due to the properties of the involved transitions. In real measurements the first vibronic (v = 1) emission mode might be quenched because of reabsorption effects.

The energetic difference between the v = 0 emission and v' = 0 absorption position is known as *Stoke's Shift*, which has its origin in the Franck-Condon-principle, see 2.2.2.

2.3. Excited states in conjugated polymers

After a polymer has absorbed an incident photon and the created excited state has lost its vibrational excess energy, the S_1^0 state has numerous routes for decay. Since many of these decay channels involve the production of temporal intermediate states, it is

useful to give an overview of the most important occurring *quasi-particles*.

2.3.1. Excitons

As said in 2.1 the optically excited electron is not delocalised over the whole conjugated polymer chain but located near its correlated hole. Such an electron – hole pair, together with the polymer chain distortion arising from the excitation, can be treated as a pseudo – particle and is known as exciton. Two important species are distinguished depending on their multiplicity: firstly the singlet – exciton (short: *singlet*), which is for example formed after a typical $\pi \rightarrow \pi^*$ transition and secondly the triplet – exciton (*triplet*), which in optically excited conjugated polymers is basically populated via ISC from the singlet state. Commonly, the triplet energy is about 0.7 eV smaller than the corresponding singlet energy. This fact can be understood qualitatively. The Pauli Exclusion Principle does not allow two electrons with the same spin to occupy the same orbital; hence the triplet electron and hole are accommodated in different orbitals. This leads to a reduced Coulombic electron – electron repulsion compared to the corresponding singlet state and therefore the triplet energy is relatively lower.

2.3.2. Dimers and excimers

The term *dimer* describes a situation in which two identical molecules (or in the case of polymers, repeat units) are close together and new bonds are created that did not exist in either of the original molecule. For an illustration one might think of two identical aromatic ring molecules in a sandwich structure. The dimer emission spectrum is considerably broader and shifted to lower energies than the corresponding monomer spectrum; the maximum shifts from the $v = 0$ to $v = 1$ vibronic mode. As dimers exhibit a real (weak) chemical bond they do also have a ground state and therefore an absorption spectrum can be attributed.
Another class of excited species is known as *excimers*. These refer to dimers that are bound only if one molecule is excited. Therefore the ground state of an excimer is dissociative and they are not detectable with absorption techniques. The excimer fluorescence emission is comparable to the dimer emission, structureless and red shifted.

2.3.3. Polarons

When an electron is added to or removed from a perfect polymer chain, it will cause this chain to be deformed and create a characteristic pattern of bond deformation about 10 repeat units long. Such an electron or a hole together with its chain distortion is called a charged polaron, P^- and P^+, respectively. In a polymer charges have to be treated as polarons rather than free electrons or holes.

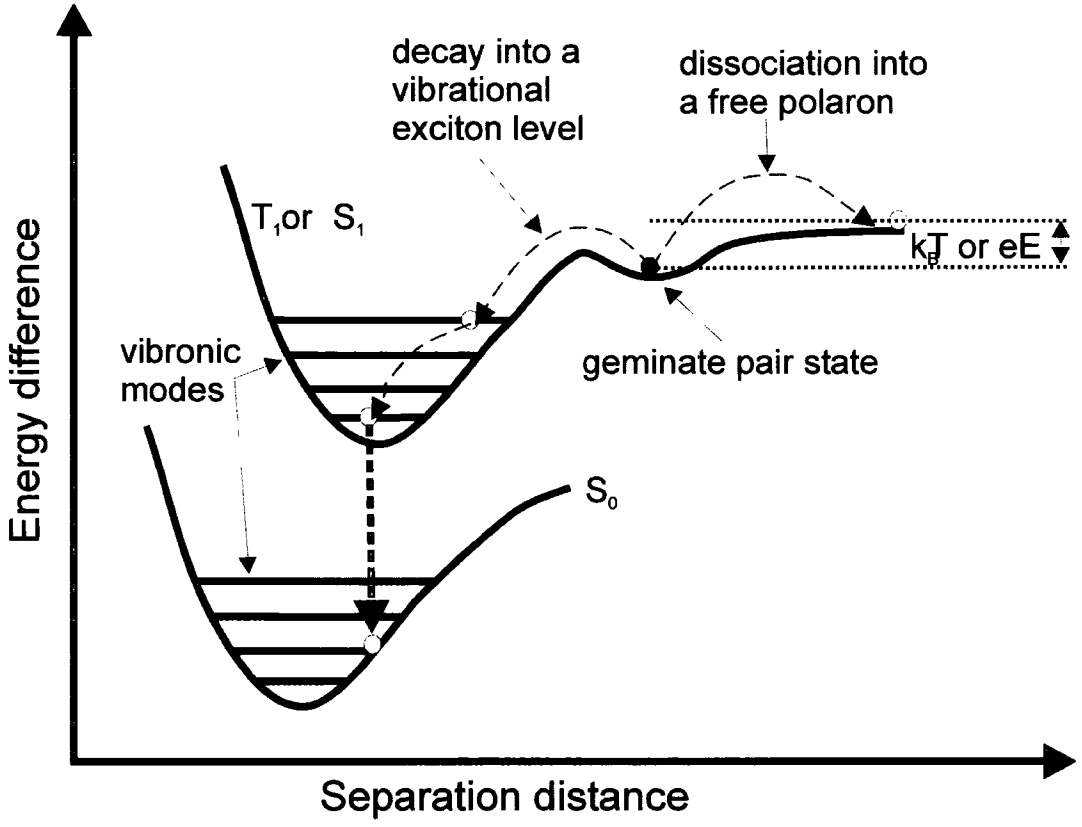

Figure 2-4 Diagram illustrating the differences in potential energy between free charge carrier, geminate pair state and exciton state

Important for conjugated polymers, polarons are formed in electroluminescent devices following the charge carrier injection.

2.3.4. Geminate pairs

This term is used to describe charged particles feeling their mutual Coulomb attraction but not directly forming singlet or triplet excitons. For example, two oppositely charged polarons located on neighbouring polymer chain segments form a geminate pair. Thermal activation energy or an applied electric field can lead to its dissociation into two free polarons. Figure 2-4 illustrates the potential energy levels for the different processes. Visible from that figure is also that in the absence of an electric field and at low temperature such a pair can not overcome the barrier to form an exciton and is therefore a long-lived particle. In this situation, recombination due to tunnelling of the electron may give rise to delayed fluorescence.

2.4. Transport of energy in conjugated polymers

After optical excitation the main part of the absorbed energy is stored in terms of excitons. Consequently, one way of transporting energy involves *exciton migration*. The second important possibility of moving energy is direct *energy transfer*. Subsequently, the main characteristics of these two transport mechanisms are briefly outlined.

2.4.1. Resonant or Förster energy transfer

This mechanism depends upon an overlap between the emission spectrum of an initially excited donor site and the absorption spectrum of the finally excited acceptor site. In early works it was assumed that the transfer is coherent and the composite total wave function is a linear combination of donor and acceptor states. The energy then oscillates between both states (similar to a coupled pendulum). However, the calculated transfer rates were much too high and it was Förster in 1959 who focused the attention on the vibrational acceptor states.[7] Since these and similar electronic states will strongly couple to the excited acceptor state and a quick decay to lower energy states will happen, the resulting irreversibility of the whole process makes a new description necessary. In this context, Förster distinguished three different cases; for applications in this thesis and for polymers in general the *very – weak – coupling limit* is the most important one. Here, the transfer rate is expressed in experimental parameters by:

$$K_{D\to A} = \frac{1}{\tau_D}\frac{1}{R^6}\left(\frac{3}{4\pi}\int\frac{c^4}{\omega^4 n_0^4}F_D(\omega)\delta_A(\omega)d\omega\right)$$

Equation 2-4

where the important parameters are τ_D, the natural donor lifetime (in absence of the acceptor), and R, which represents the donor-acceptor separation distance. The integral basically evaluates the overlap between the normalized acceptor absorbance and the donor emission spectrum. A nonzero *overlap integral* is therefore essential for long–range Förster– type transfer. Figure 2-5 illustrates the overlap of both spectra.

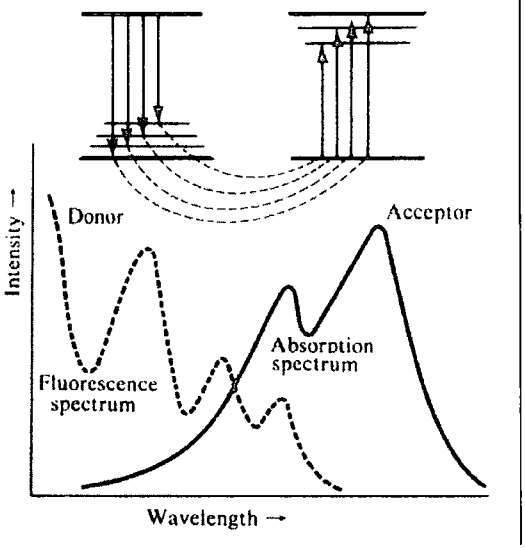

Figure 2-5 An example overlap between acceptor absorption and donor emission spectrum (taken from REF 8).

One can rewrite Equation 2-4 to

$$K_{D\to A} = \frac{1}{\tau_D}\frac{R_0^6}{R^6}$$

$$R_0^6 = \frac{3}{4\pi}\int\frac{c^4}{\omega^4 n_0^4}F_D(\omega)\delta_A(\omega)d\omega$$

Equation 2-5

where for the distance R_0 the energy transfer from donor to acceptor equalizes the radiative decay of the donor. A further simplification towards easier observable quantities introduces the characteristic radius $\overline{R_0}$, which corresponds to the distance at which energy transfer equally competes with the total rate of decay of the donor:

$$K_{D\to A} = \frac{1}{\tau}\left(\frac{\overline{R_0}}{R}\right)^6 = \frac{1}{\tau_D}\left(\frac{R_0}{R}\right)^6 \quad \text{with } \tau = \Phi_F \tau_D$$

Equation 2-6

where Φ_F denotes the donor fluorescence quantum yield in the absence of the acceptor. For conjugated polymers $\overline{R_0}$ is typically of order 40 – 50 Å.

2.4.2. Electron exchange and Dexter transfer

From the overlap integral in Equation 2-4 one infers that resonant energy transfer is forbidden for triplet excitons because the necessary absorption is vanishingly small. However, if excited donor and acceptor sites are close enough such that their orbitals overlap then an electron on one excited site will have a probability to appear on the other site. This process is termed *electron exchange energy transfer*. Typical donor-acceptor distances are in the range of 10 to 15 Å. Dexter has developed a theory, which is especially applicable for the important triplet – triplet energy transfer process. The corresponding equation reads:

$$K_{D\to A} = \frac{2\pi}{\hbar}\left|\beta_{DA}\right|^2 \int F_D(E) F_A(E) dE$$

Equation 2-7

where β_{DA} represents the exchange energy interaction between the donor and acceptor. Here the overlap integral is not taken from the fluorescence but from the normalized phosphoresce spectrum of the donor.

For singlets, electron exchange energy transfer is less important than resonance excitation energy transfer.

2.5. Exciton annihilation

Besides so-called *unimolecular* non-radiative decay processes *bimolecular annihilation* cause the decay of excited states at high generation doses. In the following, the most important cases shall be briefly discussed.

2.5.1. Triplet–triplet annihilation

This in organic solids (and solutions) important process involves the collision of two triplet excitons. Triplet-triplet annihilation (TTA) is also the major depletion mechanism for the triplet density in solid state conjugated polymers as shall be shown in detail in Chapter 4. Generally, the annihilation process is given by:

$$T_1 + T_1 \Rightarrow \left\{\begin{matrix} \frac{8}{9}(S_0 + T_n) \\ \frac{1}{9}(S_0 + S_n) \end{matrix}\right\}$$

Equation 2-8

where the right hand part should be considered as final states since also intermediate quadruple states are involved as well. The singlet exciton S_n relaxes quickly to the S_1 state and may then be observed as *delayed fluorescence* [DF].

TTA has short-range electron exchange character (see 2.4.2). Two neighbour triplets on the *same* polymer chain are assumed to interact, whereas the

annihilation of triplets located on different chains is unlikely.

Geminate pairs (see 2.3.4) are metastable particles as well and give rise to a similar delayed fluorescence. In fact, one of the aims of this thesis is to clarify whether TTA or geminate pair recombination dominates the observed delayed fluorescence in conjugated polymers.

2.5.2. Singlet-triplet annihilation

The lifetime of the triplet is much longer compared to the singlet making possible the generation of high triplet concentrations. On this account especially triplet-excited states may act as efficient quenchers for singlets, for example in electro-luminescence devices. A bimolecular reaction where an excited singlet S_1 passes its energy in a spin allowed transition from a lower to an upper triplet state is termed *singlet-triplet annihilation [STA].* The following equation expresses the mechanism:

$$S_1 + T_1 \Rightarrow T_n + S_0$$
$$T_n \Rightarrow T_1 + heat$$

Equation 2-9

The mechanism is similar to Förster energy transfer (2.4.1); the overlap occurs between the fluorescence of the singlet and the absorption of higher lying triplet levels. Note, the reverse process, when triplet energy is transferred to a singlet state, is spin forbidden since it involves a transition from T_1 to S_0.

2.5.3. Singlet-singlet annihilation

This process is very similar to STA; the energy of an excited singlet state S_1 is not transferred to a triplet but to another already excited singlet state. It is again a matter of the Förster energy transfer. The reaction can be summarized by the following equations:

$$S_1 + S_1 \Rightarrow S_n^* + S_0$$
$$S_n^* \Rightarrow S_1 + heat$$

Equation 2-10

SSA leads to a non-linear excitation dose dependency of the fluorescence emission for high doses and is frequently observed in solid state conjugated polymers.

3. Experimental – Time-resolved excited state measurements

3.1. Introduction

The majority of the experimental data of this study was obtained with a single experimental set-up – time-resolved luminescence spectroscopy. The heart of this state of the art spectrometer, the ICCD camera *4 PICOS*, combines subnanosecond time resolution with superb light sensitivity, thus allowing to probe luminescence under experimental conditions which are not within reach for common cw spectrometers. In order to get the most out of this complex system a certain level of experience and careful handling is necessary. In the present chapter the set-up shall be described in detail. Strong and weak points of the experiment, which are of importance for the reader in order to judge the experimental results presented in the following parts, are analysed as well.

The second part of this chapter is dedicated to the time-resolved transient absorption set-up. This powerful experiment has mainly been used to study the triplet exciton accumulation in a working device.

3.2. Time-resolved emission spectroscopy

In the following, with the help of the schematic drawing, shown in Figure 3-1 below, the time-resolved spectroscopy experimental set-up is briefly outlined.

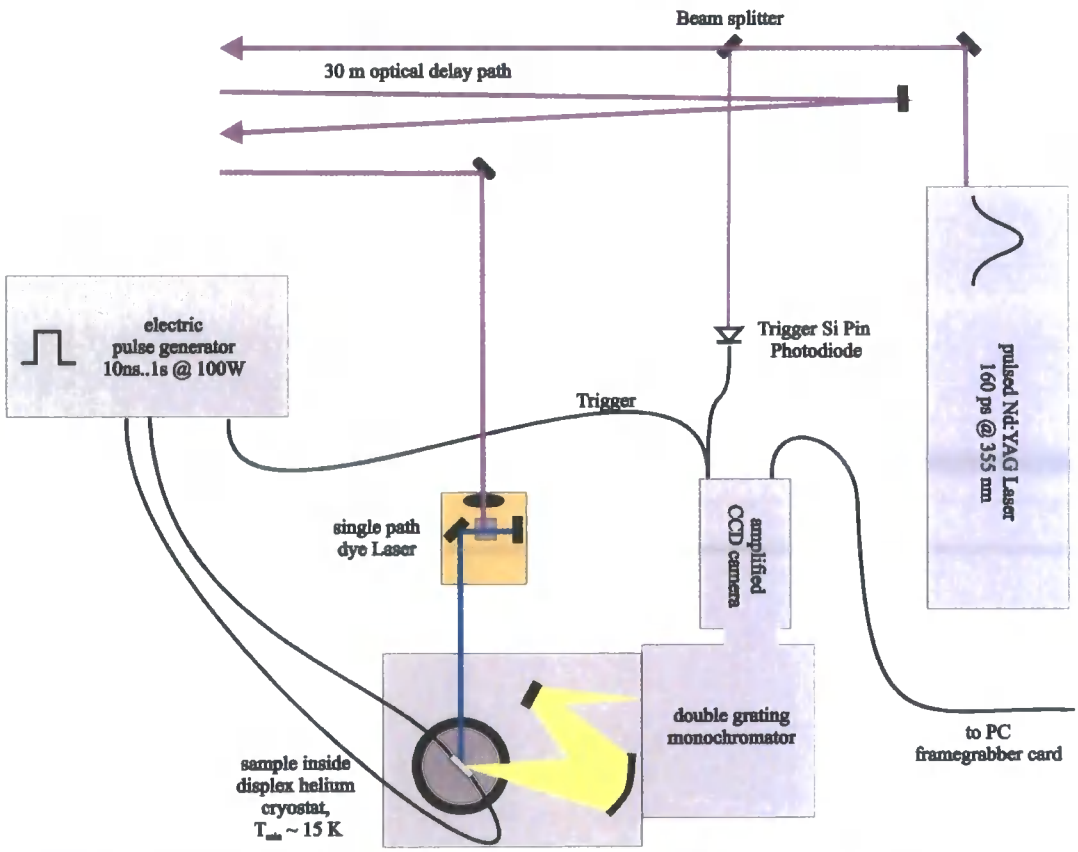

Figure 3-1 Schematic drawing of the time-resolved luminescence spectrometer.

Depending on the mode of excitation both photo and electro luminescence can be investigated. In the first case a pulsed Nd-YAG laser provides intense (>5 mJ) 160 ps light pulses at a repetition rate between 1 – 10 Hz. For the vast majority of photo excitation experiments the third harmonic in the ultraviolet at 355 nm, respectively, 3.5 eV has been used. Additionally for excitation energy dependent experiments, the green second harmonic of the Nd-YAG laser at 532 nm as well as a home-built single path dye cell laser have been employed. The latter was pumped with the above Nd-YAG laser and as such generates excitation pulses of the same duration but of longer wavelength. Upon using different laser dyes, five further wavelengths were obtained, whose (slightly broader) energy profiles are depicted in Figure 3-2.

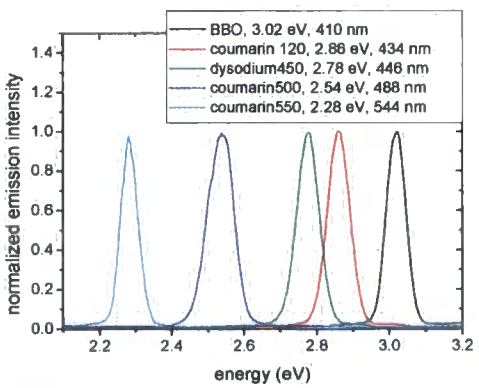

Figure 3-2 Dye laser emission profiles after excitation at 355 nm.

For excitation dose dependent experiments the laser power could easily be varied by means of a tunable half wave plate that maintains the polarization of the excitation beam perpendicular to the optical table. For this kind of experiments the dose was accurately measured between 1 nJ up to 6 mJ using a pulse power meter. Regarding electric excitation, a pulse generator is employed that has specially been designed to test light emitting diodes. This sophisticated piece of equipment features a maximum cw power output of 100 W combined with rectangular voltage pulses of adjustable duration as short as 10 ns up to DC superimposed on a variable either positive or negative DC voltage offset. Furthermore, the electrical pulse can be delayed with respect to a trigger signal at time zero, which offers a great flexibility especially for combined electro-optical excitation experiments for example time-resolved photo luminescence quenching.

The thin film sample or device under investigation is mounted on the cool finger of a closed cycle, optically accessible, helium cryostat. If not stated otherwise, then the sample is held at a vacuum better than 10^{-4} mbar. A specially-made, sealed cylindrical quartz viewport can alternatively be attached to the cold finger of the cryostat, in order to investigate frozen solutions. A temperature control unit equipped with a feedback resistor heater allows to precisely (0.1 K) measure and set any desired temperature between 15 and 300 K. The cryostat can also easily be removed and in such give way for a

quartz cuvette for the investigation of liquid solutions at ambient temperature. In any case, the light emitted by the sample is passed through an appropriate cut off filter to reject the excitation beam in case of photo excitation and then focused onto the entrance slit of a grating spectrograph, which is equipped with a 300 lines/mm grating of either 500 or 1000 nm base wavelength. Finally, the luminescence is detected by a computer-controlled, intensified ICCD camera that replaces the exit slit of the "image" spectrograph. Thus, the raw data initially obtained with this experiment, is a two dimensional image of 572 x 736 pixels, showing an approximately 300 nm wide section of the dispersed sample emission. Within the framework of this study the energetic rather than the spatial distribution of the luminescence is of importance. Therefore, the vertical component of the image is generally integrated in order to obtain a common one-dimensional emission spectrum.

3.2.1. Spectral resolution

The spectral resolution of the whole set-up was measured as the full width at half maximum (FWHM) of either the third harmonic of the Nd-YAG laser itself or a 780 nm laser diode. With a narrow spectrograph entrance slit in both cases a value of ~ 1 nm was found, which exceeds the maximal theoretical resolution of 300 nm/736 pixel, ~ 0.4 nm. This divergence has several origins, for example the ICCD camera may not be at exactly the right angle with respect to the spectrograph. Nevertheless, for the present study on conjugated polymers, the spectral resolution never limited the width of the observed emission spectra, which are generally much broader.

3.2.2. Energy to pixel calibration

The section of the dispersed sample emission that is monitored by the ICCD detector mainly depends on the chosen spectrograph grating position. Since there is no built-in correlation between grating position and ICCD camera, it is necessary to calibrate the obtained spectrum, i.e. relate the horizontal pixel number to the correct wavelength for a certain fixed grating position. This was achieved by placing a spectral calibration lamp with a number of known and sharp emission features into the focus point of the spectrograph and then monitoring the spectrum for several grating positions. The peak wavelengths were then associated to the corresponding pixel numbers. In doing so the pixel spectrum is correlated to the true energy scale with an accuracy of ± 1 nm, which was estimated from the variance of the linear pixel to wavelength relation.

The whole procedure had to be repeated for each desired grating position and a re-calibration was necessary after every move of the ICCD detector. In this context, the

known wavelength of scattered excitation laser light (first or second order of the Nd-YAG laser third harmonic) was employed as a simple test whether an active calibration curve was still accurate.

3.2.3. Energy intensity calibration

After calibrating the energy position, the measured emission spectra needed to be further corrected for the energy dependent response of the whole set-up, since both, the ICCD detector and the spectrograph, do not respond uniformly for various light energies. For the calibration, the known emission profile of a tungsten calibration lamp was compared with the one actually measured. In doing so, a correction curve was obtained, which needed to be multiplied to every experimental spectrum in order to obtain the true emission profile. Again this had to be repeated for each grating position.

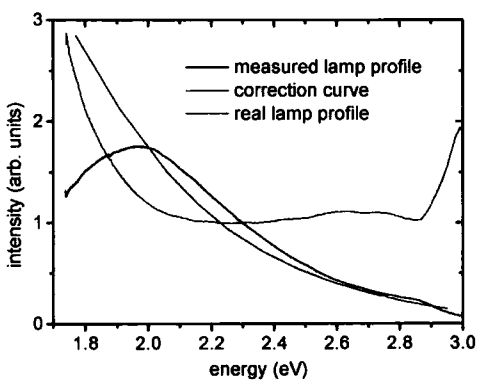

Figure 3-3 Experimental and theoretical tungsten calibration lamp profile and the resulting spectral intensity correction curve.

Representative results (for one grating position) are shown in Figure 3-3. The steep increase of the correction curve observed at ~ 2.9 eV is caused by a 385 nm UV rejection filter in front of the spectrograph, which was employed to block excitation laser light on the ICCD detector. The dispersion of the spectrograph is proportional to wavelength and indirectly proportional to the photon energy. However, the measured ICCD camera intensity (the quantum efficiency) is for a large spectral region nearly independent of the incident photon energy. As a consequence, for identical photon flux the photon density per pixel is lower in the red as compared to the blue energy part of a spectrum. This is the cause of the observed loss of sensitivity on the low energy side of the shown tungsten emission spectrum in Figure 3-3. In a way the situation is comparable to a monochromator, because the physical horizontal width of a pixel acts like the slit width for the monochromated light. Using different grating positions the overall useful wavelength range of the whole spectrometer ranged from the deep ultraviolet to the near infrared up to ~ 920 nm, which is the sensitivity limit of the red-enhanced photocathode of the intensified ICCD camera.

3.2.4. The time resolution of the spectrometer

As a matter of fact one of the most important parameters for a time resolved photo luminescence set-up is the very time resolution, governing the quality of the decay curves of excited

species. In all of such experiments (that do not apply deconvolution techniques) including the present one, the overall time resolution is determined by the slowest component. Therefore it is justified to separately consider the detector - in the present case a gated ICCD camera - and the pulsed excitation.

The here used intensified or gated ICCD camera electronically opens its 'shutter' by reversing a 100 V blocking voltage on its input stage, which is the photocathode. The delay between time zero and the opening of the shutter is known as *gate time,* the time period during which the camera detects, i.e. the shutter is open, will be referred to as *detection time*, respectively, *detection window*. The time resolution of the ICCD camera on its own is then equal to the maximum of the time it takes to open the shutter and the smallest step width for the change of the gate time. For the ICCD camera *4 Picos* both values are 100 ps, thus this is the maximum theoretical time resolution of the camera as well. In the latter reasoning only the opening of the shutter is considered; this implies that with 100 ps time resolution only *integrated decay kinetics* can be obtained. In such an experiment a set of independent, i.e. point wise, measurements is taken, with for example the delay time increasing in 100 ps steps while the detection time covers a very long period. In order to obtain the true decay curve the measured data must be differentiated. This, however, is often a haphazard task, since the noise gets over proportionally amplified. Therefore, all the decay curves taken for this study are measured with a detection width small compared to the decay process itself in order to directly, i.e. without differentiation, obtain the true kinetics. Apparently, for those kinds of measurements the time resolution is reduced to the shortest detection width, which is stated as 200 ps by the manufacturer. However, such a detection width does not give any signal intensity, since it roughly takes 200 ps to open and close the shutter. Therefore the shortest useful detection window of the ICCD camera on its own is 300 ps. If in a single experimental run different detection windows are combined to obtain the decay kinetics (compare 3.2.5), it becomes necessary to know whether the intensity response of the detector is linearly dependent on the chosen detection width, for example: does a 3 ns detection window result in ten times more signal intensity compared to a 300 ps width? In the latter example this would certainly not be expected considering the fixed 200 ps it takes to open and again close the shutter. The dependency of the set detection time compared to the time really applied by the ICCD camera can experimentally be obtained by measuring the intensity of a continuous

light with variable detection width. This was done using a battery driven (i.e. very stable) LED and the obtained correlation is shown in Figure 3-4.

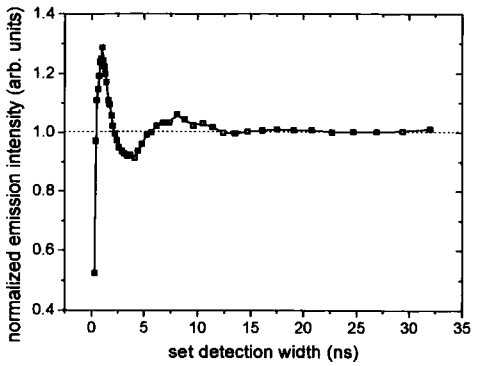

Figure 3-4 Normalized (divided by the gate width) experimentally measured intensities as a function of the detection width for the ICCD camera.

Plotted in this figure is the measured intensity divided by the set detection width, which was further normalized to unity for long gate times. Apparently the behaviour is far from being simple and oscillations are visible, i.e. the measured, relative intensity can even be higher than expected from the set detection width. Note, the ICCD camera is an electronic Gigahertz device and the 100 ps that it takes to reverse the voltage on the photocathode (i.e. open or close its shutter) is more or less already limited by the speed of light as the potential change travels through the detector. Therefore, the observed non-linearity is not really surprising. The error becomes small for detection times exceeding ~10 ns. Note, no correction is necessary for measurements with a fixed detection width but if an experiment with various light integration windows is required (compare 3.2.5) then the width dependent response of the ICCD camera must be accounted for, which was done by dividing the measured intensities by an appropriate correction curve similar to the one shown in Figure 3-4.

In the above paragraph the time-resolution for the intensified ICCD camera is estimated to be 300 ps. The latter value, however, is not automatically equivalent for the overall system if the camera is not the slowest component of the set-up. In the present experiment excitation is provided by a (165 ± 5) ps pulsed Nd-YAG laser. Ideally, the moment when the laser pulse hits the sample should coincide with the start of the gate width by the ICCD camera. Since there is no predefined zero time in the experiment the ICCD camera needs to be triggered by the laser. This can be achieved in two ways. The laser provides an electronic trigger pulse prior to the laser fires. However, the delay time between electrical and optical signal has a jitter of 30 ns, thus, in this way measurements with nanosecond time resolution are not feasible. Therefore the ICCD camera must be electro-optically triggered, i.e. by the excitation pulse itself. Here, the pulsed excitation beam is split into two components: one is used to excite the sample, the second is focused on a fast trigger diode (compare Figure 3-1). After detecting the trigger signal the ICCD camera has a 30 ns processing time,

i.e. the trigger needs to arrive 30 ns early in order to detect an event at time zero for example prompt fluorescence. That is why the excitation beam (not the trigger beam) is passed through a ~ 20 m optical delay path, i.e. the trigger is applied at the ICCD camera about 65 ns before the laser hits the sample (compare Figure 3-1). The true zero time of the experiment, that is the time when the excitation pulse hits the sample, can now be estimated by measuring the laser light intensity as a function of gate width using a small integration window.

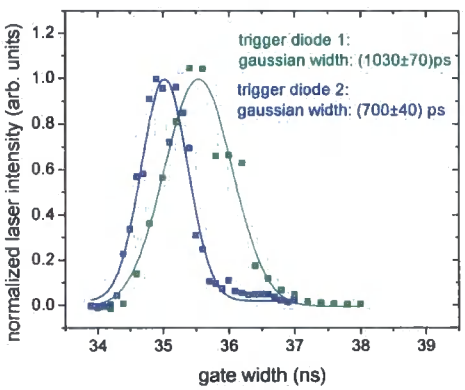

Figure 3-5 Laser excitation intensity versus delay time taken with a fixed detection window of 300 ps for a very fast (blue) and a slightly slower (green) trigger diode.

Typical results, which were obtained with a 300 ps detection window, for two different trigger diodes are shown in Figure 3-5. For the green curve (diode 1) the optical delay path was longer, thus the signal is detected later. For these special geometries, it appears that the zero times are 35.0 and 35.5 ns, respectively. This offset needs to be added to the set gate width for all measurements in order to obtain the true physical delay time of a certain spectrum. However, in the subsequent result chapters only the true, corrected gate times with respect to the zero time are stated. As it depends on the precise length of the optical delay path, this offset in time needs to be remeasured after each change in the geometry of the set-up.

Apparently the experimental results shown in Figure 3-5 also serve as a measure for the true time resolution of the overall system. If the experiment is able to trace the laser excitation pulse, i.e. allows determining the correct pulse width then the time-resolution of the system is even better than the applied laser pulse width. Otherwise the measured response is identical to the time-resolution of the system. From the previous two paragraphs (laser pulse width 165 ps and shortest detector detection window 300 ps) a resolution close to 300 ps is expected. Obviously the time resolution is not as good and even depends on the trigger diode chosen. Using Gaussian curves to fit the measure points one arrives at 1 ns and 700 ps respectively. These striking discrepancies compared to 300 ps are caused by laser intensity fluctuations resulting in intensity fluctuations of the trigger diode electric signal, which translate into a time jitter as the ICCD camera responds to a certain threshold voltage. Details are given in section 3.2.6. By using trigger diodes with fast rise time this jitter can be minimized.

Therefore the faster (40 ps rise time) trigger diode was used for the majority of the experiments. In any case, it is safe to state that the photo luminescence system has an overall subnanosecond time resolution. Accordingly, excited state decay curves were measured with typically 1 ns smallest gate width.

In the present paragraph only photo luminescence has been discussed, i.e. pulsed laser excitation, although the system is also able to measure time resolved electro luminescence. This is because for electro luminescence the time resolution of the set up is very short (10 ns) compared to the RC time of a typical device, which is of the order 0.1..2 μs depending on the applied voltage. Therefore the resolution of the set-up is far better compared to the rather slow electro luminescent processes that can anyway be investigated.

3.2.5. The method of the dynamically increasing detection width

In the above paragraph the minimum detection width, i.e. the maximum time resolution, of the instrument is stated as better than one nanosecond. However, an actually "adequate" width for a certain experiment does also depend on the time domain, in which the observed process decays, i.e. emits luminescence. This is a simple consequence of the fact that the time resolution of every experiment is inversely proportional to the signal strength. Translated to the present case: As the detection window is chosen shorter fewer photons are emitted during this period, and in an extreme case the measure falls below the noise level. The implications of the above shall be further examined by means of an example close to the phosphorescence decay observed in conjugated polymers: Considered is a hypothetical excited state decay featuring a mono exponential radiative lifetime of one second, of which initially no more that 10000 states can be populated at once. The sensitivity of the ICCD camera is arbitrarily fixed to one, i.e. if during a certain detection window one photon is emitted by the sample the camera will see it, if the emission rate falls below one only noise is obtained. Of interest are (i) the emission spectrum and (ii) the decay kinetics of the excited state. For (i) the width has to be chosen >100 μs in order to distinguish the signal from the noise. The practical background for this question is that additional decay mechanisms, apart from emitting luminescence, might be operative reducing the true lifetime of the excited state. So, if in the present example additional non-radiative decay mechanisms are effective to quench all the excited states within the first 100 μs no emission at all could be observed. For (ii): in order to obtain the lifetime it

is not only necessary to simply 'see' the luminescence, it must also be possible to follow its decay for, say, one order of magnitude. Thus the detection window is chosen to be one millisecond, which enables one to observe the luminescence decay up to 2.3 s and obtain the lifetime with an error of one millisecond.

The aforesaid applies to the simple case of a mono exponential decay, in which the process is fully described by a single number – the decay time. This, however, is the rare exception when studying emission processes in conjugated polymers in the time domain that follows the decay of the prompt fluorescence. Due to the nature of conjugated polymers the vast majority of delayed emission processes obey algebraic decay laws, i.e. processes that have their natural base in the logarithmical rather than linear time. This has rather drastic implication for the choice of the 'adequate' detection width: In the initial time regime such decays will be fast and therefore require a relatively short detection window in order to maintain a reasonable time-resolution. As the delay time increases the decay becomes much slower, i.e. the emission strength drops and thus a longer detection width would be needed in order to achieve a good signal to noise ratio. Apparently, a constant detection width in linear time cannot solve the problem. What is needed is a constant width in logarithmical time, i.e. a dynamically increasing detection width. A further visualization of the problem is given in Figure 3-6. In case (a), power law kinetics with an exponent of -1 are probed using a fixed detection window. Here the obtained emission intensities are immediately proportional to the luminescence decay. However, the detection window has to be chosen such that a decent signal within the dynamic range of the ICCD camera is obtained, with the latter being basically the difference between saturation and noise level (shown as

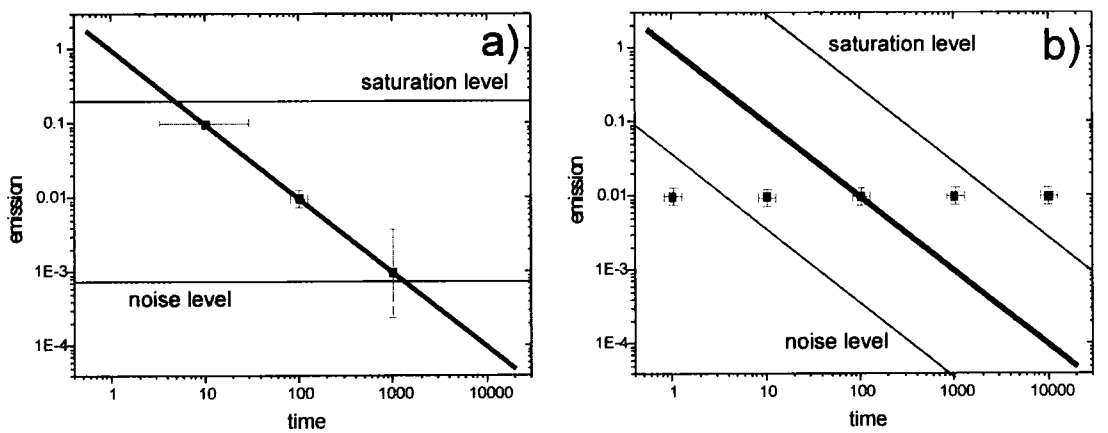

Figure 3-6 Visualization of the effect of a fixed (a) and a logarithmically increasing (b) detection width to measure an algebraic decay with exponent -1. The true decay (thick solid line) is shown in a double logarithmic fashion.

horizontal solid lines in Figure 3-6). For this fixed detection window a large uncertainty in time in the initial decay regime is unavoidable as the detection window becomes comparable to the time in which the luminescence decays. On the other hand, the emission intensity in the late time domain is too low to be distinguished from the noise level.

In case of (b) the gate width dynamically increases for longer delay times. The shorter detection window at early times means the resolution is higher in the initial time period but lower for later times compared to (a). However, the time resolution is adequate throughout the whole measurement region compared to the actual decay. Furthermore, the actually measured intensities are constant and as such exhibit a low noise as well since they are adjusted in the optimum response region of the detector. In order to obtain the true decay kinetics from (b) the measured data points need to be scaled by the corresponding detection window.

In applying the aforesaid, a set of delay times (t_x), equally spaced on a logarithmical time scale, was chosen to cover the time region of interest. The detection window was always taken a tenth of the delay time, which has proven to be a reasonable compromise between time resolution and signal strength. Thus, the measured intensity at point t_x can be expressed as:

$$I_{t_x}^{meas} \propto \int_{-\frac{t_x}{20}}^{+\frac{t_x}{20}} I(t)dt$$

Equation 3-1

with $I(t)$ being the true time-dependent intensity. As the gate width is always a tenth of the delay time, the true emission intensity can simply be regained by dividing the measured intensities and the gate time:

$$I(t) \propto \frac{I_{t_x}^{meas}}{t_x}$$

Equation 3-2

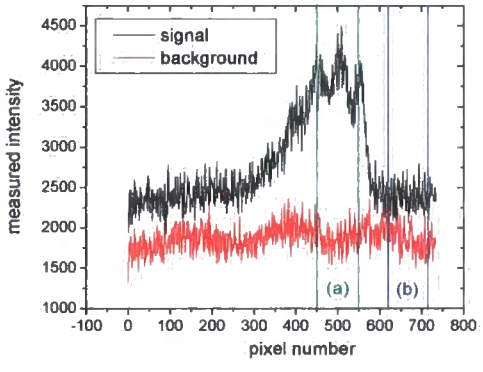

Figure 3-7 A representative raw data spectrum (of 2-fluorene, compare section 6.3.2) and the corresponding background versus pixel number.

In practice, the luminescence decays are obtained in three steps. First the emission intensities for a set of pre defined times t_x are taken as well as a single background under identical conditions but without excitation. The actual measurement is greatly simplified by means of a self-written computer program which successively sets the appropriate gate time and detection width for each data point automatically.

A typical (fairly strong) signal together with a background spectrum is shown in Figure 3-7. Apparently, the signal noise consists of two different contributions. There is the real noise, i.e. the flatness of the background, which is about ~400, but there is also a baseline shift, which for the shown example is of order ~500. The latter is a random offset of the whole baseline and is caused by the readout electronics of the ICCD camera. Therefore, simply subtracting the background would cause a certain negative or positive offset from the true signal. In order to avoid this problem, the background is dynamically corrected for each spectrum. Thus, the second step involves the integration of all emission spectra and the background spectrum over the desired wavelength/pixel region (in Figure 3-7, region (a)) but also over a region where there is no luminescence (in Figure 3-7, region (b)). Subsequently, it is possible to correct for the background using the formula:

$$I_{t_x}^{corr} = I_{t_x}^{meas(a)} - \frac{I_{t_{background}}^{meas(a)}}{I_{t_{background}}^{meas(b)}} I_{t_x}^{meas(b)}$$

Equation 3-3

where the offset of the measured intensities is subtracted for each spectrum and a prefactor, which is obtained from the background (red curve in Figure 3-7), accounts for the not necessarily identical width of the two integration regions. After dynamically subtracting the offset background, the final step in order to obtain the true time depend emission intensities *I(t)*, is to multiply each data point by t_x^{-1}, i.e. its individual inverse detection width according to Equation 3-2.

However, for measurements in the nanosecond time regime (t < 10 ns) this simple normalization does not give correct results, because of the non linearity of the ICCD camera at short detection windows, compare 3.2.4. To account for this situation, a true calibration curve was measured. To do so, a stabilized, battery-driven LED (780 nm) was placed in the focus point of the spectrograph and its emission monitored under the same time settings (t_x) as for the real decay experiment. Therewith, a function is obtained, which increases linearly with t_x and has a ringing noise (compare Figure 3-4) superimposed for short detection windows. This point-wise calibration curve is then plugged into the denominator of Equation 3-2 instead of t_x in order to normalize the experimentally measured emission intensities.

To summarize the above: the method of dynamically increasing the detection width allows for significantly enhanced signal to noise ratios and, correspondingly, the dynamic range for the whole measurement is substantially enlarged compared to the fixed range

of the ICCD camera – without losing time resolution. Thus, emission decays of up to 15 (!) orders in intensity have been taken in *one* (of course point-wise) measurement. Note, in all double logarithmic decay curves shown in the following result chapters the noise and the saturation level are not constants in time, but obey an algebraic law with slope -1 similar to those shown in Figure 3-6 (b). Apparently, a constant measure such as shown in Figure 3-6 (b) is only obtained if the true emission decays with an exponent of exactly -1. Any faster decaying process will result in decreasing measured signal intensities as time is increasing. This can not be further compensated for with a detection width which increases faster than linearly, since this would be accompanied by an unavoidable loss in time resolution. For example it is not possible to apply a quadratically increasing detection width in order to compensate for an algebraic signal decay with slope of –2. Nevertheless, even for such faster decaying emissions the linear dynamically increased width enables one to observed the decay for longer within the fixed dynamic range of the ICCD camera.

In conclusion, the greatest strength of this time resolved luminescence experiment is neither its subnanosecond time resolution nor its high sensitivity. It is rather the ability to dynamically change the detection width during the same experimental run. This makes it an especially powerful tool to study the delayed luminescence processes occurring in conjugated polymers - far superior to any linear light detection systems such as for example photodiodes or photomultipliers.

3.2.6. Laser intensity fluctuations

A major obstacle within the experimental measurements of photo luminescence decays employing the above time-resolved detection set-up is the instability of the Nd-YAG excitation laser.

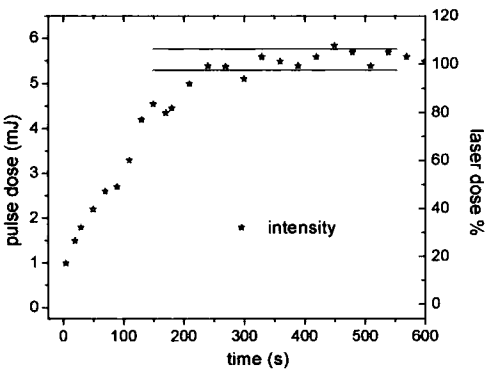

Figure 3-8 Evolution of the Nd-YAG laser intensity (3rd harmonic) after switch on at time zero. 100 laser shots were averaged for a single data point.

In Figure 3-8 the laser intensity after switch on is shown versus time. Apparently it takes about 5 min to reach a stable intensity plateau, which however is still characterized by intensity fluctuations of the order of 10 %. Even these 10 % are only achieved by averaging 100 laser shots; the true shot-to-shot fluctuation is close to 50 %. This instability in intensity is accompanied by a tiny spatial

movement of the laser beam, which however, is aggravated by the 30 m optical delay path, compare Figure 3-1. As a consequence, different areas of the sample are excited. Because only a small section of the illuminated sample is monitored by the ICCD camera, it follows that the actually observed sample luminescence is subject to the combined spatial and excitation dose fluctuation and can in shot-to-shot mode be as large as 70 %.

The situation would still be controllable if the laser fluctuation would have a true random nature. In such a situation a higher number of averages will give decent signals. However, the laser used here additionally exhibits long time intensity instabilities of about 30 %. The only practical way to account for these variations is to repeat the whole measurement several times.

There is also an impact of the intensity fluctuations on the time resolution of the set-up. The ICCD camera is electro-optically pre-triggered by the fluctuating laser that triggers a photodiode. Consequently, the rise of the electrical potential in the photodiode is also subject to shot-to-shot variations. The fixed trigger threshold of the ICCD camera then translates these intensity variations into a jitter in time relative to the true arrival of the laser pulse on the sample. For relatively low laser shots the trigger is late, and for high intensity early. This is the why the laser pulse is measured much wider than theoretically expected, i.e. compare 3.2.4 and Figure 3-5. In order to reduce the problem one needs to steepen the rise of the potential, i.e. use a very fast trigger diode. As seen in Figure 3-5 this indeed narrows the observed laser profile within certain limits.

The above fluctuations have a different impact on specific experimental situations. If the excited state features a logarithmical luminescence decay that lasts over several orders of magnitude in time then measured intensity variations from the true decay of even 50 % will hardly have any impact on the appearance of the decay curve if plotted in a double logarithmical scale. The latter is the typical situation for the decay of the delayed fluorescence in conjugated polymers. On the other hand, if the observed luminescence changes are comparably small then intensity fluctuations by 50 % basically make the whole experiment impracticable. This situation applies for the mono exponentially decaying phosphorescence, which can only be observed for about two orders of magnitude in time. Temperature dependencies belong to the same category as here the signal changes only by typically ~ 50 %.

Finally, intensity fluctuations with all their implications could be avoided almost completely by using a stable excitation source other than the Nd-YAG laser. As an example, for electrical excitation all the aforesaid problems do

not exists and excited state decay kinetics are generally much easier to measure so that the final curves appear smoother. Also, for photo excitation one could employ a laser diode, which again would be much more stable as compared to the pulsed Nd-YAG laser. However, neither the electric excitation nor the laser diode is fast enough to allow for measurements in the nanosecond time regime, which actually is the unique feature of the time-resolved spectrometer. Therefore, one has to use the Nd-YAG laser as it is and try to reduce the fluctuations as much as possible.

3.3. Time-resolved transient triplet absorption

In order to study quasi particles in conjugated polymers the second widely-used approach besides emission spectroscopy is to observe their transient excited state absorption. The goal of the present experiment is to measure the accumulation of the triplet density as a function of time after the switch-on of either electrical or optical excitation and compare it with the singlet fluorescence strength under identical conditions. As shall be seen in chapter 5, with such experimental data several important parameters about working electro luminescent devices can be gained.

The experimental set-up is outlined with the help of the schematic drawing of Figure 3-9. As shall be shown in chapter 5, for this experiment it is important to suppress thermally activated exciton migration. Therefore, the device is mounted in a helium cryostat that allows reaching about 15 K. Optical excitation is provided by a400 nm laser diode module, which can be switched on in about 5 ns. The latter rise time also corresponds to the time resolution of this experiment. In order to maintain auniform illumination of the sample the laser beam was slightly expanded. Furthermore, the optical excitation intensity could be varied by means of a neutral density filter wheel.

Electrical excitation of the sample was provided by a powerful and fast electric pulse generator. For the whole experiment this pulse generator also acted as the trigger master source for the optical and electrical excitation, and for the oscilloscope.

In both excitation modes the singlet emission intensity was measured by focusing the emitted fluorescence on the input photodiode of a transimpedance amplifier. An appropriate cut off filter was employed to reject excitation laser light on this detector. The electrical signal, which is in both excitation modes proportional to the fluorescence intensity, is then recorded by a fast digital oscilloscope that has a recording depth of four giga samples per second. However, all data shown in this study are interpolated from the original data set in order to obtain a reasonable data point density.

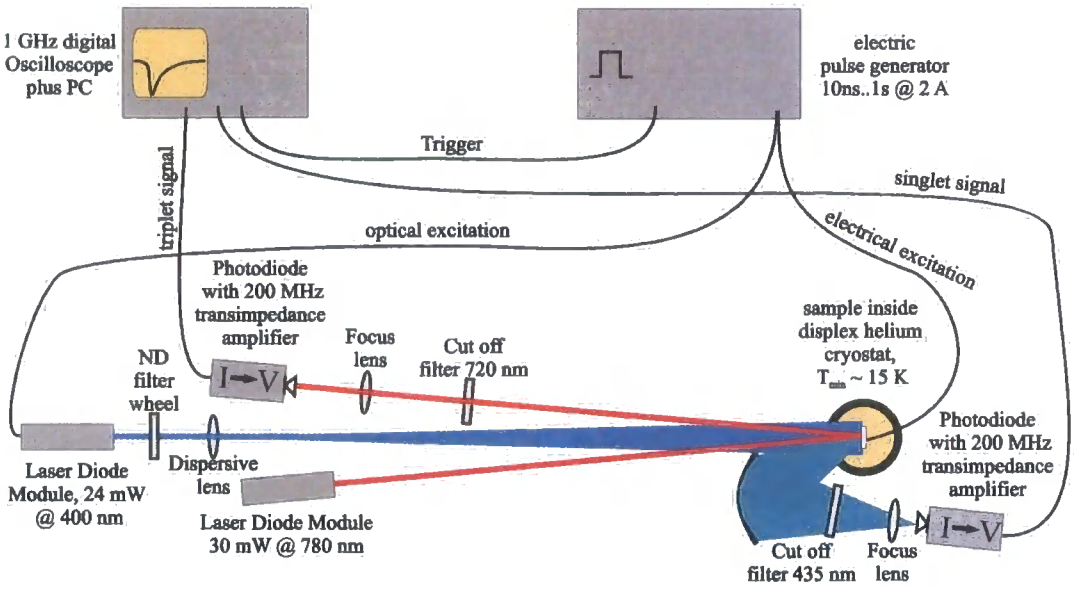

Figure 3-9 Schematic set-up to simultaneously probe the transient triplet absorption as well as the fluorescence intensity after both electrical and optical excitation of a device at low temperature.

Unlike the singlet, the triplet exciton was probed by its transient absorption. Here a cw laser diode module served as a stable probe beam with an energy close to the maximum of the transient triplet absorption spectrum of all fluorene-type conjugated polymers, 780 nm, compare Figure 4-8. After being reflected at the device cathode, any excitation laser light but also the sample fluorescence was filtered from the red laser beam by passing it through a 720 nm cut off filter. The red laser was then detected by a fast photodiode coupled to a transimpedance amplifier and finally recorded by the digital oscilloscope.

The geometry of the whole set-up was arranged such that no changes were necessary for either probing the fluorescence or the transient absorption in both electrical and optical excitation mode. Additionally, it was possible to study both the transient absorption as well as the fluorescence of the device under simultaneous or sequential optical and electrical excitation.

The experiment was run at a typical repetition frequency of 0.2 Hz in order to allow for a sufficient depletion of the long-lived triplet exciton reservoir. Depending on the signal strength between 100 and 1000 excitation runs were averaged for each final data set.

4. Triplet migration and relaxation in a photo excited polyfluorene

4.1. Introduction

Following simple spin-independent charge carrier recombination statistics, the triplet as compared to the singlet state is of equal importance for electroluminescent device applications based on conjugated polymers. However, there is much more knowledge about the singlet exciton, which is mainly caused by the fact that the fluorescence unlike the phosphorescence is easy to observe. On the other hand, a profound knowledge about the triplet exciton is of vital interest in order to optimise state-of-the-art devices, which consist of a polymer layer that is doped with a heavy metal containing complex. In best cases the latter acts as combined singlet and triplet emission centre and at the same time as an energetic trap for the triplet excitons to prevent back transfer to the host polymer. In this context it would be valuable to elucidate the rate limiting factors for the guest population and depopulation in terms of triplet migration and triplet energy transfer. Also of interest is the amount of bimolecular triplet annihilation, which will reduce the luminescence yield of the device. A necessary first step towards a full understanding of these complicated guest-host systems is a profound knowledge about the triplet processes in the host polymer layer. However, apart from the energetic levels little is known about triplets even in pristine conjugated polymers. The present chapter is intended to close this gap as it illuminates migration as well as energy relaxation phenomena of the triplet exciton in a prototypical conjugated polymer by means of time-resolved absorption and luminescence spectroscopy.

Typically for such studies is the population of the triplet manifold via photo excitation followed by inter-system-crossing (ISC), which is more or less efficient depending on the conjugated polymer.[9] In principle short current pulses could alternatively serve as a direct excitation source, which was done in chapter 5. However, the latter method has some disadvantages regarding triplet migration studies. First of all, the current source is in practice a voltage source, thus the initial charge carrier density, concomitantly the triplet density, is unknown. Further, the comparatively long excitation pulses (>1 µs) limit the time resolution; charge carriers remain, which might influence the triplet concentration long after excitation; and the technique is restricted to thin films. Thus, for the present study pulsed laser excitation is deemed the superior method.

Such pulsed photo excitation enables the observation of phosphorescence (Ph), originating from the radiative (spin forbidden) decay of the first excited triplet to the singlet ground state, $T1 \rightarrow S0$. However, this is, independent of the excitation mechanism, only possible in

the long-time region after excitation (>10 ms) when combined with low temperature (<100 K).[10-12] This very low time resolution is not due to a lack in sensitivity but follows from the long radiative lifetime of the triplet state in pristine conjugated polymers. As an example, from the radiative lifetime of the triplet, roughly one second, it follows that only every 100000th triplet created would decay radiatively in the first ten microseconds. Aggravating this, the ISC rate (for photo excitation) and the phosphorescence quantum efficiency, are far from unity, hence temporally resolved phosphorescence detection at early times after excitation is impossible. Even at intermediate measurement times, (µs to ms) the Ph signal is superimposed on the strong delayed fluorescence (DF), whose low energy tail extends into the spectral region of the Ph emission. Thus, a study of triplet migration in conjugated polymers cannot only rely on the photo excited phosphorescence observation because the migration of the triplet excitons is much faster compared to their radiative lifetime. Alternatively, information about the triplet exciton in the initial, dark period could be gained by studying the time-resolved transient triplet absorption, which, however, requires comparably high excitation doses. In those conjugated polymers where the DF after photo excitation originates from triplet-triplet-annihilation (TTA) of course the latter contains information about the precursor triplet states as well and therefore studying the DF offers a powerful tool for gaining information about the triplet state, especially in the first 10 ms after excitation.

Employing time-resolved spectroscopy at low temperature, Romanovskii *et al.* observed both, Ph and DF, emitted by the conjugated polymer methyl-poly(para-phenylene) (MeLPPP).[12] Recently, similar observations have been reported for polyfluorenes[10, 13, 14] and polythiophenes.[15] For the present photo luminescence study a polyfluorene derivative was chosen, as here the DF originates undoubtedly from triplet-triplet-annihilation (TTA),[16, 17] whereas the analysis of photo emission experiments under applied bias voltage suggests the DF of MeLPPP to be caused by delayed charge carrier recombination.[18]

The emphasis of this investigation is to examine the already observed delayed luminescence in greater detail and as such gain a deeper insight into the nature of the triplet state in conjugated polymers in general. Special attention is focused on the migration and energy relaxation of the triplet excitons and on their lifetimes at various temperatures including the important case of thin films at room temperature. To do this, mainly the DF kinetics of the polymer were investigated as a function of temperature and excitation dose in different environments covering

solution, frozen solution, film and blended into an inert matrix polymer. The results obtained were further complemented by time-resolved transient triplet absorption studies and analysed in the framework of a well-established migration theory relying on the hopping of localized particles in a distribution of energy states, which is briefly outlined below.

4.2. Theory

In general, delayed fluorescence in organic conjugated systems potentially originates from charge carrier recombination (either geminate or non-geminate), inter-system-crossing, or triplet-triplet-annihilation. The charge carriers for the first case are for example available in electrical excitation mode[11] or following high excitation doses due to singlet-singlet-annihilation.[19] For the current considerations this mechanism for delayed fluorescence is neglected, as there is no indication of a prominent charge carrier density after photo excitation. Also the second possibility, where a singlet manifold is repopulated by the conversion of triplet excitons due to inter-system-crossing, can safely be discarded on account of the large singlet-to-triplet energy splitting in conjugated polymers, which prevents any thermally activated back transfer. On the other hand there is abundant proof, either from our own, but also from other research groups, that the delayed fluorescence in polyfluorene-type polymers originates from triplet-triplet-annihilation.[10, 16, 17]

After bimolecular triplet annihilation nine excited states are formed with equal probability of which three have singlet character and might potentially be observed as delayed fluorescence.[20] Since the actual triplet fission is an electron exchange interaction, its interaction radius is comparable to the triplet exciton delocalization length, which is of the order of 2 nm only. Rate limiting for the annihilation process is the triplet exciton migration that needs to bring two species within the interaction radius. Thus, the triplet migration is the key to the understanding of the delayed fluorescence in conjugated polymers. A consistent picture in turn allows gaining information about the triplet migration from the experimentally accessible delayed fluorescence. In the following the scenario of triplet migration and annihilation in an energetically distributed material is briefly outlined.

Starting from the classical rate equation, an excited triplet density is depopulated by a combination of monomolecular (k, representing impurity quenching and radiative decay) and bimolecular decay processes (γ):

$$\frac{dn(t)}{dt} = G(t) - kn(t) - \gamma n(t)^2$$

Equation 4-1

Following pulsed photo excitation the population of the triplet manifold due to

inter-system-crossing occurs during the singlet lifetime, which is short (<1 ns) compared to the typical phenomena related to the triplet exciton. Therefore the triplet excitation can still be considered as pulsed respectively time independent and the time dependent triplet generation term in Equation 4-1 vanishes. Next, the monomolecular term in Equation 4-1 is neglected under the premises that non-radiative quenching is not a major decay mechanism and only the early time period after (pulsed) photo excitation (typically t < 100 ms) is considered. For this simplified situation bimolecular annihilation is left as the only decay mechanism and the DF observed at a delay time t is directly proportional to the triplet decay, i.e. the change of the triplet density, at the same time:

$$DF(t) \sim \frac{dn(t)}{dt} = -\gamma_{TT} n(t)^2$$

Equation 4-2

therefore the initially excited triplet density, n_0, decays according to:

$$n(t) = \frac{n_0}{1 + \gamma_{TT} n_0 t}$$

Equation 4-3

or in general for a time dependent γ_{TT}:

$$n(t) = \frac{n_0}{1 + n_0 \int_0^t \gamma_{TT}(u)du}$$

Equation 4-4

According to Smoluchowski's theory of bimolecular reactions (in the asymptotic time-independent limit) the annihilation constant γ_{TT} is proportional to the triplet diffusion coefficient (D), the interaction radius (R) and the fraction of triplets annihilated after encounter (f)[21]

$$\gamma_{TT} = 8\pi f R D$$

Equation 4-5

Using a classical, time independent diffusion coefficient (D), Equation 4-1 to 4-5 have been applied successfully for several organic crystals. Usually, the results were classified whether the radiative decay or the bimolecular annihilation is the major decay mechanism for the triplet excitons: If the latter applies then DF and triplet density obey algebraic decay laws with exponent of -2 and -1, respectively. On the other hand, if annihilation does not lead to a significant depletion of the triplet reservoir (low excitation dose) then the triplet density decays exponentially with its characteristic lifetime and the corresponding DF decays twice as fast. Typical values for γ_{TT} and D are of order 10^{12}cm^{3}s^{-1} and 10^4cm^{2}s^{-1}, respectively.[20]

Unlike organic crystals, which exhibit a nearly isoenergetic site distribution, characteristic of conjugated polymers is their inherent energetic and spatial disorder. While the latter prevents coherent motion such as in inorganic semiconductors, the former leads to temperature dependent energy relaxation phenomena during the exciton migration. This twofold disorder renders the diffusion time-dependent, making the mathematical treatment

more complex than in the case of the classical organic crystal work. In the following the highlights of several earlier theoretical work[22-24] as well as Monte Carlo simulations[25-27] on non-equilibrium diffusion and energy relaxation in localized state distributions are briefly outlined. In the framework of these theories the triplet diffusion is treated as a series of incoherent jumps among spatially and energetically localized states. The jump rate between two such localized states (*i,j*) separated by R_{ij}, which possess the energies ε_i and ε_j, is governed by the Miller-Abraham equations:

$$v_{ij} = v_0 e^{-2\alpha R_{ij}} e^{-\frac{\varepsilon_j - \varepsilon_i}{k_B T}}, \quad \varepsilon_j > \varepsilon_i,$$
$$v_{ij} = v_0 e^{-2\alpha R_{ij}}, \quad \varepsilon_j < \varepsilon_i$$

Equation 4-6

where v_0 is the so-called attempt-to-jump frequency, which is close to a typical phonon frequency ~10^{12} s^{-1}, and α denotes the inverse localisation length of the triplet exciton. Thus, jumps downhill in energy only depend on the separation of the considered sites, uphill jumps additionally require thermal activation energy. In the context of Equation 4-6 the diffusion is referred to as "in equilibrium" if the back and forward jump rate between any two sites *i* and *j* is of nearly equal probability, i.e. $k_B T >> |\varepsilon_i - \varepsilon_j|$. Otherwise the system is characterised by motion due to non-equilibrium diffusion.

For organic systems, a Gaussian distribution is always the best choice to describe the DOS:

$$n(\varepsilon) \sim e^{\frac{(\varepsilon - \varepsilon_T)^2}{2\delta^2}}$$

Equation 4-7

with δ being the standard deviation (width) of the distribution and ε_T the centre energy.

After pulsed excitation at random energy within the DOS the diffusion of the triplet excitons evolves in two fundamentally different migration regimes. Firstly, motion is governed by fast energy relaxation towards low energy sites within the DOS. For the migrating triplet, neighbouring sites that qualify for the next jump with a lower energy become fewer after each successful (arriving at lower site energy) jump. Since the attempt-to-jump frequency does not change, successive jumps to even lower energy sites take longer with the elapse of more and more time after excitation. This renders the diffusion (and concomitantly γ_{TT}) time-dependent or dispersive, respectively. The exact behaviour of *D(t)* is strongly dependent on the width of the DOS and the available thermal activation energy, i.e. the temperature of the environment, and is not trivial to cast into an explicit analytical expression. Nevertheless, in an attempt to solve the migration problem analytically in the zero-

temperature limit (absence of thermal activation energy) for a Gaussian energetic site distribution Movaghar *et al.* derived an expression for the time dependence of the average hopping, which is directly proportional to the diffusivity and thereby to the triplet-triplet-annihilation constant, γ_{TT}:[23]

$$\gamma_{TT}(t) \sim D(t) \sim \nu(t) \sim \frac{1}{t \ln(\nu_0 t)}.$$

Equation 4-8

This expression can be approximated by $\nu(t) \sim t^{-1.04}$ in the long time limit.[26] During the thermalization period the same zero temperature treatment of Movaghar *et al.* predicts a temperature independent relaxation of the average energy relative to the centre of the Gaussian DOS, which in a simplified version yields:[23]

$$\varepsilon(t) \sim -\delta\left[\ln(\ln \nu_0 t)\right]^{1/2} \quad \text{as } t \to \infty.$$

Equation 4-9

Both of these asymptotic dependencies, which hold true for *any* Gaussian-type DOS, were confirmed several times using Monte Carlo techniques for example in Ref. [27]. In this approximation neither the diffusivity nor the average energy reach an equilibrium value.

Even at $T \neq 0$ the excitons, which at $t = 0$ are excited at random within the DOS, initially thermalize to lower energy sites, accordingly in this time period Equation 4-8 and 3-9 are still valid. However, for such a finite temperature the diffusivity will approach a quasi (only quasi because the triplet is a transient particle) equilibrium value after a certain delay time. At this (temperature dependent) segregation time t_s the diffusion due to thermalization within the DOS equalizes the thermally activated hopping; afterwards triplet migration is governed by thermally assisted jumps. Now the non-dispersive, classical, regime is attained, which is described by a time-independent, but still temperature dependent, diffusion constant, D_∞. Using an effective medium approximation, an analytic expression for the segregation time was calculated as:[28]

$$t_s(T) = t_0 e^{\left(\frac{c\delta}{k_B T}\right)^2}$$

Equation 4-10

where c is a constant depending on the dimensionality of the migration; with c = 0.93 or 2/3 for one-dimensional or three-dimensional migration, respectively.[29] Again, Equation 4-10 has been systematically confirmed by employing Monte Carlo techniques, for example in Ref. [26]. t_0 is not simply the inverse attempt-to-jump frequency ν_0 from Equation 4-6 but it denotes the dwell time for triplets that migrate through a hypothetical isoenergetic ($\delta = 0$) equivalent structure, i.e. the exchange interaction strength and the spatial site distribution are already included. Thus, both parameters are related to each other by

$$t_0 = \left[6\nu_0 e^{(-2\alpha R_{ij})}\right]^{-1}$$

Equation 4-11

For the study of transient particles, such as triplet excitons, a certain temperature region exists (typically $T < 90$ K) in which equilibrium diffusion after completed energy relaxation might in principle be reached according to Equation 4-10; however, this is impeded by the finite mono molecular lifetime of the excitons. In other words, the segregation time t_s exceeds the mono exponential triplet lifetime. Obviously, in such a situation only the dispersive migration regime can be observed.

Likewise for the diffusivity, also the mean energy of the migrating triplets takes a definite, but temperature dependent value in the non-dispersive regime that is given by:

$$\varepsilon = \varepsilon_T - \frac{\delta^2}{k_B T} \qquad \text{for } t > t_s .$$

Equation 4-12

The schematic drawings of Figure 4-1 and 4-2 are intended to illustrate the turnover from dispersive to non-dispersive triplet migration for finite temperatures. Figure 4-1 shows the triplet population (green) within the energetic DOS directly after excitation (a), within the dispersive time regime (b), and finally in the non-dispersive regime (c). During thermalization, only sites with lower energy as compared to the actual one are accessible for each triplet out of the green area. Once the thermal activation energy ($k_b T$) has been reached, any further migration can, unrestricted by energetic considerations, proceed within this low energy submanifold of the whole system. Within this framework a reduced site density or a larger site separation R_{ij} can be compensated for by increasing the temperature and vice versa.

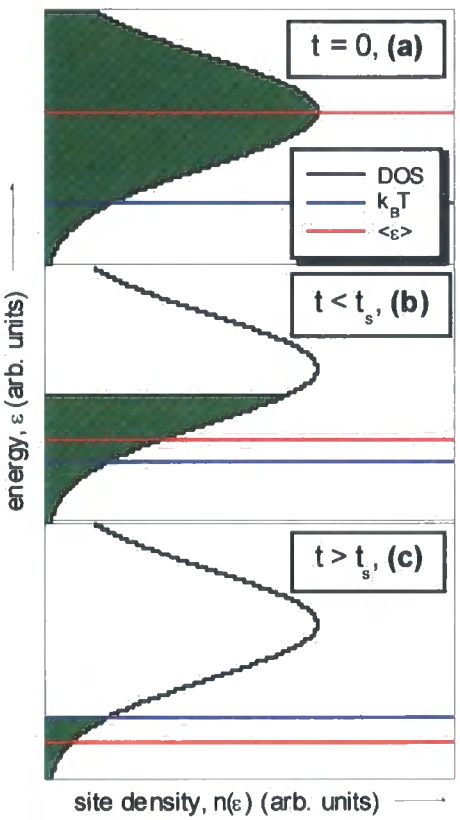

Figure 4-1 The population (green) of the Gaussian DOS (black solid line) at three different times after excitation as indicated. The blue line denotes the thermal activation energy and the red line the average triplet energy.

The green area is at all times proportional to the average hopping rate, i.e. the migration efficiency. Note, according to Equation 4-9, the energy relaxation from (a) to (b) occurs much

faster than from (b) to (c). The time-dependent shift of the average triplet energy <ε> can be observed as a time dependent shift of the corresponding triplet emission.

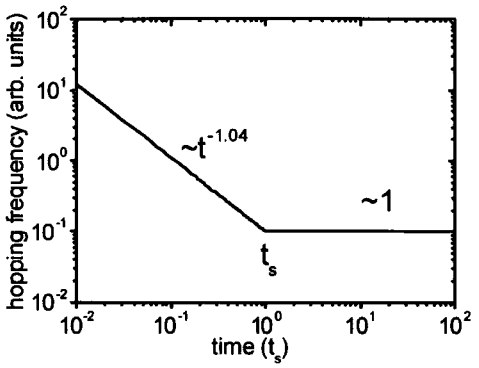

Figure 4-2 Time dependence of the average hopping frequency covering dispersive and non-dispersive diffusion.

Figure 4-2 qualitatively shows the jump rate versus time, whereby the time is given in multiples of the segregation time t_s. According to Equation 4-8 in the dispersive time regime the number of jumps in a certain unit time asymptotically decays with a slope of -1.04 and approaches a constant value once equilibrium diffusion has been attained.

Of course, the initial behaviour of the hopping frequency in the dispersive regime has to have some sort of cut-off frequency for scaling reasons, which, however, is difficult to cast into an explicit expression and anyway occurs in a time domain, which is not accessible within the present study.

4.3. Sample Preparation

The synthesis of the polyfluorene derivative poly(9,9-bis(2-ethylhexyl)fluorene-2,7-diyl) end-capped with *N,N*-bis(4-methylphenyl)-*N*-phenylamine (PF2/6am4) (see Figure 4-3 below for chemical structure) is described in the literature.[30] This polymer rather than a more common polyfluorene was chosen because it shows much less tendency to form keto-defect sites.

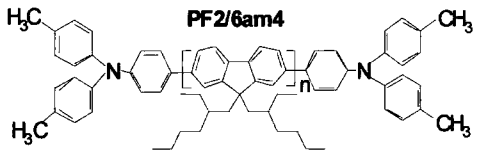

Figure 4-3 The chemical structure of the investigated amine-endcapped polyfluorene derivative.

In order to investigate the concentration dependence of the decay kinetics, dilute solutions of PF2/6am4 in either 2-methyltetrahydrofuran (MTHF), methylcyclohexane (MCH) or toluene have been prepared. The polymer fractions were 10^{-3}, 10^{-4}, and 10^{-5} by weight, which for the lowest concentration corresponds to ≈ $5*10^{-6}$ mol repeat unit/mol solvent. After transferring the solutions into a sealed degassing cell, attached to a quartz cuvette, the air dissolved in the solutions was removed by three freezing-thaw-cycles. Additionally, MTHF and MCH/toluene form clear glassy matrices at low temperature making possible the investigation of low polymer concentrations imbedded in a rigid matrix. To do so, a sealed cylindrical quartz view port, loaded inside the glove box under nitrogen atmosphere with pre-deoxygenated

polymer solution, was attached to the cold finger of the helium cryostat. A disadvantage of frozen solution is their natural restriction to low temperature. This limitation has been circumvented by embedding the investigated polymer into zeonex - a cyclo olefin, from ZEON. In order to fabricate films, zeonex containing 10^{-4} or 10^{-5} by weight PF2/6am4, was dissolved in toluene and subsequently drop cast onto silicon wafers. With this procedure perfectly clear films were obtained, exhibiting the purple colour of PF2/6am4 solutions as compared to the bluish appearance of PF2/6am4 films. To compensate for the low absolute absorption of these (thin, dilute) films, typically 20 films where stacked together forming one sample of about 2 mm overall thickness.

The behaviour of these, supposedly matrix isolated, polymer chains was compared with solid-state polymer films that have been prepared by spin coating a 2% by weight solution of PF2/6am4 in toluene at 2500 rpm onto previously cleaned quartz substrates.

4.4. Results and Discussion

4.4.1. Fluorescence decays in solid state and frozen solutions

In Figure 4-4 the isoenergetic prompt (PF) and delayed fluorescence (DF) as well as the red-shifted phosphorescence (Ph) spectra are shown as observed for a thin film at 15 K. For the purpose of comparison the 300 K absorption spectrum of the same film is included as well. Very similar spectra were obtained for the other systems, frozen solution, solution and thin film. Furthermore, the curves are consistent with data published for similar polyfluorene derivatives,[10, 16] in particular confirming that the different end groups do not alter the photo physics.

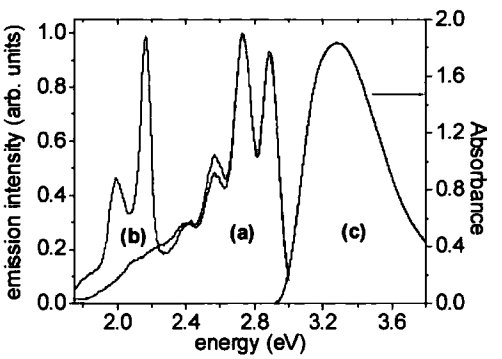

Figure 4-4 Normalized prompt and 10 ms delayed emission spectra of a PF2/6am4 film at 15 K. Prompt and delayed fluorescence appear identical in spectral position and shape (a). Only for the delayed spectrum phosphorescence is detected peaking at 2.17 eV (b). Also shown is the 300 K absorption spectrum of the same film (c).

Even if the spectral appearance of the (normalized) PF and DF is identical, the difference in intensity between both kinds of emission is remarkable – some ten orders of magnitude for the spectra presented in Figure 4-4. Representing the numerous decay curves measured for this study, two typical temporal decay patterns of the spectrally integrated fluorescence obtained from zeonex films are presented in Figure 4-5 in a double logarithmic fashion. The spectra of Figure 4-4 represent roughly

the start- and endpoints of the low temperature curve of Figure 4-5.

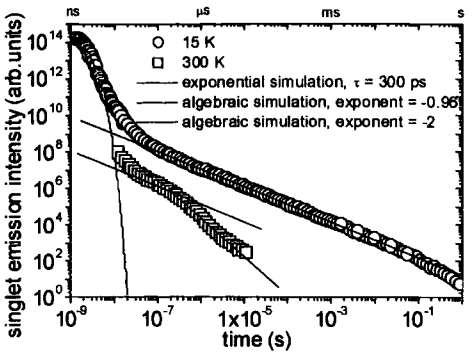

Figure 4-5 Double logarithmic presentation of the fluorescence versus time of 10^{-4} PF2/6am4 imbedded into zeonex. For the sake of clarity the 300 K curve is offset by two orders of magnitude compared to the 15 K curve. The solid lines are guide lines corresponding to algebraic and exponential decays, respectively.

Apart from the initial time domain, the kinetics are far from being simply mono-exponential and, depending on experimental parameters such as temperature and excitation dose, up to five decay regimes with different kinetics can be distinguished as follows: Extending over the initial four nanoseconds and only shown for the low temperature curve, the tail of the PF decay is visible featuring a nearly mono-exponential decay, which was simulated using a 300 ps characteristic lifetime, green solid line of Figure 4-5. This (slightly temperature dependent) PF lifetime of PF2/6am4 agrees well with data obtained using the time-correlated single photon counting method that are given in section 6.3.2.

Extending over the next 100 ns after photo excitation, a fast decaying DF (subsequently called DF1) is just about visible, which obeys algebraic decay kinetics with an exponent between –2 and –3. This emission, which has not been mentioned in the literature before, is truly delayed rather than the tail of the PF as the double logarithmic graph might suggest. For example, at 20 ns the measured intensity is ~ 10^{10} times stronger than that expected from the exponential PF decay (compare with exponential simulation). There are many reasons not to assign the origin of this kind of DF to TTA.

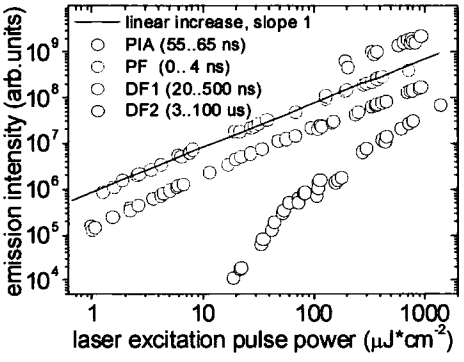

Figure 4-6 Laser power dependency of transient triplet absorption (blue), prompt fluorescence (green), early time (red) and late time delayed fluorescence (black) component. The measurements have been taken using a 10^{-4} MCH solution at 300 K rather than a film. In order to see that the gate times employed indeed correspond to DF1 and DF2 refer to the solution decay kinetics shown in Figure 4-13. The solid line depicts a linear increase with laser power.

One is the laser excitation dose dependency shown in Figure 4-6, which was measured for a 10^{-4} MCH solution. Here, gate windows were chosen such that the intensity dependencies are obtained selectively for the PF, DF1 and the subsequent long-time DF. The clearly linear dependence for the early,

fast DF1 component on excitation power points to a monomolecular rather than bimolecular origin, such as TTA. The latter findings are identically recovered in zeonex films and solutions. A detailed characterisation of this kind of DF is given in chapter 6.

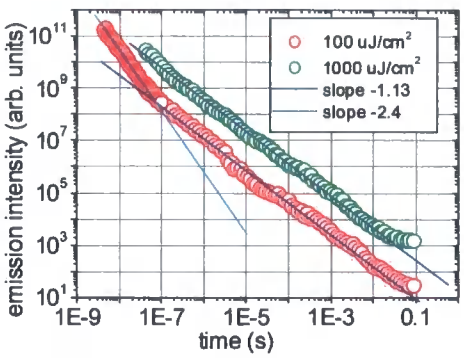

Figure 4-7 Fluorescence decays at two excitation doses of 10^{-5} wt% polymer in a toluene:MCH frozen solution at 20 K. The curves are not normalized. Solid lines indicate algebraic decays. The additional signal at 0.1 s is caused by phosphorescence.

With delay times exceeding the DF1 regime, the delayed fluorescence (hereafter called DF2) decay becomes slower obeying an algebraic law with slope –0.96±0.01 in the case of zeonex and solid thin films. A slightly faster decay is found for all kinds of frozen solution, -1.13±0.01. Representative decays are shown in Figure 4-7. These slopes within the given error limits have been observed without exception (20 times for films and zeonex, 4 times for different frozen solutions), therefore they represent firm results rather than random deviations from an ideal slope of –1 caused by inaccuracies of measurement. The slopes are independent of experimental conditions, for example they do not depend on the excitation dose as shown in Figure 4-7. For sufficiently high temperatures, i.e. the 300 K curve in Figure 4-5, a further turning point ($t_{S(300\ K)} \approx 200$ ns) in the fluorescence decay kinetics is observed, after which the decay becomes faster again exhibiting a slope of ~ -2. These general decay patterns (a slope of ~ -1 which is, only at higher temperatures, followed by a slope of ~ -2) were always observed in zeonex as well as for polymer films and frozen solution. This kind of delayed emission (DF2) originates from TTA, which was shown independently by us and Hertel *et al.*[16, 17] For example, the bimolecular nature of the annihilation process manifests itself in super linear excitation dose dependencies as shown in the lower curve of Figure 4-6. Naturally any additional triplet decay beside TTA will result in reduced DF2 emission intensities. This is the cause of the fifth decay regime, the accelerated DF2 decay for delay times > 100 ms, as seen in the upper curve of Figure 4-5, as here the radiative triplet decay (Ph) becomes increasingly important. In Figure 4-7 the long time behaviour of the DF2 kinetics actually curves in the 'wrong way'. This is caused by the very weak DF2 signals as compared to the Ph signals in frozen solutions, which makes selective integration difficult. Thus, the 'fluorescence kinetics' actually contain a phosphorescence contribution.

The decay pattern of the DF2 emission is fully consistent with the theoretical expectations of bimolecular triplet annihilation of 4.2: In the initial time domain after excitation and independently of temperature, dispersive triplet decay is observed, which lasts up to a temperature dependent segregation time and afterwards turns into a non-dispersive decay. In fact, this full pattern is observed only for the room temperature decay in Figure 4-5. At low temperature the radiative triplet lifetime is shorter than the segregation time $t_{s(15\ K)}$ – the non-dispersive part of the fluorescence decay cannot be observed. The non-dispersive, classical decay of the ambient fluorescence curve occurs in a time domain much shorter (<10 μs) than the mono exponential triplet lifetime (~1 s). Therefore the observed –2 slope directly reflects the classical high excitation dose situation, where TTA is the main deactivation channel for the triplet population, which itself decays with an algebraic law of slope minus one.

What is the meaning of the exponents that were observed in the dispersive regime, - 0.96 and –1.13 for films and zeonex films, respectively? Again, it is useful to consider, whether these data represent the high or low excitation case, or in other words, whether the observed delayed fluorescence does significantly deplete the triplet reservoir or not. According to Equation 4-2, in the first case a slope of –3 (time dependence of the triplet-triplet-annihilation 'constant' from Equation 4-8 multiplied with the square of the decaying triplet population) in the second case a slope close to –1 (time dependence of the triplet-triplet-annihilation constant from Equation 4-8 multiplied with a constant triplet population) are expected. Apparently, the observed decay parameters only fit to a situation with constant triplet population. To gain confidence in this assumption the transient triplet absorption, which is directly proportional to the total triplet density, has been measured as a function of time.

4.4.2. Photo induced triplet absorption decays of solid state and frozen solution

The inset of Figure 4-8 shows a photo-induced transient triplet absorption (PIA) spectrum of 10^{-4} by wt polymer in zeonex. This spectrum, which was measured using the ICCD camera, is consistent with quasi steady state transient triplet absorption spectra of similar polyfluorene derivatives.[31] The main part of the figure compares the temporal decay of the photo induced triplet absorption signal at 15 and 300 K, measured using the same zeonex film as in Figure 4-5. Due to a lack of a fast transimpedance detector at the time of the measurements, the data points are combined from two

different experiments: whereas the noisy initial points represent integrated triplet absorption spectra obtained with the ICCD camera (compare section 3.2), the later time region is covered by an oscilloscope trace (compare section 3.3). At first glance the triplet decay patterns resemble those of the DF2, seen in Figure 4-5. However, in the same time regime where the DF2 intensity decreases by some eight orders of magnitude the PIA signal is only reduced by approximately 30 %. Thus, the above assumption of a nearly time-independent triplet density during the dispersive triplet migration regime is in fact confirmed.

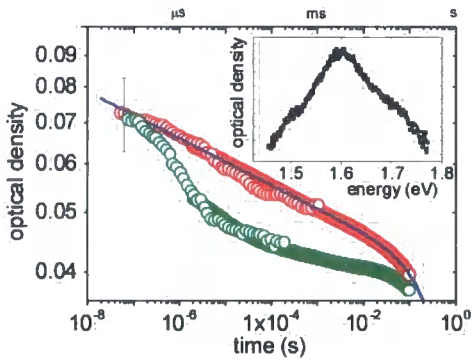

Figure 4-8 Time resolved transient triplet absorption signal of 10^{-4} polymer in zeonex at 15 K and 300 K. The curves are composed of two data sets obtained independently with ICCD camera and oscilloscope in order to cover the initial and the late time regime, respectively. The ICCD camera results are smoothed; an error bar of the original data is given. The solid line fit of the 15 K curve corresponds to Equation 4-13. The inset shows a TRA spectrum at 15 K, which was obtained using the ICCD camera.

At variance to the DF kinetics, the weak time dependence (slope –0.04) of the triplet decay also extends into the first 100 ns, thereby confirming the lack of any sort of fast initial decay comparable to the DF1 kinetics. This observation once more proves that, unlike the DF2, the DF1 does not originate from TTA. However, the turning point in the DF2 kinetics from slope ~ -1 to -2 is accompanied by a similar change in the PIA curve at the same (temperature dependent) delay time t_s. This observation might be visualized by comparing the 300 K zeonex curves of Figure 4-5 (DF2) and Figure 4-8 (PIA), in both cases $t_s \approx 200$ ns. After t_s the PIA signal declines by some 25 % (relative to the slope of –0.04). Then the decay again slows down until the radiative triplet lifetime becomes dominant. Likewise, this long lasting tail has its counterpart in the DF2 kinetics.

The low temperature, time dependent, PIA signal (red data set of Figure 4-8) can be fitted extremely well (blue solid line) using a simulation of the form

$$Ph(t) \propto t^{-s} e^{-\frac{t}{\tau}}$$

Equation 4-13

The characteristic radiative triplet decay lifetime τ is found to be 1.43 s. This value slightly exceeds the phosphorescence decay time, 1.1 s, found by Hertel *et al.* for a similar polyfluorene derivative in frozen solution.[16] However, the authors assumed only exponential triplet decay and thereby neglecting the additional algebraic component, hence a smaller exponential decay time is expected. In Equation 4-13 the exponent s describes the power law contribution to the triplet

decay, s = - 0.04. An inherent problem of the PIA experiment is the low sensitivity, which required very high excitation doses (~2000 μJ) as compared to the delayed fluorescence measurements in order to achieve decent signal-to-noise ratios. On this account it might be more realistic to consider the actually measured slope as an upper limit rather than the true triplet decay that corresponds to the given above delayed fluorescence decays. Indeed, for very high excitation doses (>2000 μJ/cm^2) the measured DF2 decay becomes slightly faster. However, the experiment is difficult as at such excitation doses the sample already degrades. The latter obstacle also impeded to gain solid state PIA data.

4.4.3. The experimental slopes within the framework of the theory

Next, the measured DF2 slopes in the dispersive regime, - 0.96 and –1.13 for thin film/zeonex and frozen solution, respectively, are discussed in the background of a nearly constant triplet density. Plugging the observed time-independent triplet density ($T(t)$) in Equation 4-2, the delayed fluorescence decay should be proportional to the triplet-triplet-annihilation constant γ_{TT}. The latter is proportional to the triplet diffusivity, which in the dispersive regime is approximated by Equation 4-8 as $\gamma_{TT}(t), D(t) \sim t^{-1.04}$. Although close, neither the DF2 slopes in frozen solutions nor those in thin films and zeonex exactly match the expected decay exponent of -1.04. Furthermore, the deviation from the expected slope (0.08 for both cases) clearly exceeds the error limit of the experimentally measured slopes (0.01). However, Equation 4-8 describes the dispersive triplet diffusivity only for the special case of three-dimensional motion. For example, in two dimensions the decay is predicted to be faster featuring an exponent of -1.5. As shall be shown below, the polymer chains in frozen solutions are neither fully isolated nor do they behave like solid state. Instead frozen solutions take an intermediate position between these two extremes, which in some (theoretical) publications is treated as motion in systems with fractal dimensionality. Bearing this in mind the observed faster decay becomes, at least at a qualitative level, reasonable. But why is the DF2 slope in solid state even slower than the annihilation constant γ_{TT}, -0.96 versus -1.04? Independent of any dispersive or non-dispersive theory, from the basic Equation 4-2 such a situation would require an increasing triplet population, which is absurd. Even on a more general level, nothing can asymptotically decay slower than –1 as this would require an infinite excitation density (the number of decaying particles approaches infinity as $t \to \infty$). Thus, Equation 4-2 is an over

simplification and does not exactly describe the present solid-state situation, although the observed delayed fluorescence is certainly caused by triplet-triplet-annihilation. Triplet quenching sites might account for these observed discrepancies. The quenching rate would have the same time dependence as the annihilation rate[32] because the diffusivity is rate-limiting here as well. Therefore both processes balance in time making it possible to see delayed fluorescence, which still obeys a power law but with a smaller slope. At this point it is impossible to perform the whole calculations, starting from a modified Equation 4-2 that includes a mono molecular decay term, in order to analytically confirm the above hypothesis. Nevertheless, a large number of materials having different quality were tested within this study and experience proved that materials of low quality decayed with a slower rate, i.e. showed the largest deviations from the ideal slope of –1.04 in the dispersive decay regime. Whether a material is good or bad was mainly distinguished by the amount of keto defect emission that is additionally observed in the nanosecond time domain.[33] In general the DF2 decays slower than –1.04 for any material. Only few polymers, namely polyspirobifluorene but also some new batches of polyfluorene, reach the latter, theoretical limit.

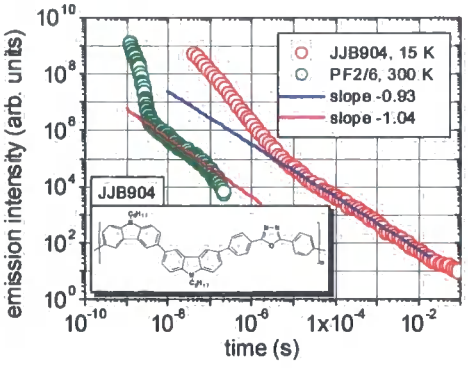

Figure 4-9 Solid state fluorescence decays of polyfluorene (PF2/6) at 300 K and a carbazole and oxadiazole containing copolymer at 15 K.

For illustration purposes, two DF2 decays that represent different scenarios are given in Figure 4-9. The green dataset was obtained from a clean and new polyfluorene derivative with a molecular weight corresponding to 20 repeat units. Here the room temperature prompt fluorescence decay directly turns into the DF2 emission i.e. the latter is strong enough to completely mask the DF1. During the dispersive decay the DF2 decays with the ideal slope of - 1.04. For this room temperature dataset, the segregation time between dispersive and non-dispersive triplet migration is visible at ~ 100 ns. The red dataset stems from a carbazole and oxadiazole containing copolymer (see inset of Figure 4-9 for chemical structure). Following the prompt fluorescence decay (not shown), the fast decaying DF1 emission is clearly visible. Subsequently (~ 5 µs) the decay turns into the dispersive DF2 regime, which here features an algebraic exponent of – 0.93. Because the measurement was

taken at low temperature no turn over into the non-dispersive regime is observed. Likewise for frozen solution (compare Figure 4-7), the increasing signal at long delay times is caused by an underlying phosphorescence contribution in the fluorescence spectrum. The clearly slower decay slope is consistent with a high proportion of defect emission that is observed in this material.

To summarize, the slope actually observed is independent of experimental conditions for a certain batch of a polymer and in such should be considered as a material constant likewise the mono exponential singlet lifetime. Qualitatively, the difference of the experimentally observed and the ideal slope is an indication of the amount of triplet quenching sites.

4.4.4. The segregation time in the framework of the theory, the variance of the triplet DOS

Next the temperature dependence of the segregation between dispersive and non-dispersive triplet migration, $t_s(T)$, shall be investigated. To do so, a compendium of decay curves covering frozen solution, thin film and zeonex film at several temperatures is shown in Figure 4-10 on a common time axis. First of all, these curves are not normalized. Therefore, the DF2 intensity is almost temperature independent as long as the dispersive regime is valid. This is consistent with the above finding that during the non-equilibrium diffusion regime no significant depletion of the triplet reservoir occurs. Obviously the accelerated decay of the DF2 starts earlier with increasing temperature, and, concomitantly, the turning point shifts to shorter delay times after photo excitation.

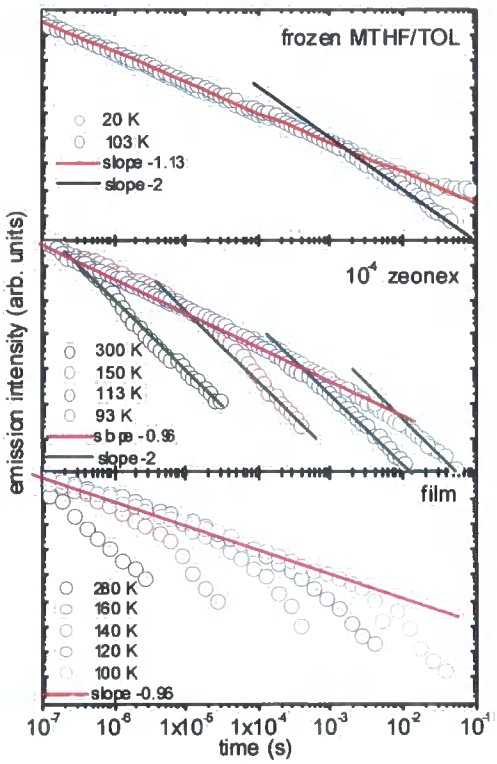

Figure 4-10 Compendium of non-normalized fluorescence decay curves at different temperature for 10^{-4} frozen solution, film and 10^{-4} by wt PF2/6am4 in zeonex.

In Figure 4-11 the segregation times from Figure 4-10 and other decay curves are plotted in a semi-logarithmic fashion versus the inverse squared temperature according to Equation 4-10. The values were obtained from the intersections of -1 and –2 slopes fitted to the appropriate time regimes in the DF2 kinetics. Within experimental

error a linear behaviour is found. A least squares fit yields δ = (41±1) meV (for three-dimensional migration) and an intersection with the $1/T^2$-axis at t_0 = (70±20) ns.

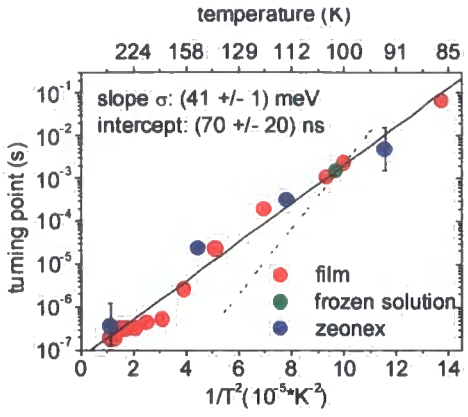

Figure 4-11 The turning point of several DF2 decay curves (among others taken from Figure 4-10) as a function of the inverse squared temperature according to Equation 4-10. The true turning point is assumed to lie within one order of magnitude in time around the values found in Figure 4-10, indicated by the error bars. The dashed line corresponds to data obtained experimentally by Hertel et al.[16]

An independent measure of δ can also be gained employing a Gaussian profile analysis of the high-energy tail of the inhomogenously broadened T1 → S0 phosphorescence spectrum. To do so it would be necessary to examine the unrelaxed Ph spectrum at zero time delay because in the course of relaxation the Gaussian distribution narrows (compare Figure 4-1). Unfortunately, it is experimentally not possible to observe an instantaneous Ph spectrum as a consequence of the long radiative triplet lifetime, therefore δ cannot be measured directly.

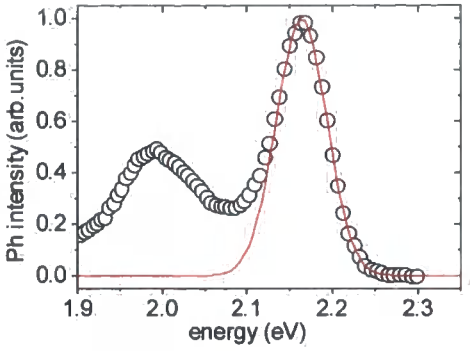

Figure 4-12 Baseline corrected 10 ms delayed Ph spectrum from Figure 4-4. Its first vibronic mode is fitted to a Gaussian curve with fwhm = 61 meV (red line).

Nevertheless, in Figure 4-12 the baseline-corrected Ph spectrum from Figure 4-4 was analysed yielding fwhm = 61 meV and δ^t = 25.9 meV, respectively. This Ph spectrum was taken at 15 K corresponding to a disorder parameter of $\hat{\delta} = \frac{\delta}{k_B T} > 20$.

Under such conditions, known as the strong disorder case, the Gaussian distribution narrows by ~ 70% of its initial value as $t \rightarrow \infty$.[34] Thus the experimentally observed distribution (after the elapse of five decades of normalized time) $\delta^t \sim 0.65\delta$ is an expected and reasonable result.

Recently, Hertel *et al.* investigated the temperature dependence of the DF turning points of a polyfluorene derivative imbedded into frozen MTHF, between 100 and 130 K.[16] These authors analysed their data according to Equation 4-10 but obtained a slope with rather different parameters, which is included for comparison as a dashed line in Figure 4-11. However, as the

glass transition temperature of MTHF is below 100 K, the solvent does not act as a true rigid matrix in this temperature regime, thus TTA is artificially accelerated. This explains the unphysically low value for t_0 obtained by Hertel *et al.*, 100 ps. For the same reasons Figure 4-11 does not contain any frozen solution data points for temperature higher than 100 K. Note, for temperatures lower than 90 K the segregation time is longer than the radiative triplet lifetime, concomitantly the turning point cannot be observed.

4.4.5. Delayed fluorescence and triplet decay in liquid solutions

Figure 4-13 shows the triplet (measured as the photo induced absorption signal) as well as the delayed fluorescence decay of a degassed toluene solution at room temperature. In order to achieve a high time resolution for the PIA experiment, the ICCD based set up has been used, i.e. this is a point wise measurement. In the whole measured

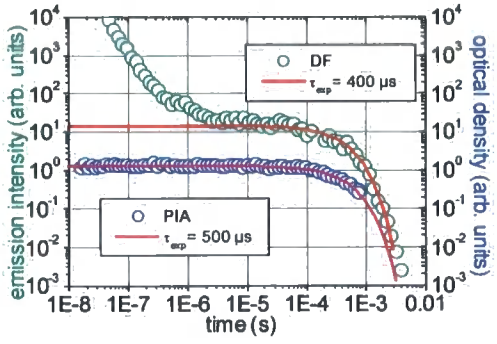

Figure 4-13 Photo induced absorption and delayed fluorescence decay of a degassed 10^{-4} wt% toluene solution. Solid lines correspond to single exponential decay.

time region the triplet decay is perfectly described by a single exponential lifetime of 500 µs. Likewise the solid state data, the decay of the delayed fluorescence initially shows a fast decaying DF1 contribution that obeys an algebraic decay law. Worth noting, this fast DF1 decay occurs in a time domain where the triplet density is nearly time independent. Again, this observation proves that the DF1 is not caused by triplet-triplet-annihilation. Subsequent to the DF1 regime (~1µs), the delayed emission turns into a mono-exponentially decaying contribution, featuring a lifetime of 400 µs. This emission has its equivalent in the DF2 emission of the solid state data and is caused by triplet-triplet-annihilation, which shall be shown by three experimental observations: First the bimolecular nature of the DF2 is confirmed by the super linear laser excitation dose dependence Figure 4-6.

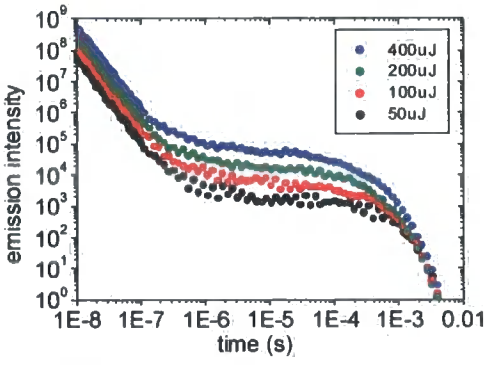

Figure 4-14 Laser excitation dose dependency (given in cm^{-2}) on the fluorescence decay of a 10^{-4} wt% MCH solution. The curves are not normalized to each other.

Unlike the latter experiment with its fixed delay times, in Figure 4-14 the full

delayed fluorescence decays were measured for four different laser doses. Consistent with the linear dependence of Figure 4-6, the DF1 contribution each times doubles for double the excitation dose. For the same changes in laser dose the DF2 contribution increases nearly by a factor of four, i.e. super linearly. Apparently, the exponential decay of the DF2 does not depend on the excitation dose. From this, one concludes that the bimolecular annihilation is not rate limiting for the triplet decay, which must have another origin.

Secondly, Figure 4-13 shows that both triplet and DF2 decay are closely linked to each other, as here the delayed fluorescence signal drops immediately once the triplet density decays. Finally, oxygen strongly quenches the DF2 component, which is shown by Figure 4-15 below. This is expected if triplets cause the observed DF2 emission.

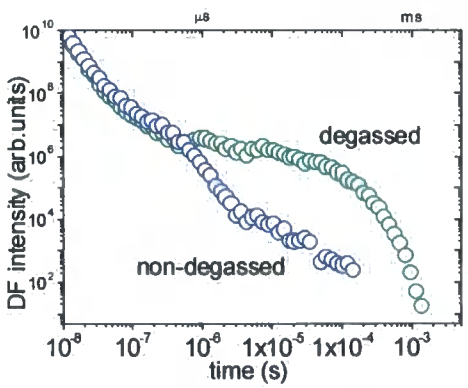

Figure 4-15 The effect of oxygen on the DF2 decay kinetics of a 10^{-3} wt% toluene solution at 300 K. The curves are not normalized.

Therefore, liquid solution is the only exception where the typical algebraic decay pattern of the DF2 kinetics is not observed at all. This is not astonishing considering the rather different situation in liquid solution, where the triplet resides on truly isolated polymer chains, as compared to the three dimensional migration in solid state. The exponential triplet decay kinetics of Figure 4-13 show that the mono molecular term of Equation 4-1 dominates the decay. On the other hand the observed lifetime is much shorter than the radiative triplet lifetime, ~1s. Therefore, the triplet decay is caused by a mono molecular quenching process.

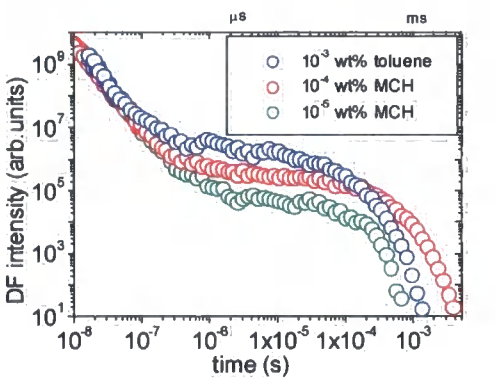

Figure 4-16 Fluorescence decay kinetics at 300 K of three degassed solutions containing different polymer concentrations. The laser pulse power was fixed to 100 µJ/cm². The emissions are scaled to the DF1 signal thereby accounting for the reduced absorption at lower polymer concentrations.

Regarding the solid state, three dimensional triplet diffusion was found to be rate limiting for the delayed fluorescence. But what is rate-limiting for the relatively small DF2 emission observed in liquid solutions? There are two potentially rate limiting mechanisms that need to be considered: either intrachain triplet annihilation or the

diffusion of the host polymer chain. Both cases can be distinguished by measuring the delayed emission strength as a function of polymer concentration.

In Figure 4-16 the room temperature DF decay is shown for liquid solutions at three different polymer concentrations *c*. These curves are scaled to the DF1 emission, which, according to Figure 4-6 and Figure 4-14, has mono molecular origin. Thus, the applied normalization in Figure 4-16 basically accounts for the increasing absorption of the solutions with increasing concentration. It is found that with increasing concentration more DF2 is emitted relative to the (de facto normalized) absorption. i.e. a super linear increase of the DF2 emission contribution. Expressed in absolute numbers the DF2 intensity relative to the laser absorption is reduced by a factor of six for a tenfold dilution of the polymer, thus DF2 ~ $c^{1.8}$. A linear concentration dependence is expected if the DF2 is caused by intrachain triplet-triplet-annihilation. The observed super linear dependence of the DF2 on polymer concentration clearly points to an interchain origin of the delayed fluorescence. The triplet annihilation in solution is then governed by the diffusion of the host polymer chain. However, the actual triplet annihilation has only a minor influence on the triplet density and is not rate limiting for the triplet decay. This means there is a faster quenching mechanism for the triplet excitons compared to the polymer chain diffusion. If one considers the PF2/6am4 polymer chains to be a semi rigid coil in solution, from light scattering data[35] one can calculate the collisional transfer rate of polymer chains (carrying the triplets) in solution using the Einstein-Smoluchowski relationship.[36] For two polymer chains at 1.5 10^{14}/cm^3 this encounter rate is ~ 2 s^{-1} (this corresponds to γ_{TT} of Equation 4-1), which is far slower than the observed ~ 2 10^3 s^{-1} (k_n of Equation 4-1) triplet decay. Again this confirms that bimolecular annihilation is not rate limiting for the observed mono exponential triplet decay. Very likely the latter is caused by the diffusion of a dilute triplet quencher, which together with the solvent encounters the polymer chain (the triplets) with a rate of ~2 10^3 s^{-1}. In this context oxygen is not the quencher, as more than three freeze thaw cycles (used here) have no effect on the triplet lifetime. On the other hand, in the course of the degassing, during the melting of the solvent, a residual water contamination is always visible. This water pollution, which is present in any non-treated solvent, is a likely candidate for the triplet quenching.

4.4.6. The triplet decay of liquid as compared to frozen solution

It is now further illuminated how important interchain migration is, as common opinion only considers intrachain triplet migration in conjugated polymers. Triplet-triplet-annihilation is a short-range exchange process, which relies on the wave function overlap of the two triplets concerned.[8] Therefore, an essential precondition for the occurrence of DF2, which originates from TTA, is the existence of more than one triplet on a polymer chain. In liquid solutions this is achieved by polymer chain diffusion that occurs with a rate of ~2 s^{-1}. A similar process in frozen solution cannot occur, accordingly no delayed fluorescence (DF2) is expected. However, a strong DF2 component is actually observed upon freezing these at ambient temperature dilute solutions.

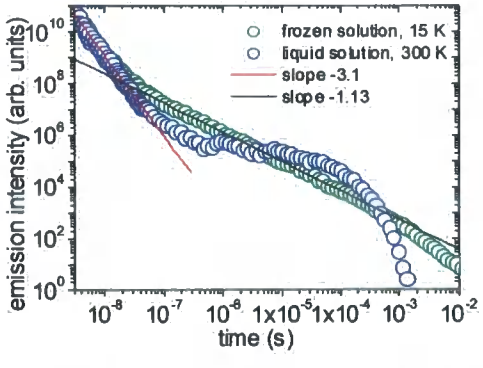

Figure 4-17 Comparison of the delayed fluorescence decays of a 10^{-4} wt% MCH/MTHF mixture, either in frozen and in liquid solution. The curves are scaled to the initial DF1 component.

This might be visualized by looking at Figure 4-17. These decays were taken using the same solution. For clarity the curves are scaled to the mono molecular DF1 component, thereby accounting for the potential small differences in excitation dose. The transition from the exponential, blue curve towards the algebraic green decay occurs smoothly at intermediate temperatures. The observed graph in frozen solutions is the typical decay pattern for the solid state. Also the triplet-triplet-annihilation needs to be of interchain nature. This was already concluded from the polymer concentration dependence in 4.4.5. An independent proof that interchain triplet migration indeed occurs comes from the average number of initially created triplets on a polymer chain. The molecular weight of the PF2/6am4 investigated, 29200 g/mol corresponds to a chain density of ≈ $1.5 \times 10^{14}/cm^3$ for the 10^{-5} by weight diluted polymer. The absorption at the laser excitation wavelength, 355 nm, of such solutions is 0.8 (for one cm path length). Therefore, the maximum laser excitation dose used for this study, 1 mJ/cm^2, as a first approximation homogeneously absorbed throughout the sample, corresponds to ~ 10 initially created singlets per chain. Employing the inter-system-crossing rate for polyfluorene in solution, 0.03,[9] on average approximately only 0.3 triplets per chain are created. Because the latter estimate is an upper limit for the initial triplet density per chain (calculated for the maximum laser

dose, typical laser dose was ten times less ~ 80 μJ/cm^2) intrachain TTA can be safely ruled out as main contribution to the observed DF2. As diffusion is also impeded, this can only mean that, unlike in room temperature solutions, in frozen solution the polymer chains form clusters or aggregates, thus the case of isolated chains *no longer* holds true. This also consistently explains why supposedly isolated polymer chains show the solid state DF2 decay pattern. So far, no temperature dependent light scattering experiments have been done but one can assume that the solubility of the polymer in any solvent is reduced upon lowering the temperature, which could in the extreme case lead to phase separation effects.

Exactly the same holds true for zeonex films, which might be considered as a frozen solution as well. Certainly, 10^{-2} by wt (1%) PF2/6am4 blended into zeonex forms clusters, which is evident from the opaque appearance and the absorption spectra of these films. Initially, the author hoped to achieve truly isolated polymer chains upon reducing the amount of PF2/6am4 in zeonex to 10^{-4} and finally 10^{-5} by wt%. However, even in these perfectly clear films TTA occurs, which on its own already shows that the polymer chains are not isolated. Thus, one has to conclude that the PF2/6am4 chains imbedded in zeonex cannot be considered as truly isolated either. With this background knowledge, it also becomes possible to discuss another experimental result, which is surprising at first glance but can easily be explained by non-isolated polymer chains. Recall the compendium of turning times, t_s, from dispersive to equilibrium triplet diffusion, as plotted in Figure 4-10. There seems to be no difference in t_s between the 10^{-4} diluted zeonex film and the 10^{-4} frozen solution on the one hand and the solid film on the other hand, although the chain number per unit volume between both systems should in principle differ by some four orders of magnitude. In accordance with intuitive reasoning, Ries *et al.* employing Monte Carlo techniques, found that halving the site concentration results in an increase of t_s by about one order of magnitude in time.[27] Thus, translated to the present situation, the difference should easily be visible even within experimental error. This is at variance to the experimentally observed unchanged turning times, which further confirms the presence of polymer chain clusters or aggregates. Thus, all frozen solution experiments probe the bulk rather than isolated polymer chains. Finally, one could also argue the other way round as was done by Hertel *et al.*:[16] Starting from the assumption that the polymer chains are truly isolated in frozen solution. In this case the unchanged turning times when comparing frozen solution and film point to an intrachain nature of the triplet migration in both

cases. This, however, is clearly disproved by the large amount of evidence for the interchain origin of the DF2 emission.

In this context, intrachain triplet migration in frozen solution as proposed by Romanovskii *et al.* should be considered with caution.[37, 38] As shown in Ref [31], true intrachain TTA is only observed by using very long polymer chains (~ 1000 repeat units) combined with extreme laser excitation doses (mJ regime). In conclusion, the preparation of a truly matrix isolated polymer chain is still a challenge.

4.4.7. Triplet energy relaxation as a function of time

In the theory of migration within an energetic site distribution another aim, beside the time dependence of the diffusivity, was to describe the energy relaxation towards the tail states of the DOS with time and temperature. In section 4.4.4, the dwell time and the Gaussian width for triplet migration in PF2/6am4 could be gained from the temperature dependent analysis of the diffusivity (derived from the annihilation rate). In the following, it shall be verified whether this set of parameters also accounts for experimentally accessible energy shifts.

In the upper half of Figure 4-18, the maximum energy of several phosphorescence spectra taken at 15 K with successively increasing delay times, obtained by fitting to a Gaussian shape, is plotted versus logarithmic time for two polymer films, which possess different thickness.

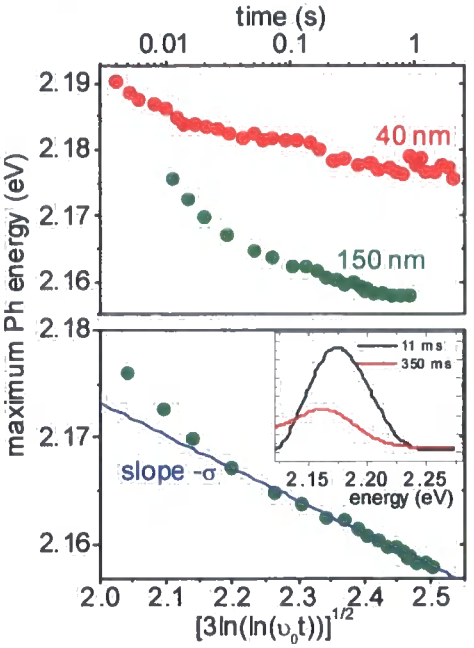

Figure 4-18 Upper half: Ph shift versus logarithmic time for two films of different thickness. Lower half: the thick film dataset replotted versus double logarithmic time according to Equation 4-9. Data points were derived from Gaussian fits to the first vibronic of 15 K Ph spectra taken with increasing delay. The inset shows two typical Ph spectra after different delay times.

The graph proves that triplet relaxation is sensitive to film thickness, which again clearly confirms the interchain nature of the triplet migration. This important fact is further validated by the absolute extent of the energy shift compared to δ, as much less energy relaxation is expected in the case of one-dimensional migration.[39, 40] At 15 K the case of strong disorder, defined by $\hat{\delta} > 10$ (for PF2/6am4 fulfilled for T < 48 K), applies, therefore only dispersive triplet migration occurs and the energy relaxation should be

described by the analytical $T \rightarrow 0$ treatment of Movaghar *et al.*, Ref [24] compare 4.2. In the lower half of Figure 4-18, the centre energies of the T1→S0 transition of the thicker film have been replotted according to Equation 4-9. Consistent with the theory,[23, 26] the energy relaxation is faster in the initial time regime (in fact most of the relaxation is expected to happen between 7 and 700 ns, i.e. $0.1 - 10t_0$) and turns into an asymptotic linear behaviour for long times described by Equation 4-9. The exact version of the latter equation (please refer to Ref. [23, 27]) also contains a site concentration dependence, which explains the thickness dependence of the energy relaxation of the polymer films studied. In connection with Equation 4-9, it has been shown that different site concentrations can be accounted for by a linear scaling of the attempt-to-jump frequency v_0 to an effective time scaling factor that includes the site concentration.[27] This situation was already illustrated in Figure 4-1, where the diffusion rate is determined by the green area under the DOS, which is proportional to the height of DOS and thus scales with the site density. According to this approach, v_0 was varied until the slope of Figure 4-18 yielded $-\delta$. The interception of this linear fit with the energy axis yields the non-relaxed triplet energy $\varepsilon_T = (2.26 \pm 0.01)\,\mathrm{eV}$, which is of course slightly higher than the T1→S0 band shown in Figure 4-12. Consistently, the same value is obtained for the thin film data set but, of course, using another v_0. This triplet energy is in excellent agreement with the value found for polyfluorene in pulsed radiolysis triplet energy transfer experiments, 2.3±0.1 eV[41] bearing in mind that the latter result was obtained using a solution at room temperature, thus bathochromic shifts can be expected. In conclusion, solid state phosphorescence spectra do not show the actual triplet energy as they are typically shifted to the red spectral region by ~100 meV.

4.4.8. Triplet energy relaxation as a function of temperature

In contrast to the strong disorder case, where the diffusivity never approaches an equilibrium value, for intermediate disorder the average triplet energy settles δ^2/k_BT below the centre of the DOS after equilibrium has been reached, i.e. for $t > t_s$, compare Equation 4-12. Therefore plotting the T1→S0 maxima versus inverse temperature should in principle provide an easy and independent possibility to determine δ. Unfortunately, in the present situation the onset of equilibrium diffusion is accompanied by efficient TTA causing rapid triplet decay. Consequently, in analogy to the initial Ph spectra but for different reasons, the observation of relaxed Ph spectra is prevented as well. Such a

spectrum would correspond to case (c) of Figure 4-1.

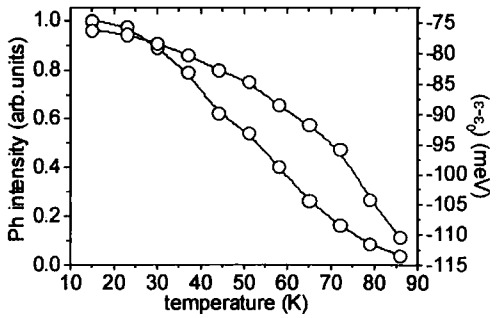

Figure 4-19 Ph intensity (blue) and absolute (including the shift that already occurs during the delay time) energy shift (green) as a function of temperature. Data points were derived from Gaussian fits to the first Ph mode of 10 ms delayed Ph spectra.

Nevertheless, in Figure 4-19, the centre energies $\varepsilon(T)$ obtained from the experimentally accessible Ph spectra are plotted versus temperature together with the declining Ph intensity (fixed delay 10 ms). In the equilibrium time domain $\varepsilon(T)$ should decrease proportional to $1/T$. This criterion is obviously not met as $\varepsilon(T)$ decreases monotonically upon raising the temperature, which confirms the non-equilibrium nature in the whole temperature region covered for times up to at least 10 ms, the delay time used to take the Ph spectra. For 10 ms delay, from Figure 4-11 one would expect to approach equilibrium at ~ 93 K. The mean energy of the relaxed DOS should then be shifted by $-\delta^2/k_BT$ ~ 210 meV relative to ε_T. Please note, choosing a shorter delay time would still not enable the observation of the energetically relaxed Ph spectra, but only shift the onset of equilibrium to higher temperatures and vice versa. As soon as equilibrium diffusion has been achieved then the phosphorescence spectrum cannot be observed anymore.

4.5. Conclusions

In this chapter, time-resolved delayed fluorescence and photo-induced triplet absorption of a prototypical conjugated polymer have been investigated in detail. The results are consistent with predictions of theories relying on incoherent hopping in an energetic Gaussian-like distribution of localized states exhibiting a variance of 41 meV and a hopping time of 80 ns, which includes the site density. This simple set of parameters fully determines the triplet migration as well as the triplet energy relaxation as a function of time and temperature for solid state polyfluorene films.

The triplet migration evolves in two time regimes initially characterized by dispersive and subsequently by non-dispersive diffusion. In the bulk in both time regimes, triplet-triplet-annihilation is observed, which decays proportionally to t^{-1} and t^{-2}, respectively. Bimolecular triplet annihilation only becomes a major decay mechanism for triplets in the non-dispersive regime. It follows that only sufficiently low temperature enables the observation of phosphorescence, because here migration is exclusively dispersive and no other major triplet decay mechanism apart from the radiative one is active.

Therefore, all observed phosphorescence spectra belong to the dispersive time regime. These spectra neither match the triplet DOS nor can they ever stem from thermally relaxed triplet excitons. The actual centre of the triplet DOS (the triplet energy) is blue shifted by approximately 100 meV as compared to the centre energy of the actually observed phosphorescence band.

For dilute solutions, triplet annihilation is limited by the polymer chain diffusion and again bimolecular annihilation is not important for the triplet decay. Instead, rate limiting is the diffusion of a dilute quencher, probably water.

In the framework of this study, clear evidence is found supporting the interchain nature of triplet migration. In this context it was also shown that so-called matrix isolated polymer chains, either using frozen solutions or inert matrix polymers, actually form aggregates and in such are not isolated.

5. Triplet excitons in devices

5.1. Introduction

From both a theoretical and application-oriented point of view the formation ratio of singlet to triplet excitons during charge recombination is one of the most important issues regarding the electro luminescence of conjugated polymers. From simple quantum statistical arguments one predicts that for every fluorescent singlet another three non-emitting triplets will be created, which would limit the maximal achievable intrinsic quantum efficiency to 25 %. The importance of the question has triggered an extraordinary number of publications that claim a measure of the singlet-to-triplet generation ratio. However, already for the widely-studied archetypical conjugated polymer poly(2-methoxy, 5-(2'ethyl-hexyloxy)-*p*-phenylene vinylene) (MEH-PPV), the published data contradict each other as they cover any value between 15 and 95 % percent singlet yield. The reason why there is such a large spread within these published data is simple – they are without exception incorrect. Either they require absolute values of many quantities, which are usually difficult to determine without complicated and indirect interpretations, or they bank on wrong assumptions. The following list of experimental work on the singlet-to-triplet generation ratio is not intended to be exhaustive, but it exemplarily covers the different experimental approaches that have been tried so far. It shall briefly be discussed why a correct measure of the singlet generation yield for conjugated polymers still remains an outstanding challenge.

5.1.1. Absolute and partly relative measurements

Several studies about the singlet exciton generation ratio are based on a comparison of the absolute electro and photo luminescence yields of a particular polymer in device configuration. This was for example done by Cao *et al.*[42] and Kim *et al.*[43] for PPV derivatives. However, the measurement of absolute photo luminescence quantum yield in solid state is involved and requires a large number of corrections, thus the values should be treated with great care. Even more difficult to determine are electro luminescent quantum yields as here one is confronted with dark current, space charge layers, losses in the ohmic ITO electrode and the like. In the context of these various quenching mechanism, the electro luminescence quantum yield is generally dependent on the driving current, i.e. is not a single value as implied by the above authors. Especially, for PPV derivatives there is another problem as these polymers suffer from backbone oxidation resulting in ketone formation. In electrical excitation mode these defect sites trap electrons and act as recombination sites. Since these

defects act as non-radiative quenching mechanism more efficient for electrical as compared to photo excitation the ratio of the two quantum yields does not give a correct answer.

An interesting approach was chosen by Segal *et al.*[44]. Like Cao *et al.*, the fluorescence emission ratio between optically and electrically excited fluorescence is the measure. But instead of relating these emissions to the driving current with the help of luminescence quantum yields, the authors measured the photocurrent in reverse bias in order to normalize the emission quenching. The ratio of emission quenching to photocurrent combined with the ratio of forward current and electro luminescence then yields the singlet exciton generation ratio. Apart from uncertainties that the latter ratio might again be influenced by dark currents, capacity effects and the like, the crucial point is the assumed photocurrent yield of 100 %, as otherwise the measured emission quenching is only proportional but not identical to the measured photo current. However, this critical assumption is by far not fulfilled, as time resolved delayed collection field experiments by Hertel *et al.* imply an upper limit of the photocurrent yield at the highest applied fields of about 10 % only[45] and as such significantly lower than unity. Thus, the experiments by Segal *et al.*, although interesting, will not tell anything about the exciton branching ratio either.

Dhoot *et al.*[46] tried to determine the singlet-to-triplet exciton generation ratio in an electrically excited MEHPPV device at 20 K straight away by comparing the absolute emission quantum yield with the absolute electrically induced triplet absorption strength. Considering dark currents etc., it may be questioned whether it is possible to correctly determine the emission quantum yield of any device. The main criticism concerns the determination of the triplet generation rate, where the authors applied a common lock-in technique to measure the induced triplet absorption. Extracting the triplet generation rate from this signal requires knowledge of the triplet-triplet-absorption cross section and the triplet decay kinetics. Albeit applying independently obtained results for the former, for the latter the authors simply assumed mono exponential decay kinetics with a voltage dependent life time of 250 µs. However, in view of chapter 4 the triplet decay at such high excitation doses is nowhere near exponential but is dominated by bimolecular annihilation. Also the mono exponential triplet lifetime of typical conjugated polymers is about 2000 longer as compared to the above employed value.[10, 13] As a result, increasing excitation dose (increasing voltage) causes enhanced

bimolecular annihilation and the 'mono exponential' lifetime appears even further reduced. Consequently the triplet generation rate is drastically underestimated and a lower limit for the singlet generation of 83 % (more than four singlets per triplet), which increases even further for increasing voltages, has been obtained.

5.1.2. An example of a true relative measurement

Lin *et al.* measured the ratio of the electrically and optically induced triplet absorption under identical fluorescence emission.[47] Upon applying the singlet lifetime and the inter-system-crossing rate, the singlet exciton generation ratio is found. An implicit condition for this approach to work is that the ratio between the differently excited triplet excitons needs to be preserved (during a measure run). This in turn implies that only mono molecular processes (generation, radiative decay, quenching) may (of course equally) influence the two triplet densities. But this is in fact not the case. The triplet was probed at room temperature with a quasi steady state lock-in technique. The assumption of Lin *et al.* that the room temperature triplet decay is mono exponential with a lifetime of only 100 µs is in best case naïve[48] and contradicts the findings of chapter 4. Thus, the necessarily fixed rate of electrically and optically excited triplet excitons does not hold true. As a result, at higher excitation doses (higher applied voltages) the authors observe an increase of the singlet-to-triplet generation rate, but this reflects nothing else but the increased bimolecular triplet annihilation activity that reduces the triplet relative to the singlet density. In conclusion this approach in principle would work but at present has generated arbitrary values, because bimolecular triplet annihilation has not been accounted for.

Besides, the above cited work, which up to now has been the only one of its kind, is additionally subject to a fundamental mistake as most likely a combination of triplet and polaron induced absorption has been probed at room temperature rather then a pure triplet induced absorption signal.[48, 49]

5.1.3. Phosphorescent and fluorescent dopants

Exemplary experiments are performed by Baldo *et al.*[50] Here the investigated polymer in device configuration is doped with a singlet and a triplet acceptor. After recombination on the host polymer, both singlet and triplet excitons are assumed to transfer selectively and completely to their corresponding guest molecule, i.e. the transfer rate approaches unity. Upon applying the emission quantum yields of the two dopants, the exciton generation ratio can be easily worked out.

Weak points are the assumed 100 % transfer rates to the dopants, which implies the absence of any singlet or triplet quenching during or prior to their transfer. Further, the emission quantum yields of the guest molecules are usually measured in dilute solutions and might change within the polymeric environment, especially on account of the frequently observed cluster formation of such dopants. However, the most serious objection concerns the implicitly assumed equivalence of the exciton generation in a doped and an undoped polymer film after electrical excitation. This is clearly not the case as the phosphorescent dopants act as charge traps, therefore the recombination already takes place on the dopant sites. This fact is for example shown by the increasing capacity[51, 52] and the accompanying increasing turn-on voltages for doped devices.[50] Therefore, for polymeric systems, the approach via selective doping so far did not yield any useful data. In addition, chemical bonding of the dopant to the polymer backbone[53] does not circumvent the fundamental problem of charge trapping at dopant sites and in such is unsuitable to measure the exciton branching ratios of pristine polymers as well.

Finally, current research unveiled an even more fundamental problem, which impedes the use of any heavy metal containing materials for the determination of the singlet-to-triplet branching ratio. Recently, evidence of a remote, resonantly-enhanced heavy metal effect has been provided, which substantially increases the inter-system-crossing rate in the presence of heavy atom materials.[54] Thus, even if it is assumed that the charge carrier recombination in a phosphorescent doped material occurs on the polymer chain rather than on doping sites, the initial branching ratio is not preserved during the singlet lifetime and can neither be reconstructed from the measured relative doping emissions.

5.1.4. Spin-resonance measurements

This approach is rather different from the others as it seeks to infer the formation cross section for singlet and triplet excitons from the observation of the polaron absorption signal under magnetic resonance conditions. A more detailed analysis of these experiments is given at the end of the chapter in 5.4.10.

5.1.5. The present, truly relative measurement

The present approach is very similar to the experiments by Lin *et al.* (5.1.2) as the fluorescence to triplet induced absorption ratios are measured each for optical and electrical excitation.[47] In order to detect the induced triplet absorption commonly used lock-in techniques cannot account for bimolecular triplet annihilation, i.e. they will underestimate the triplet generation

rate. Also this technique requires the triplet life time, which is an ill-defined quantity (compare chapter 4). Thus, at variance to all previous studies, the present measurements are truly time-resolved, which enables one to either avoid or account for bimolecular triplet annihilation in a straight forward manner.

In previous studies mainly PPV derivatives have been used that are known to be susceptible to backbone oxidation that causes keto defect formation thereby preventing an accurate comparative measurement. Here hermetically sealed devices with either a polyspirobifluorene (PSF) or a polyspirobifluorene with a copolymerized hole transport moiety as active materials were investigated. Unlike many common polymers, PSF is inert against backbone oxidation, as a consequence of its doubly bonded spiro bridge. Though it was not explicitly mentioned, optical singlet exciton generation with a potential efficiency less than unity, i.e. direct charge carrier generation, is another problem with earlier measurements. In this context commonly used PPV derivatives exhibit quantum yields in dilute solutions that are considerably smaller than unity and it is unclear what the cause for this drop in efficiency is. Again polyfluorene derivatives seem to be much better suited to perform accurate measurements on the singlet generation ratio, because here the sum of the photoluminescence - plus inter-system-crossing quantum yield approaches 98 % (in dilute solutions) and in such leaves little or no room for a significant amount of photo generated charge carriers. However, in order to further reduce potential charge carrier generation, here the sample is excited right on the absorption edge at 401 nm. For a typical polyfluorene absorption spectrum refer to Figure 4-4 in chapter 4.

In typical devices as used in the above referenced works, charges are present in high concentrations as the driving current through common devices is space charge limited. This is for example confirmed by the voltage dependent induced absorption spectra as here strong polaron features are visible that even occur *before* the turn-on of the device.[47, 48] In the context of a singlet-to-triplet generation ratio experiment such a charge density is unwanted, because exciton-polaron interactions cannot be excluded. However, for polyfluorenes, but not for PPV's, it is possible to alter the current flow from space charge to injection limited by using oxygen plasma cleaned ITO electrodes.[52, 55] The capacity, i.e. the charge carrier density of such a device is significantly lower as compared to commonly fabricated devices, which is for example demonstrated by reduced turn-on voltages. For the present studies such state-of-the-art devices are used, and,

as shall be demonstrated, the results are not influenced by exciton polaron interactions.

The outcome of the present investigation is manifold. The singlet-to-triplet generation ratio seems to be consistent with the theoretically expected 1:3 limit; ratios of order 1:1 or even higher can safely be excluded. Also, the existence of a certain charge carrier recombination zone for electrical excitation is confirmed by applying a model that describes the time dependent triplet accumulation in a polymer film at continuous excitation in the framework of bimolecular triplet annihilation. Depending on the material, exponential layer thicknesses of 6 and 12 nm are obtained. Furthermore and unlike the classical treatment, the triplet-triplet annihilation in the dispersive triplet migration regime needs to be described by an annihilation constant that depends on excitation density. A quantitative value for this figure has been estimated. Finally, the interactions of the singlet and triplet excitons with an applied electric field have been studied. Here evidence for singlet exciton-polaron quenching is found. Also, triplet-triplet annihilation seems to be a source of geminate pairs, which might either recombine or, especially if a stimulating electric field is applied, fully dissociate.

5.2. Theory

5.2.1. Premises for a relative experiment

In the following an expression is derived that links the inter-system-crossing rate and the singlet-to-triplet generation rate to a set of four quantities, namely the singlet and the triplet density after both optical and electrical excitation. The novel feature is that this should be a truly relative measurement and this in a twofold sense. In such neither the optical excitation dose nor the driving current for electrical excitation need to be known. Instead only *proportional* singlet and triplet quantities need to be measured (individually for optical and electrical excitation) but these under *identical* excitation dose each. Furthermore, these two individual experiments (electrical and optical excitation) shall be relative to each other in an unknown but *fixed* proportion. In order to maintain this condition the triplet (respectively singlet) proportional quantity needs to be measured under the same experimental condition (geometry of the set-up) for both electrical and optical excitation.

The definitions of the triplet and singlet quantities, which need to be experimentally accessible, are introduced as follows:

T for the triplet exciton

S for the singlet exciton

As shall be shown in 5.2.3 these signals might for example be identified with phosphorescence and fluorescence but could also be transient absorption signals. It is further necessary to distinguish whether a signal originates from electrical or optical (photo) excitation, which is indicated by the superscripts *el* and *opt*, respectively. The following definitions for quantities shall be used in order to relate the measured quantities to the exciton generation rates:

$G^{el/opt}$, total (singlet and triplet) exciton generation rate after electric/optical excitation

χ, triplet generation ratio after electrical excitation

κ^{ISC}, inter-system-crossing ratio

ε, constant of proportionality between the triplet proportional signal (*T*) and the actual triplet density

δ, constant of proportionality between the singlet proportional signal (*S*) and the actual singlet density

Using these definitions the measured quantities are given by the following four equations:

$$T^{el} = \varepsilon G^{el}(\chi + (1-\chi)\kappa^{ISC})$$

$$T^{opt} = \varepsilon G^{opt}\kappa^{ISC}$$

$$S^{el} = \delta G^{el}(1-\kappa^{ISC})(1-\chi)$$

$$S^{opt} = \delta G^{opt}(1-\kappa^{ISC})$$

Equation 5-1

One might find it strange that (not measurable) exciton generation rates rather than laser flux or current are introduced in the above definitions. In principle one could replace, for example, G^{el} with φI where *I* denotes the current through the device and ϕ is a positive constant smaller than one that accounts for dark currents and the like. In view of Equation 5-3 this, however, would not yield any more information and thus is omitted in Equation 5-1. κ^{ISC} and χ are introduced as fractions of the normalized overall exciton generation in optical and electrical excitation mode, respectively, rather than as rates. In such a way they can take any value between zero and one. Usually inter-system-crossing rates are measured in dilute polymer solutions. Here, however, the experiments will be performed on devices, i.e. solid state samples. It does not matter in this context that the fluorescence quantum yields in solid state typically drop by a factor of three compared to solution, because the number of observed triplets *relative* to the number of emitting (note, not generated) singlets is still preserved. In this context the *emitting* singlets (the fluorescence), not the actually *generated* singlets, will be the measure. It is therefore legitimate to employ solution inter-system-crossing yields for the subsequent calculations. Finally, throughout this investigation κ^{ISC} is assumed identical for electric or optical excitation.

The constants δ, ε merely describe the proportionality between the measured signals and the exciton densities. In such a way they are insensitive to whether an exciton density was optically or electrically excited. Important for this whole relative approach to work is that there is only one δ and ε for both electrical and optical excitation, respectively. Therefore it is of great importance that the experimental set-up does not move between the joint optical and electrical probes.

In dividing the two sets of singlet and triplet probes in Equation 5-1 by each other, the above constants of proportionality are eliminated and two new ratios are obtained:

$$\frac{T^{el}}{T^{opt}} = \frac{G^{el}}{G^{opt}} \frac{(\chi + (1-\chi)\kappa^{ISC})}{\kappa^{ISC}}$$

$$\frac{S^{el}}{S^{opt}} = \frac{G^{el}}{G^{opt}}(1-\chi)$$

Equation 5-2.

Finally, these two ratios of Equation 5-2 are again divided by each other in order to obtain a true time and excitation independent constant that links the triplet generation constant with the inter-system-crossing constant.

$$\frac{T^{el}}{T^{opt}} \frac{S^{opt}}{S^{el}} = \frac{\chi + (1-\chi)\kappa^{ISC}}{(1-\chi)\kappa^{ISC}}$$

Equation 5-3

The optical and electrical generation rates cancel out in Equation 5-3 even if they would be time dependent rather than true rates (think of an RC time constant in a device, which would make G^{el} time dependent). The important premises for this approach to work are the identical excitation rates for the two different probes, the triplet (*T*) and the singlet (*S*) as well as the unchanged experiment conditions when going from an electrical to an optical detection. Of course, an implicit condition is that electrically and optically excited excitons are identical and furthermore the environment after both excitation modes is undistinguishable as well. Then the (differently) excited excitons are exposed to the same quenching mechanisms and should exhibit the same lifetime. For this relative experiment, the actual nature of potential mono molecular quenching mechanisms is of no importance as these cancel out in Equation 5-3 as long as they apply for both electrical and optical excitation mode in the same way. A phosphorescence emission quantum yield smaller than one in the case of a triplet proportionally measurement (*T*) is such a case. Similarly, it would not matter whether or not all emission events are collected, but an arbitrary time window can be chosen for the phosphorescence detection; however, it has to be the same for the two excitation modes in order to have an identical ε for electrical and optical excitation.

In principle all of the above also applies to exciton quenching sites as these act mono-molecularly and as such it should not matter, which excitation mode is

used. However, some quenching sites, namely keto defects but also metal impurities, act as charge traps and recombination centres predominantly in electrical excitation mode. For example optically as compared to electrically excited polyfluorene derivatives feature much lower keto defect emission strength.[56] Still, this would not be a problem as long as these electrically excited defect sites do not transfer into polymer triplets, as such a situation would still be similar to a dark current and thus would be included in the electric excitation, G^{el}. However, at present the deactivation channel via triplet transfer for the keto defect sites cannot at all be ruled out, especially as the polymer triplet energy is lower as compared to the energy of the defect sites. This opens an exclusive generation channel for the triplet excitons in electrical but not in optical excitation mode. Therefore for an accurate measurement any impurities in the active polymer layer need to be avoided.

5.2.2. How to account for bimolecular annihilation?

The above derivation of Equation 5-3 critically relies on the linearity between the measured singlet and triplet proportional probes (S, T), respectively, with their corresponding singlet and triplet generation rates. This in particular implies that any bimolecular processes such as triplet-triplet-annihilation or singlet-singlet-annihilation need to be avoided. However, singlet annihilation is certainly not a dominant quenching mechanism in the present experiments, because the maximal excitation doses employed here (< 30 mW/cm^2) are far too low to render this process possible. As such, any singlet probe will always fulfil the linearity criteria. As a consequence of its long lifetime it is the triplet which is the problematic exciton. Therefore one should mainly be concerned about bimolecular triplet annihilation. The latter triplet quenching mechanism reduces the triplet relative to the singlet density and as such produces unrealistically high singlet-to-triplet generation ratios. In fact this is one of the main reasons for the high singlet-to-triplet generation ratios obtained in most previous measurements.

Nevertheless, considering the inherent quadratic dependence on excitation dose, bimolecular quenching can be suppressed by using low doses. However, a measurement point at a single low dose on its own is not sufficient to discriminate linear from quadratic behaviour; instead here each triplet signal shall be measured as a function of excitation dose. Then a linear behaviour of the measured quantity versus the excitation dose indicates the absence of bimolecular processes and the slope of such a

relation corresponds to the required triplet generation rate.

In this context what would be the best way to linearly vary the excitation dose? In electrical excitation mode one could for example alter the driving voltage. However, there is no linear dependency between applied voltage and electrical excitation (current) for a device. Better suited here are measurements as a function of excitation pulse length for a fixed voltage. Provided the pulse length is much shorter than the triplet lifetime then the triplet excitons will accumulate within the device. Then a longer pulse corresponds to a higher excitation dose and this approach beyond doubt guarantees a linear relation between excitation dose and exciton generation (note, not the actual measured density!).

A potential source for the optical excitation would be the 170 ps pulsed Nd:YAG laser from chapter **4**. However, for the present experiments this laser is far too unstable. Instead a cw stabilized 401 nm laser diode module is used that features a rise time after switch-on of ~ 50 ns. Likewise for the electrical excitation, the optical excitation dose is then a linear function of the excitation pulse width after switch-on.

To summarize the above, for both optical and electrical excitation mode the experimental triplet quantities are measured as a function of pulse length after switch-on of the excitation. In doing so the time parameterises the excitation dose.

Having clarified the excitation mode, it remains to consider potential experimental ways to measure the quantities, which are proportional to the singlet and triplet exciton.

The simplest probe for the singlet exciton (*S*) is to monitor the fluorescence. The latter could be measured using a photodiode or a photomultiplier, whose output signal is directly proportional to the light flux rather than the singlet exciton density. As such one would probe the emission *rate* under a certain excitation dose. Another possibility is to accumulate the overall fluorescence of the excitation pulse, for example, by using the ICCD camera set-up described in section 3.3. Such an approach yields the *integrated* fluorescence intensity. In any case the singlet lifetime (~2 ns) is short compared to the excitation pulse. Therefore the singlets do not accumulate during the excitation pulse.

For the triplet excitons, unlike the singlet, it is difficult to employ excitation pulses that are long compared to the triplet lifetime, which is of the order of 500 ms. On this account it is impracticable to probe something proportional to the triplet generation rate. Instead of this for the triplet exciton, integrated signals are always measured. This could for example be the phosphorescence as a function of pulse width using the ICCD camera. In

such an experiment the variable excitation pulses need to be short (< 10 ms) compared to the phosphorescence lifetime that they can still be considered as pulsed. The phosphorescence might then be monitored by using any (fixed) detection window after the excitation pulse. Alternatively, the triplet exciton can be probed by its transient absorption. Here a photodiode, which responds to the infrared probe beam, monitors the integrated triplet signal in real time, compare section **3.3**.

On the whole, it would either be possible to use the time-resolved photodiode set-up or the ICCD camera in order to gain the necessary quantities. Furthermore, one could even network both set-ups as for example the triplet could be probed with the photo diode and the singlet with the ICCD camera. This, however, requires a change of the experiment without changing the optical excitation intensity. On this account it seems better to probe both singlet and triplet with a single experiment. And this all the more as the above experiments feature quite different strong and weak points: The ICCD camera set-up is able to detect luminescence signals over a large intensity range. However, each data point has to be measured individually; therefore relatively few points can be taken. In contrast, characteristical of the photodiode based set-up is the vast amount of data points as here whole curves are taken in one measurement. A disadvantage, on the other hand, is the relatively low signal-to-noise ratio.
For the present study no ICCD set-up results were included, because the quality of the data for low excitation doses was not sufficient. Furthermore, initial results suggested that even triplet densities, which are just about detectable as phosphorescence, are still subject to triplet-triplet-annihilation. Although even less sensitive compared to the ICCD camera, all results presented have been obtained with the photodiode set-up, because here the vast amount of data allows for a reliable extrapolation to zero dose, which is shown in the next section.

5.2.3. The time dependent triplet density

In order to fulfil Equation 5-3 triplet generation rates in the absence of bimolecular annihilation are necessary. However, in solid-state, even at low temperature, every observable triplet signal, including both phosphorescence and induced absorption, is subject to bimolecular quenching. Therefore, the only practical approach to gain the triplet generation rates is to extrapolate the excitation dose dependencies to zero dose, in such a way accounting for the triplet-triplet-annihilation. Translated into the present situation where time parameterizes the dose: one needs to determine the slope at time zero. In

practice one needs to fit the measured triplet signal (either phosphorescence or induced absorption) to a model, which correctly accounts for bimolecular annihilation. This section intends to clarify what the correct model should look like.

In 5.2.1 it was already stated that any triplet probe (either induced absorption or phosphorescence) is an integrated measurement. Therefore the triplet excitons linearly accumulate as a function of time during the excitation. For long excitation times triplet-triplet-annihilation as opposed to mono molecular decay will be the dominant decay mechanism, thus, the triplet density approaches a steady state value. Following chapter **4**, triplet-triplet-annihilation in conjugated polymers generally is a migration activated process. The migration itself can either be non-dispersive or dispersive. The first case results in efficient TTA and is mainly realized at higher temperature and longer delay times. The second case is achieved at low temperature and short times after excitation and is accompanied by inefficient TTA. If one is interested in high triplet accumulation densities without bimolecular annihilation the dispersive triplet migration regime has to be realized. Therefore, according to chapter 4 low temperatures ~20 K) shall be used as then the dispersive regime lasts longer in comparison with the triplet lifetime. Besides, following chapter **4** dispersive migration is anyway an essential requirement in order to measure triplet quantities in solid-state.

In the following the scenario for triplet accumulation as a function of time with bimolecular annihilation is illustrated in detail. To do so the symbols used are defined below together with the corresponding units, as this greatly simplifies the understanding of the physical meaning.

$\left[I_0^{el/opt}\right] = \frac{1}{sm^2}$; triplet generation rate

$\left[\lambda^{el/opt}\right] = \frac{1}{m}$; absorptivity

$\left[\gamma_{TT}\right] = \frac{m^3}{s}$; TTA constant

$[x] = m$; sample depth

$[t] = s$; time

$[d] = m$; thickness of the active sample layer

$[T(t)] = \frac{1}{m^2}$; triplet density per unit area as a function of time

$[T(x,t)] = \frac{1}{m^3}$; triplet density per unit area at a certain sample depth as a function of time

Likewise in chapter 4 Equation 4-2, the starting point is the rate equation for the triplet generation without the mono molecular decay term. Such a treatment is legitimate as long as the considered time span is much smaller than the mono molecular triplet lifetime

(t << 0.5 s). Any other mono molecular non-radiative quenching mechanism would only reduce I_0, which is anyway an abstract quantity within this investigation (for example neither the current through the device nor the resulting triplet density are known). Initially, and in common with all classical treatments, it is assumed that the triplet generation occurs homogeneously throughout the active layer:

$$\frac{dT(t)}{dt} = I_0 - \gamma_{TT}(T(t))^2$$

Equation 5-4

(Correctly, γ_{TT} should be considered here in terms of area, rather than volume, density annihilation constant with unit $\frac{m^2}{s}$.) Equation 5-4 yields the time dependent triplet density as:

$$T(t) = \sqrt{\frac{I_0}{\gamma_{TT}}} \tanh\left(t\sqrt{I_0\gamma_{TT}}\right)$$

Equation 5-5

However, in a more realistic scenario it is assumed that the triplet exciton generation is not homogeneous throughout the active polymer layer but mainly occurs in a thin layer with exponential density profile. The logic behind is immediately clear for optical excitation as here the penetration depth is an exponential function characterized by λ^{opt}. Thus, initially for optical excitation the triplet density is higher at the ITO surface of the device. A similar situation also holds true for electrical excitation. Here, the carrier mobility is highly unsymmetrical as all common conjugated homo-polymers, including polyfluorenes, are basically hole transporting materials. Therefore the carrier recombination is expected to take place close to the cathode where the electrons form a space charge layer. Though little is known, here the thickness profile of this potential recombination zone shall be described by an exponential function as well. Thus, the triplet generation rate is supposed to be higher in the area close to the cathode and exponentially diminishes towards the anode surface. The above arguments are of special importance as at low temperature the triplets are almost immobile, thus they cannot compensate for the initial inhomogeneous distribution by triplet migration. Then $I_0\lambda e^{-\lambda x}$ is the triplet generation at a sample depth x and Equation 5-4 needs to be modified to:

$$\frac{dT(x,t)}{dt} = I_0\lambda e^{-\lambda x} - \gamma_{TT}(T(x,t))^2$$

Equation 5-6

It is now important to note that the overall triplet-triplet annihilation is proportional to the sum of the individual layers at a certain sample depth x, rather than to the overall triplet density. However, the triplet probes (both induced absorption and phosphorescence) are proportional to the overall triplet density $T(t)$ and not sensitive to the sample depth, x. It follows that first the differential Equation

5-6 has to be solved followed by integration over all *x*. Note again, this treatment is only legitimate as long as the triplets are nearly immobile.

The solution of Equation 5-6 is identical to Equation 5-5

$$T(x,t) = \sqrt{\frac{I_0 \lambda e^{-\lambda x}}{\gamma_{TT}}} \tanh\left(t\sqrt{I_0 \lambda \gamma_{TT} e^{-\lambda x}}\right)$$

Equation 5-7

and basically describes the time dependent triplet density with bimolecular annihilation for an infinitesimally small layer of the device at a depth *x*. In contrast to this, the overall triplet density is experimentally probed, thus Equation 5-7 has to be integrated over *x*:

$$T(t) = \int_0^d T(x,t)dx$$

$$T(t) = \frac{2}{\gamma_{TT}\lambda t}\left\{\ln\cosh\left(t\sqrt{I_0 \lambda \gamma_{TT}}\right)\right.$$
$$\left. - \ln\cosh\left(t\sqrt{I_0 \lambda \gamma_{TT} e^{-\lambda d}}\right)\right\}$$

Equation 5-8

I_0 as defined in Equation 5-6 is only identical to the triplet generation rate if $d >> \lambda$, i.e. if the triplet generation area is small as compared to the sample thickness. This is nothing else but the assumption that all excitation is transferred into excitons. Then Equation 5-8 simplifies into:

$$T(t) = \frac{2}{\gamma_{TT}\lambda t}\ln\cosh\left(t\sqrt{I_0 \lambda \gamma_{TT}}\right).$$

Equation 5-9

The slope of the above equation at time zero is given as:

$$\frac{dT(t \to 0)}{dt} = I_0$$

Equation 5-10

and simply reflects the fact that at early times the triplet density follows the triplet generation rate, as here bimolecular annihilation is not yet active. In line with intuitive reasoning, the initial rate is independent of $\lambda^{el/opt}$. The second important asymptotic parameter is the triplet density under steady state conditions, which is given as:

$$T(t \to \infty) = \sqrt{\frac{4I_0}{\lambda \gamma_{TT}}}$$

Equation 5-11

In common with the classical treatment, the triplet density is proportional to the square root of the quotient of generation and annihilation rate and in addition, of course, independent of time. Unlike the classical value, for inhomogeneous triplet generation the absorptivity also occurs in the steady state value as the latter is proportional to the square root of the absorption layer thickness. For example in the case of electrical excitation a thinner recombination zone would yield a smaller steady state value for the triplet density. Again this is intuitively clear as a thin layer with high absorption coefficient leads to high triplet densities accompanied by high bimolecular annihilation efficiencies; therefore this

thin zone basically shields the incoming excitation flux from a deeper penetration into the sample.

The triplet density from Equation 5-9 depends on three variables plus time. One is independent of whether optical or electrical excitation is used (γ_{TT}), two do depend on the excitation mode (λ, I_0). For each individual experiment λ and γ_{TT} are not obtained independent of each other and it is convenient for the fitting procedure to rewrite Equation 5-9 in terms of only two abstract parameters, *a* and *c*:

$$T(t) = \frac{a}{t}\ln\cosh(ct)$$

$$c = \sqrt{I_0 \lambda \gamma_{TT}} \qquad [c] = \frac{1}{s}$$

$$a = \frac{2}{\lambda \gamma_{TT}} \qquad [a] = \frac{s}{m^2}$$

Equation 5-12

In terms of these two parameters the initial slope and the steady state value are obtained as $\frac{ac^2}{2}$ and ac, respectively.

The two graphs below are intended to illustrate the above equations. In Figure 5-1 curves according to the homogeneous (Equation 5-5) and the inhomogeneous (Equation 5-9) triplet generation model are given. All parameters are arbitrarily set to unity. Apparent from the double logarithmic inset, both curves rise with identical initial slopes (I_0 = 1). Only for this example, both curves also approach the same steady state value, because λ was set to unity. Although the asymptotic behaviour for short and long times is identical, in the intermediate region the inhomogeneous curve rises slower than the homogenous one, i.e. it takes longer to approach steady state conditions. This reflects the slower triplet generation rate for areas far away from the surface.

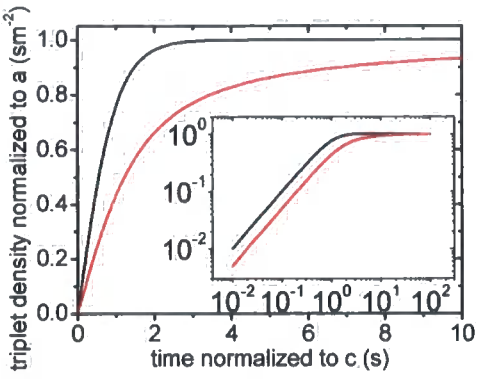

Figure 5-1 Comparison of the built in of the triplet density after homogeneous (black, Equation 5-5) and non-homogeneous triplet generation (red, Equation 5-9). Parameters are $I_0 = \lambda = \gamma_{TT} = 1$. The inset shows the same graphs in a double logarithmic presentation.

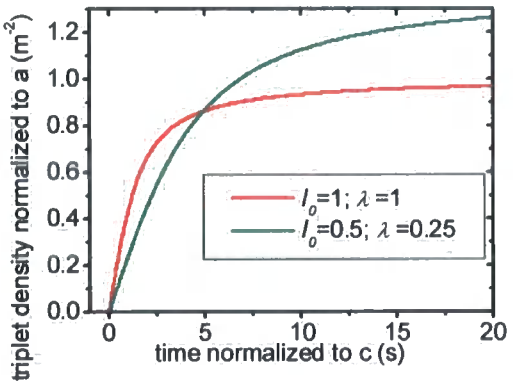

Figure 5-2 Two solutions for the in homogeneously triplet generation model (Equation 5-9) with parameters as indicated and $\gamma_{TT} = 1$.

Figure 5-2 shows two data sets according to the inhomogeneous triplet

generation model. The red curve corresponds to double the excitation rate as compared to the green curve. Hence the curve with the lower excitation dose (green) rises slower, which is consistent with Equation 5-10. Simultaneously to the higher excitation doses, for the red data set the generation layer thickness is reduced by a factor of four, i.e. λ is four times larger. For that reason the green curve, albeit rising more slowly, finally approaches a $\sqrt{2}$ higher steady state triplet density. Note, this could never happen for a homogeneous triplet generation, simply because the free parameter λ is lacking.

5.3. Experimental

5.3.1. Device fabrication

All measurements described in this chapter were made on state-of-the-art electro luminescent devices fabricated in the Philips Research Laboratories in Eindhoven. These, rather than "home-made" samples have been used because of the uniformity and quality of the individual devices, which result in a very good reproducibility of the experimental data. Another advantage of these air sealed samples is their excellent long term stability, which allows measurements to be made over months. A schematic drawing of the device structure is depicted in Figure 5-3 and a representative device is shown in Figure 5-4.

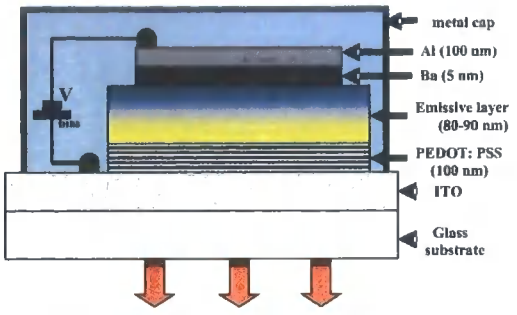

Figure 5-3 Schematic drawing of the device structure.

The PLEDs were fabricated under clean room conditions in a nitrogen atmosphere inside a glove box ($[O_2]$,$[H_2O]$ < 1 ppm) using pre-cleaned indium-tin oxide (ITO) coated glass substrates of 4.2 x 4.2 cm. The ITO was treated in a UV/O_3 photoreactor and remaining dust particles were blown away with ionised nitrogen. First a 100 nm of the hole transporting material poly-(3,4-ethylenedioxythiophene):poly-(styrenesulfonic acid) (PEDOT:PSS) was applied. These PEDOT:PSS layers were annealed at 180 °C for 2 minutes.

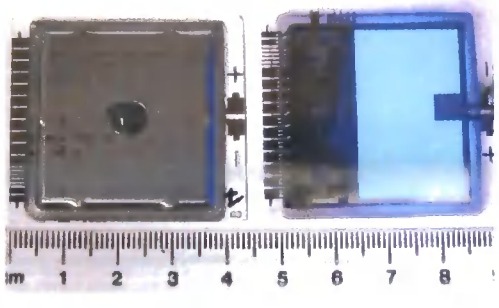

Figure 5-4 Back (left) and front side (right) of a blue emitting PSF device as used for this study. Visible are the metal seal, the electrical contacts, the presently driven large area device and the three little sub devices.

Two similar polymers were chosen as active materials: the blue emitting polyfluorene derivative

polyspirobifluorene (PSF) homopolymer and a very similar copolymer, which additionally comprises an hole transporting moiety within the polymer backbone. All chemical structures are shown in Figure 5-5. These polymers were dissolved in chlorobenzene and spin-coated on top of the PEDOT:PSS layer, resulting in $d \sim 50$ nm active layer thickness. The diode structure was completed by vacuum evaporation of the Ba/Al (5 nm Ba capped with 100 nm Al) cathode metal. Finally, the devices were sealed using a metal cap in order to prevent the oxidation of the cathode.

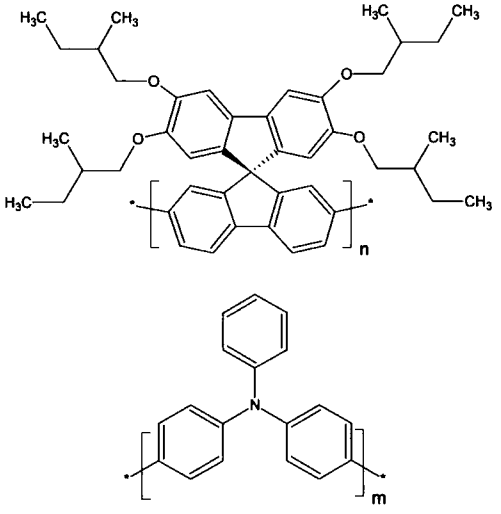

Figure 5-5 Chemical structures of the investigated polymers. Above: Repeat unit of the polyspirobifluorene homopolymer; below: the TAD type electron transport moiety that is additionally incorporated in the above polymer backbone for the copolymer.

Due to a sophisticated combination of lithographically prepatterned ITO and metal evaporation through a mask, each device contained an arrangement of nine individually accessible square diodes with 3, 1 and 0.2 mm side length as well as one large area subunit, compare Figure 5-4. For the present study the 3 x 3 mm diodes were chosen as a compromise between RC response time and sufficient emission strength.

5.3.2. Special experimental conditions

A premise in order to observe decent triplet signals is low temperature. Therefore all measurements were taken at 20 K. To do so, the devices are mounted onto a specially built sample holder that allows for electrical and optical access inside the helium cryostat, for visualization see Figure 5-6. Thermal contact between the device holder and the device was established by applying a thin layer of thermal contact paste. Furthermore, the device holder is constructed such that it masks the non active parts of the sample. This ensures that the excited areas for electrical and optical excitation are congruent. In electrical mode only the active area is excited anyway. For the optical mode the laser beam was expanded to about one square centimeter with the active electrical area of the device (3 mm in diameter) in the center. Since the other parts of the sample are masked by the device holder, only the electrically active area was excited applying a homogeneous excitation flux, compare Figure 3-9 and Figure 5-6.

As shown in Figure 3-9, in order to probe the transient triplet absorption a

780 nm laser diode module is employed, whose energy for both here investigated materials nearly coincides with the maximum of the corresponding transient triplet absorption spectra.[31] Finally, a triplet and a singlet probe are needed under identical excitation conditions. While this is no problem for electrical excitation, for optical excitation it implies that the laser relative to the sample should not move throughout the whole experiment in order to ensure a constant optical excitation flux.

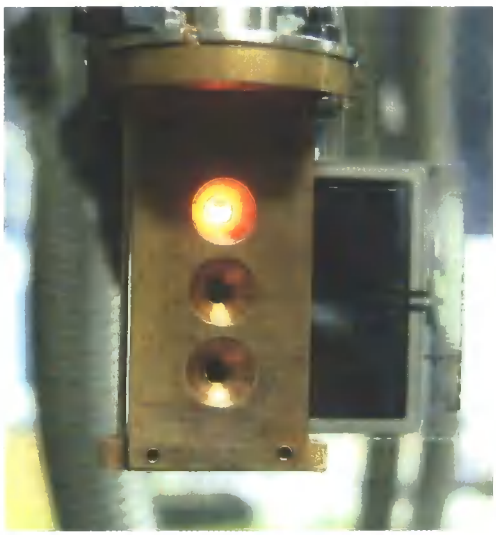

Figure 5-6 Sample holder of the helium cryostat loaded with an orange emitting device.

If not stated otherwise, all experiments in section 5.4 were carried out with a repetition frequency of 0.2 Hz in order to avoid the build up of long lived excitations such as triplets, at the beginning of a new measure cycle. The maximum optical excitation power (uncorrected for loss mechanism) was 48 mW/cm^2. As it is of no importance for the present study, no endeavor has been made to measure the driving current though the device at low temperature.

5.4. Results

5.4.1. Electrical versus optical excitation

An implicit assumption for the approach outlined in 5.2.1 is the equivalence of optically and electrically excited excitons. However, identical excitons alone (a widely accepted assumption) are still not sufficient for this experiment. One mainly needs to ensure that the experimental environment does not change for the different excitation modes. Sample heating as a consequence of the driving current in electrical excitation mode is such a case as this would imply a generally higher surrounding temperature for the electrically compared to the optically excited excitons. Another selective quenching mechanism is exciton polaron quenching, which would mainly occur in electrical excitation mode. In this context, Sinha *et al.* observed a quenching of the electrically excited delayed luminescence in polyfluorene devices with increasing reverse bias voltage, which was explained by triplet exciton-polaron quenching.[11] However, unlike in the present study, the devices in the above work were fabricated without oxygen plasma treatment of the ITO electrodes. For the present experiment such a cleaning is critical,

because treated devices exhibit significantly lower polaron density during operation.[55] Thus, by employing state-of-the-art devices the triplet lifetime (and in such the triplet density) is much less influenced by charge carrier interactions when compared to the above experiments by Sinha and co-authors.

Another example for a selective triplet excitation pathway, which was already mentioned in 5.2.1, are keto-defect sites.[56] These defects are weakly emissive with a luminescence lifetime of ~6 ns. Therefore their presence or absence can easily be verified by employing nanosecond time-resolved spectroscopy, compare section **6.3.7**. However, both spirobifluorene derivatives used for this study do not exhibit any such yellow emission. This is also consistent with the general assumption that oxygen is unable to oxidize the double bonded spiro-bridge of the spiro-fluorene repeat unit into fluorenone.[57]

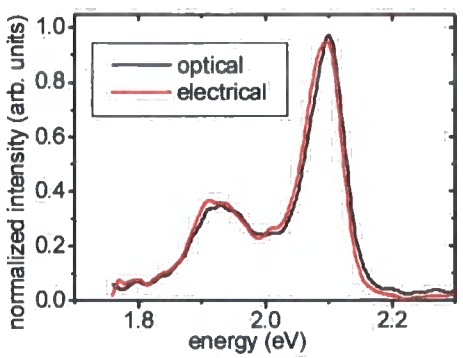

Figure 5-7 Comparison of 10 ms delayed and normalized homopolymer phosphorescence spectra after optical (pulse width 1µs) and electrical (5 V, 20 µs) excitation.

To gain confidence in the equivalence of the two excitation modes the emission spectra of both excitons as well as the phosphorescence lifetimes have been measured using the ICCD camera time-resolved luminescence set-up. Representative results for the homopolymer triplet exciton are shown Figure 5-7 and Figure 5-8.

Here the phosphorescence spectra as well as the corresponding decays are measured under identical conditions apart from the excitation mode. Although the electrical spectrum is slightly (5 meV) red shifted as compared to the optical one, the spectral shapes are identical.

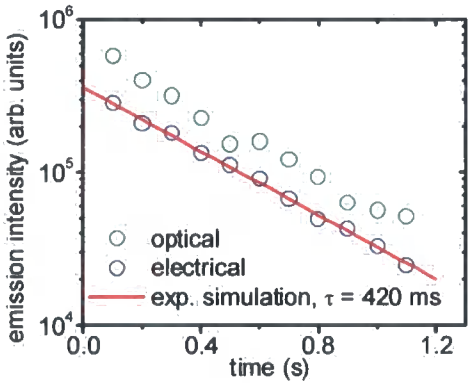

Figure 5-8 Semi logarithmical presentation of the time-dependent decay of the homopolymer Ph signals. Settings as in Figure 5-7.

Similarly, the radiative triplet lifetime is independent of the excitation mode. This reassuring observation confirms the above assumption that exciton-polaron quenching (if present at all) has no significant influence on the triplet exciton lifetime and as such on the triplet exciton density. Furthermore, there is no prominent sample heating in

electrical excitation mode as this again would cause a higher triplet mobility accompanied by an accelerated quenching. Although identical for both excitation modes, the obtained lifetimes are shorter than measured in plain photo excited thin films of the same material, 420 ms as opposed to 1 s. This discrepancy might be caused by the metal surfaces. All the above findings are nearly identically recovered for the copolymer triplet exciton.

Regarding the singlet exciton, similar to Figure 5-7 the fluorescence spectra of both materials do not change upon exciting either optically or electrically. A comparison of the singlet exciton lifetime for both excitation modes, likewise in Figure 5-8, is impossible, because here one can only measure the mutual effects of the exciton lifetime and the by far slower charge carrier drift through the device.

A straight forward way to test whether or not polarons quench some of the electrically excited singlet excitons is to measure the emission intensity under optical, electrical, and simultaneous optical and electrical excitation. If there is singlet polaron quenching then a certain amount of the optical excited singlet excitons should be quenched once the electrical excitation is switched on due to the then present polarons. In other words, the sum of the individual optical and electrical signal intensities would not be identical to the simultaneously excited intensity. The results of a corresponding experiment are shown in Figure 5-9. Here, the device is, in two milliseconds steps, first optically, then simultaneously, and finally electrically excited. The emission intensities add up perfectly, which means there is no significant singlet polaron quenching.

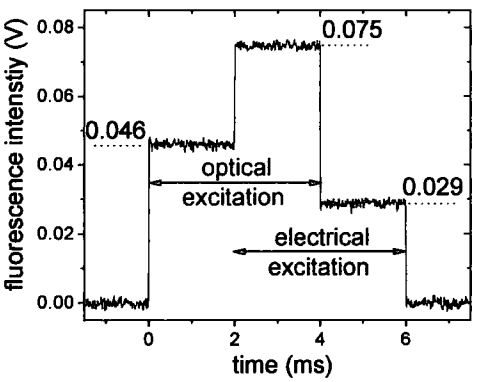

Figure 5-9 Time dependent emission intensity for a 4 ms optical and a 4 ms electrical excitation pulse. The electrical pulse is 2 ms delayed with respect to the optical one.

Thus, one concludes that the assumption of identical excitons for both excitation modes is justified.

5.4.2. Qualitative results

The aim of this section is to show the nature of the original data but also to demonstrate some qualitative results. Chosen for representative presentation are four electrical datasets that cover a large range of excitation doses, and for comparison one optical dataset, all obtained with the homopolymer. The original curves consisted of 50000 points and were generally smoothed using 500 surrounding points. In order to keep the graphics a reasonable size, only 100 points per data set are shown.

Furthermore, induced absorption signals are normalized for the transmission, i.e. are given as $-\frac{\Delta T}{T}$, which for a small ΔT corresponds to the optical density.

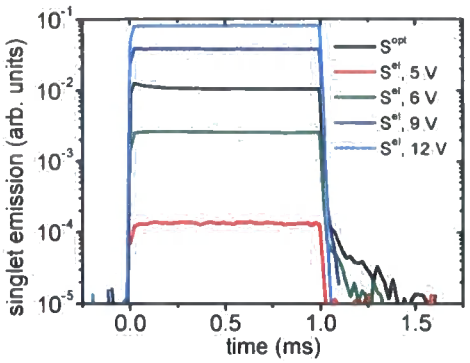

Figure 5-10 Semi logarithmical presentation of the fluorescence (S) versus excitation pulse length after optical and several electrical excitations under identical conditions for one millisecond pulse length.

In Figure 5-10 the fluorescence (*S*) signals after optical or electrical excitation for one millisecond are shown. These datasets are proportional to the singlet- as well as overall exciton generation rate for the different excitation modes. Furthermore, optical and electrical fluorescence intensities follow an absolute relation. For electrical excitation, in this time domain the singlet generation is time independent, which confirms a constant current through the device, which translates into a time independent exciton (both singlet and triplet) generation rate. In Figure 5-11 only the first ten microseconds of Figure 5-10 are shown. Unlike the optical signal, which rises instantaneously, the electrical signals now do reveal a rise time of the singlet generation rate that actually depends on the applied voltage. This behavior is caused by the RC time constant of the device. Note, even in this time domain the observed curves are still proportional to the exciton generation rates. But of course, relative triplet to singlet measurements in this initial time domain cannot rely on the constant singlet value of Figure 5-10 but instead one needs to employ the whole time dependence as observed.

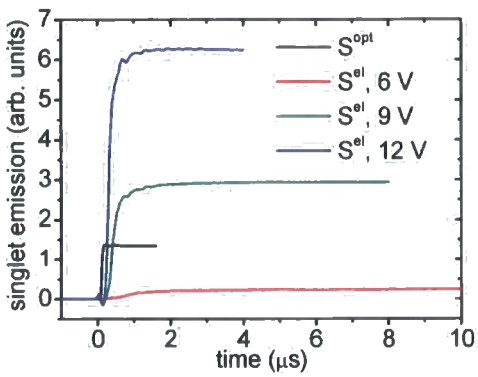

Figure 5-11 Linear presentation of the initial time domain from Figure 5-10. In this time period the 5V signal is too weak and has been excluded.

Corresponding to these singlet probes, Figure 5-12 and Figure 5-13 illustrate the interesting time dependencies of the induced triplet absorption signals (*T*). Here a linear rise is expected at early times due to triplet accumulation with fixed rate that later turns into a saturation regime caused by TTA. Such a behavior is indeed observed for the optical excitation as here the signals rises linearly in the microsecond time domain (compare black curve Figure 5-13) and subsequently saturates at around one millisecond (black curve in

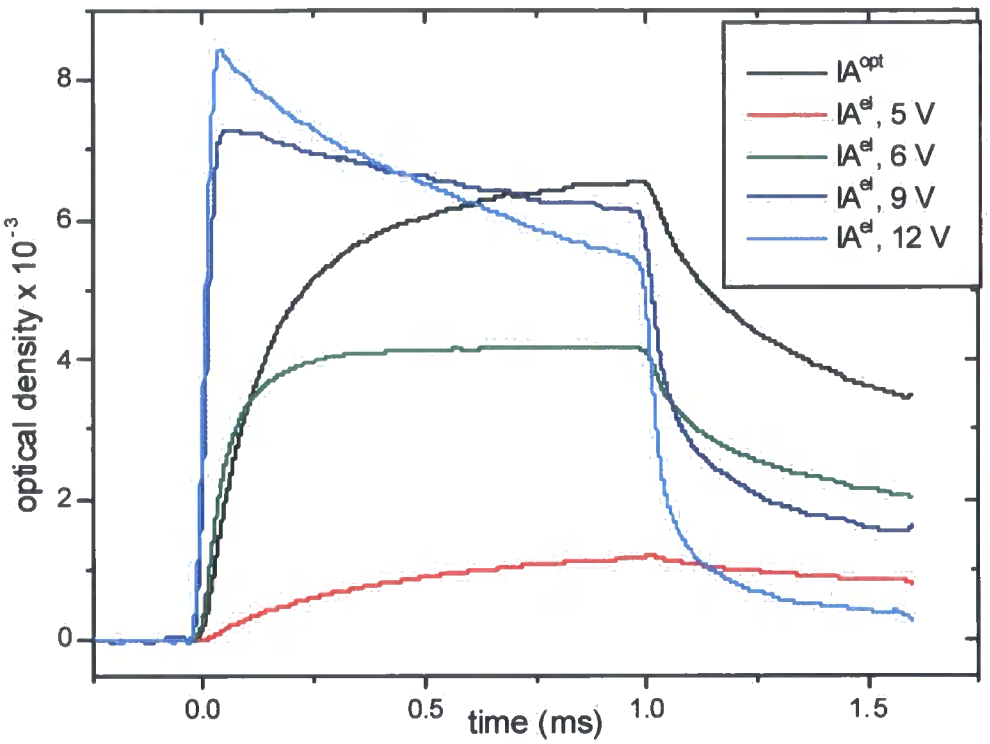

Figure 5-12 Compendium of induced absorption signals (IA) with conditions as in Figure 5-10.

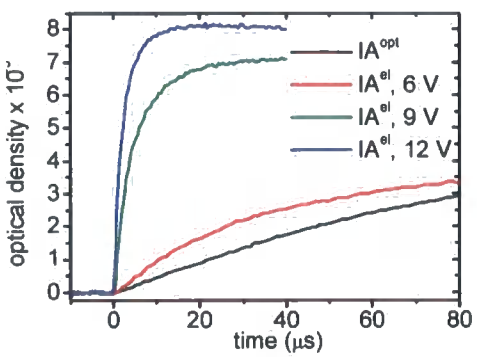

Figure 5-13 Early time period of Figure 5-12.

Figure 5-12). Qualitatively similar *T* patterns are observed after electrical excitation with 5 and 6 V. For all curves, the bimolecular annihilation still persists after the turn off of the excitation as it causes a drop off. The overall magnitude of this decay will depend on how far the bimolecular annihilation is already dominating. Therefore, if the excitation is switched off already during the linear accumulation regime then no drop of the signal should occur. Consistently, the curve with the lowest triplet generation (5 V) decays slower than the other curves. Apparently, the curves for higher electrical excitation (9 and 12 V) do not fit the pattern of a linear rise that turns into a plateau. Here, after a rapid rise of the *T* signal a plateau is approached but subsequently the signals decrease again, the higher excitation faster than the lower one. These decreases are very likely caused by the heating of the sample in consequence of the current flow. In such a situation triplet migration is no longer dispersive, which causes efficient triplet quenching by bimolecular annihilation. In terms of the

picture established in chapter 4, this would correspond to a thermally induced change from dispersive to non-dispersive triplet migration that is accompanied by a reduced average triplet lifetime. Directly after switching off the excitation the device is still warm. This explains why, the triplet level corresponding to 12 V even falls below the 5 V curve, albeit the latter possesses a significantly lower triplet generation rate.

The following discussion requires the triplet exciton generation rate relative to that of the singlet generation. As seen from Figure 5-11 the electrical singlet rates are in principle time dependent. However, this time dependence only affects an early time domain where the T signals can anyway not be observed due to a lack of sensitivity. Therefore, for the calculations, only the time independent rates as observed in Figure 5-10 are used.

The measure in Figure 5-12 and Figure 5-13 is proportional to the triplet accumulation within the active polymer layer, which in 5.2.3 has been discussed in terms of homogeneous and inhomogeneous exciton generation. Hereby, already a qualitative discussion of the experimental curves helps to choose the right model. To do so, attention is focused to a very interesting observation from Figure 5-12, the relative behavior of the optical (black) and the 6 V electrical (green) curves. Evidently from the initial time domain (see also Figure 5-13) the electrical excitation causes a higher triplet generation as compared to the optical one, i.e. in terms of section 5.2.3 $I_0^{el} > I_0^{opt}$. Following the classical bimolecular annihilation model (Equation 5-5) this fact directly implies that also the steady state value for electrical excitation should exceed that of the optical one. This is not the case as the 6 V electric signal levels off at a clearly lower value as compared to the optical excitation. Thus, the experimental situation is similar to Figure 5-2. This is, although qualitative, unambiguous proof that the homogeneous triplet distribution model cannot account for the bimolecular annihilation for these immobilized triplets. Instead one has to account for the inhomogeneous excitation, which is preserved due to the immobility of the triplets at these low temperatures. In the present situation from Equation 5-11 one concludes that the optical absorption layer is larger than the triplet generation layer after electrical excitation.

5.4.3. The modeling of the transient triplet absorption curves

As outlined in section 5.2.3, two different models might potentially describe the triplet accumulation limited by bimolecular annihilation in these devices. One emanates from spatially homogeneous excitation (Equation

5-5), the other from an inhomogeneous triplet generation with exponential profile (Equation 5-9). As both models predict rather different curves under identical excitation conditions (compare Figure 5-1), at most one will be suitable to fit the experimental data correctly and hence yield the accurate slope at time zero.

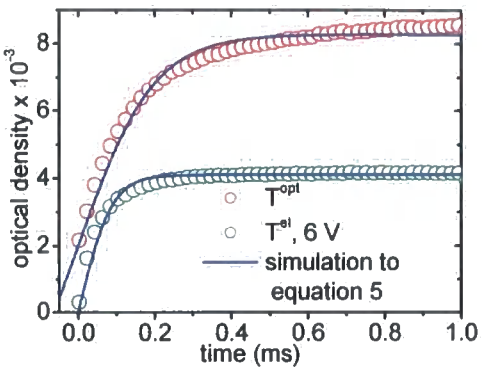

Figure 5-14 Optical and 6 V electrical T datasets fitted to the homogeneous triplet generation model according to Equation 5-5. For clarity the T^{opt} curve is offset by 0.002.

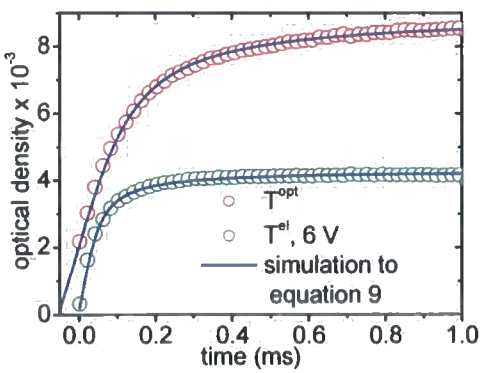

Figure 5-15 The same data sets as in Figure 5-14 this time fitted to the inhomogeneous triplet generation model, Equation 5-9.

From a qualitative comparison of the 6 V electrical with the optical curve in 5.4.2 it was already concluded that the homogeneous exciton generation model cannot describe the observed curves. Indeed, simulations according to Equation 5-5 for any of the *T* datasets only yield an unsatisfactory agreement, as the experimentally observed curves generally rise slower than predicted by the model. This is illustrated in Figure 5-14 for the two above datasets that cover optical and electrical excitation.

In contrast in Figure 5-15 the datasets of Figure 5-14 are again fitted, this time using the inhomogeneous excitation model according to Equation 5-9. Here, with the same number of free parameters as in the simulations of Figure 5-14 – only two, the agreement of the simulations with the experimental data is truly excellent.

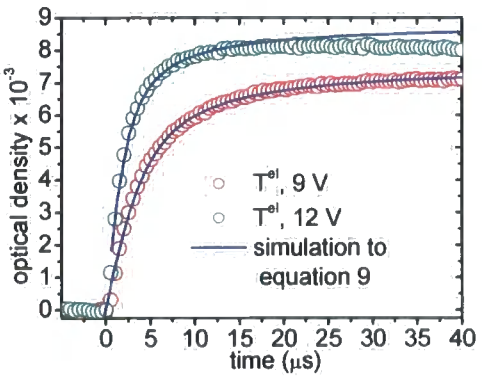

Figure 5-16 T^{el} curves for 9 and 12 V with simulations according to the inhomogeneous triplet generation model. Sample heating causes the failure of the model curve for the green dataset.

In Figure 5-16 the initial time period, before sample heating disturbs the measurements, of the T^{el} curves for 9 and 12 V electrical excitation from Figure 5-12 are fitted to the inhomogeneous model. Again very good agreement with the experimental curves is obtained. The above results

confirm that for an accurate description of the triplet accumulation at low temperature the initial inhomogeneity of the triplet generation has to be accounted for. However, much more important is that new information about the recombination zone for electrical excitation can be gained, as the layer thickness explicitly appears in the simulation model. This will be discussed in more detail in section 5.4.6.

5.4.4. The singlet-to-triplet yield

Following Equation 5-3 the relative singlet and triplet generation rates after optical and electrical excitation are required for the calculation of the singlet-to-triplet ratio, χ. According to Equation 5-12 from the two fitting parameters of the inhomogeneous exciton generation model, *a* and *c*, the triplet generation rates are simply obtained as $\frac{1}{2}ac^2$. Note, for the following the value of the layer thickness λ or even the existence of a inhomogeneous recombination zone as discussed in 5.2.3 is of no importance, because here only the initial slope l_0, which is independent of λ, is needed. The steady state fluorescence values, similar to those shown in Figure 5-8, are applied as the relative singlet generation rates.

In principle it would be sufficient to calculate χ from a single optical and electrical excitation experiment. However, it is scientifically more solid to redo the calculations for a whole range of different excitation doses, i.e. different driving voltages and optical powers, in order to obtain a more precise average value but also to either observe or rule out any dependency of χ on the excitation dose. In this context, the left hand side of Equation 5-3 can also be considered as the quotient of two ratios: one is the triplet relative to the singlet probe for *any* electrical excitation power; the other is the triplet relative to the singlet probe for *any* optical excitation power. Instead of recalculating χ for different point-wise excitation doses, it appears convenient to employ the slopes of the triplet versus the singlet rates and in such average over a large range of excitation doses. Note, higher singlet rates imply higher excitation doses, thus a dependency of the triplet versus the singlet also automatically employs a whole range of excitation doses.

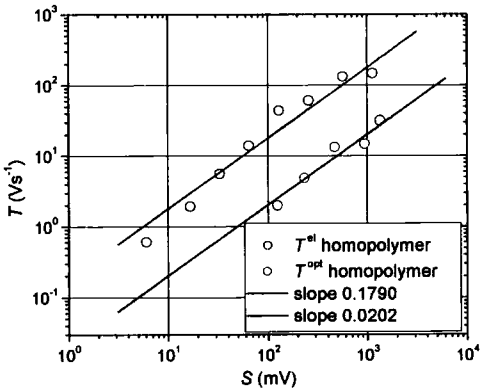

Figure 5-17 Dependency of the triplet induced absorption (T) on the fluorescence (S) for electrical and optical excitation for the homopolymer on a double logarithmical-scale.

In practice using the oscilloscope in real time rather than averaging mode, first datasets for the lowest but still detectable triplet induced absorption signals (T) as well as the corresponding fluorescence levels (S) were independently recorded for both excitation modes. By adjusting the driving voltage for electrical or the optical power for photo excitation, the singlet levels (i.e. the excitation doses) were then repeatedly approximately doubled in order to obtain an equally spaced graph on a logarithmical scale.

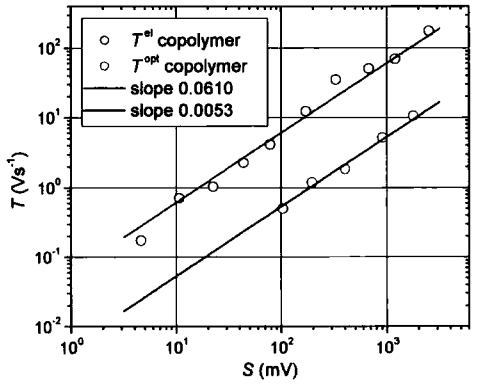

Figure 5-18 The same as Figure 5-17 for the copolymer.

The outcome of this procedure for the homo- and the copolymer is shown in Figure 5-17 and Figure 5-18, respectively. The fluorescence levels are given in mV, because this is the original measure of the oscilloscope. For the triplet signal the slope at time zero has units of volt per seconds, i.e. volt is the original measure. Considering the homopolymer the data points cover the region from 5.5 to 7.9 V and 3 to 30 mW/cm^2, for electrical and optical excitation respectively. Similarly, the copolymer datasets were measured between 4.6 to 7.5 V and 1.5 to 30 mW/cm^2. In both these driving voltage regions the datasets are not influenced by sample heating as observed at higher voltages, compare Figure 5-12. Only the graphs within the same figure can be compared with each other but there is no absolute relation among the two figures. This arises from the necessary sample change, which as a consequence of slight changes in the experimental geometry implies that neither the singlet nor the triplet quantities were recorded under unchanged conditions when going from one to the another sample.

The lowest data points of the two graphs in Figure 5-17 roughly exhibit the same triplet density but the singlet density is more than ten times higher for the optical excitation. This translates into an about ten times higher triplet generation rate in electrical as opposed to optical excitation. For the quantitative analysis, the data were fitted on a double logarithmic scale to a linear relation of the kind $y = a + x$ with a being the logarithm of the desired slope and the only free parameter of the fit. Such obtained straight lines are included in both graphs as solid lines. Apparently, all fits describe the measured data very well, which means there will be *no* dependency of χ on the excitation dose – neither in optical nor in electrical excitation mode in the range of excitation doses used. Therefore the obtained quotients of the

slopes for each polymer are universal and as such can be employed in Equation 5-3.

An obstacle for the final determination of χ are the unknown exact values of the inter-system-crossing rates of both materials. To measure these yields in dilute cyclohexane solutions, two relative experiments were performed by M. Jose in the laboratories of Prof. Burrows. Flash photolysis experiments based on a known polyfluorene as standard yielded 0.0897 and 0.0517 for the homo- and the copolymer, respectively. On the other hand, from singlet oxygen quantum yield measurements based on phenalenone as standard, inter-system-crossing yields of 0.016 for the homo- and 0.0396 for the copolymer were obtained. On account of the large discrepancies between these results, which are caused by the inherent inaccuracy of both experiments, Prof. Burrows suggested the true triplet quantum yield of both materials to be of order 5±3 %. This, however, implies that the singlet-to-triplet generation rate, χ, can also only be obtained with an uncertainty of ±60 %, because in Equation 5-3 χ scales almost linear with κ_{ISC}. Nevertheless, the outcome of Equation 5-3 is given in the second column of Table 5-1 below. One could also go the other way round and assume that the quantum statistical limit for the singlet yield after charge carrier recombination holds true, i.e. $\chi = 0.25$. Then with the data obtained here it becomes possible to calculate the inter-system-crossing yield. This has been done in the first column of Table 5-1. The given error limits on these values, 20 % for the homopolymer and 10 % for the copolymer, are derived from the uncertainties of the slopes of Figure 5-17 and Figure 5-18, respectively.

	if $\chi = 0.25$ then κ_{ISC} =	if $\kappa_{ISC} = 0.02 - 0.08$ then χ =
homo-polymer	0.042 ± 0.008	0.136 - 0.386
co-polymer	0.032 ± 0.003	0.174 - 0.456

Table 5-1 Results according to Equation 5-3: in the first column χ was fixed to 0.25 and κ_{ISC} calculated, in the second column χ was calculated from given κ_{ISC} yields.

The inter-system-crossing rates obtained with χ = 0.25 are typical values for conjugated polymers[9] and as such suggest the validity of the quantum statistical limit for the singlet generation after charge carrier recombination also for conjugated polymers. Furthermore, the relative difference between the two investigated materials is consistent with the different singlet lifetimes, 2.3 versus 1.7 ns for homo- and copolymer, respectively. Although clearly included, the large error margins of the second column do not allow for an accurate differentiation whether or not the quantum statistical limit holds true. Nevertheless, singlet generation rates of 50 % or more as proposed by several authors[46, 47, 58, 59]

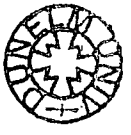

are clearly ruled out even within these generous error margins.

In conclusion, there is clearly need to acquire more accurate values for the inter-system-crossing yields. Here, one way is to employ photoacoustic calorimetry, which was used in the past for other conjugated polymers.[9] An alternative relative method, which does not require any standard, is the observation of the bleaching signal recovery after optical excitation. Here, in the absence of any significant charge state production, the survival signal after the decay of the fluorescence, which is proportional to the long lived triplet excitons, relative to the initial signal directly reflects the inter-system-crossing yield.

On the whole, one tends to assume that the quantum statistical limit for the singlet generation holds true for the charge carrier recombination in conjugated polymers.

5.4.5. The dependency of the fitting parameters a and c on the excitation flux

So far the results of the fitting of the triplet induced absorption curves according to the inhomogeneous exciton generation model have only been used in order to determine the slope at time zero. For this purpose one could have even employed an unphysical model for the fitting procedure. Provided it would acceptably reproduce the initial slopes then the correct singlet-to-triplet generation ratio would still be obtained. However, considering the excellent agreement of the model with the experimental data, and this with only two parameters, hereafter it shall be assumed that the model indeed describes the underlying physics correctly. Then valuable information about working devices are obtained as the fitting parameters, *a* and *c*, are directly linked to several material constants.

At first glance a ($a = \frac{2}{\lambda \gamma_{TT}}$) only depends on material parameters that are independent of excitation dose and as such should be a true constant itself. This then allows to determine the thickness of the electrical charge carrier recombination layer relative to the optical absorption one, with the latter, λ^{opt}, being accessible using ellipsometry. Furthermore, from the corresponding optical definition of *a* one could simply calculate the triplet-triplet-annihilation constant, γ_{TT}.

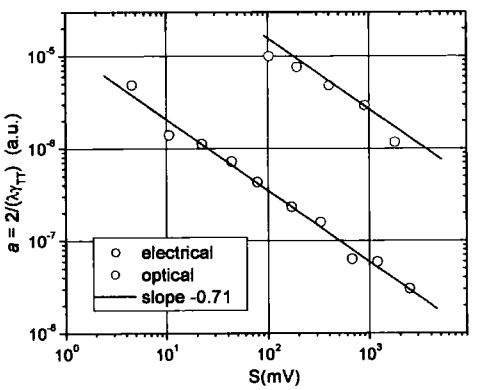

Figure 5-19 Dependency of the fitting parameter a on the overall exciton generation rate for optical and electrical excitation for the copolymer.

In Figure 5-19 *a* as derived from the copolymer datasets is plotted versus the fluorescence level, which itself is proportional to the overall excitation dose, on a double logarithmical scale for both optical and electrical excitation. Apparently, *a* is far from being constant but instead follows a power law dependency on the excitation dose with an identical exponent for both excitation modes, - 0.71. These at first glance puzzling observations are in fact expected as shall be demonstrated in the following. In chapter 4 it was shown that the triplet migration, which is rate limiting for bimolecular annihilation, at the temperatures employed here, is dispersive. This means γ_{TT} is not constant but depends on time, which makes γ_{TT} also depend on the triplet density.[25] A very simple example might help to illustrate this statement. Consider an immobile triplet exciton density, *G*, under classical and time-dependent diffusion. The latter is assumed to be ~ $t^{-0.6}$. The half-lives of these triplet densities can easily be calculated and yield $t_{1/2} \sim G^{-1}$ and $t_{1/2} \sim G^{-2.5}$ for the classical and the dispersive diffusion, respectively. Now, an increase of *G* by, say, a factor of two reduces the triplet lifetime in the classical case (inversely proportional) by a factor of two but for the dispersive diffusion by a factor of more than six. One could say that unlike the classical in the dispersive regime the lifetime of the excitons does not scale linearly with the average distance between the triplets. The reader is referred to Scheidler *et al.* for a more detailed analysis of this issue.[25]

In conclusion γ_{TT} depends on the triplet exciton density and might for the copolymer be described by

$$\gamma_{TT} = \gamma_{TT}^{0}\left(\frac{I_0}{I_{norm}}\right)^{0.71}$$

Equation 5-13

In chapter 4 it was already stated that the time dependence (concomitantly also the density dependence) cannot be cast into an explicit analytical expression, although, asymptotically a power law with slope of -1.04 is obeyed in the zero temperature limit.[26] However, important for the present experimental situation is the initial (measured in terms of the attempt-to-jump frequency) and intermediate time domain as here most of the migration events occur. Here for practical purposes all authors approximate the time dependence of the diffusion with the help of algebraic decay laws.[22, 25, 32, 60, 61] Although it remained questionable to what extent such a procedure is legitimate,[27] slopes between 0.6 and 0.8 have been reported in the literature, which agrees well with the value of 0.7 found here.[25]

Within the modeling of the transient triplet absorption curves the parameter *c* is independently obtained and as such allows a crosscheck of Equation 5-13. Following the definition of *c*

($c = \sqrt{I_0 \lambda \gamma_{TT}}$) one expects a power law dependence on the excitation dose with a slope of 0.86, which is in excellent agreement with the experimentally observed algebraic law with slope 0.88, compare Figure 5-20.

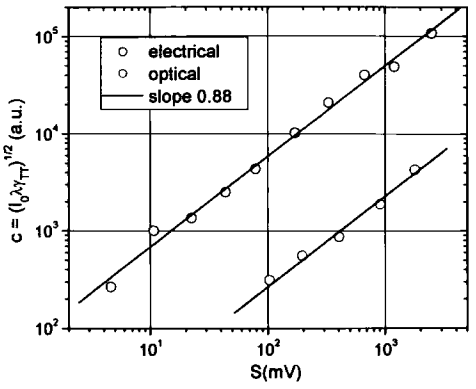

Figure 5-20 Dependency of the fitting parameter c on the overall exciton generation rate for optical and electrical excitation for the copolymer.

5.4.6. The thickness of the charge carrier recombination layer

Having established the triplet density dependence of the bimolecular annihilation constant, attention is now focused again on the parameter *a* – this time with respect to the second material constant, λ. These considerations aim for a determination of λ^{el} relative to λ^{opt}. From the excitation density dependence of γ_{TT} it follows that the optical and electrical values of *a* can only be compared at identical triplet density (note, *not* overall excitation dose!). In Figure 5-21 the parameter *a* of the copolymer is plotted versus the relative triplet generation rate for both excitation modes. Apparently, even for equal triplet densities the datasets are still offset to each other, which implies $\lambda^{el} \neq \lambda^{opt}$.

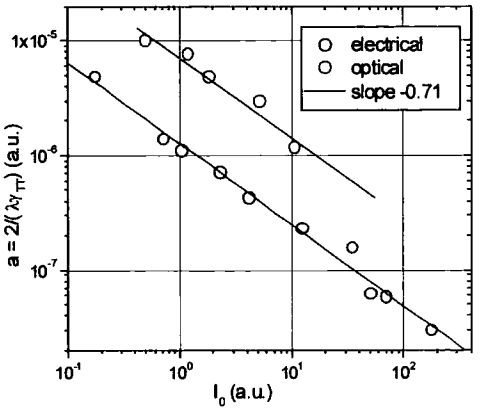

Figure 5-21 Dependency of the fitting parameter a on the triplet generation rate after optical and electrical excitation for the copolymer.

In fact, identical exciton generation layer thicknesses for both excitation modes would be a surprising coincidence and have already been excluded from a qualitative analysis of Figure 5-12. From Figure 5-21 one gains for the copolymer $\lambda^{el} = 5.6\lambda^{opt}$.

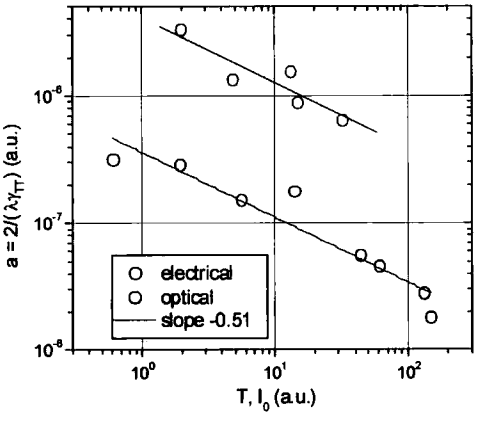

Figure 5-22 The homopolymer fitting parameter a versus the triplet generation rate for optical and electrical excitation.

So far only copolymer data were shown, because these exhibit a higher signal-to-noise ratio compared to the homopolymer ones, and as such are better suited for presentation.

Nevertheless, in repeating the above procedures for the homopolymer one obtains an algebraic triplet density dependence of γ_{TT} with slope 0.51 and $\lambda^{el} = 11.2\lambda^{opt}$. Corresponding results are shown in Figure 5-22.

Having found the ratio between optical and electrical layer thickness, an independent measure for the absorptivity is required in order to gain the absolute electrical recombination layer thickness. In this context ellipsometry is a straightforward and exact method in order to obtain the optical absorptivity of thin films. Unfortunately, for the polyspirobifluorene derivatives investigated here no data are available so far. Nevertheless, common polyfluorene is very similar in absorption and emission characteristics and here $\lambda^{opt} = 1.5 \times 10^8 m^{-1}$ at 400 nm has been reported.[62] In Table 5-2, the latter value is also assumed for both materials investigated here in order to calculate the electrical inverse layer thicknesses.

	$\lambda^{opt}[m^{-1}]$	$\lambda^{el}[m^{-1}]$
homopolymer	1.5x10^7	1.7x10^8
copolymer	1.5x10^7	8.4x10^7

Table 5-2 Compendium of the inverse exciton generation layer thicknesses.

With the optical absorption layer being ~ 70 nm, for electrical excitation charge carrier recombination layers of 6 and 12 nm for the homo- and the copolymer, respectively, are found. The larger value for the copolymer relative to the homopolymer is well understood on a qualitative level in terms of the dissimilar electron mobilities. The electron transport unit within the copolymer increases the mobility of the electrons in this material relative to the homopolymer, which means on average electron and hole meet each other further away from the cathode. This effect is then consistently observed as a wider recombination layer.

5.4.7. An estimate of the triplet-triplet-annihilation constant

Following Equation 5-12, from the two modeling parameters, *a* and *c*, the triplet generation rate per unit area is obtained as $I_0 = 1/2\,ac^2$. Of course, I_0 does not depend on either λ or γ_{TT}, which was a main ingredient for the determination of the singlet-to-triplet generation ratio in 5.4.4. Provided the absolute value of I_0 is known then it becomes possible to normalize the detector response to the actually present triplet density, i.e. determining the constant of proportionality ε from section 5.2.1.

In practice the absolute value of I_0 is estimated from the copolymer dataset with the highest optical dose, which is very similar to the red homopolymer dataset of Figure 5-15. The maximal overall optical laser dose was measured as 48 mW/cm^2. However, due to reflections on the cryostat windows and the device but mainly due

to the finite sample thickness, only 55 % percent of this flux is absorbed by the active polymer layer. At 401 nm such an optical flux excites $4.8 \times 10^{20} s^{-1} m^{-2}$ singlet excitons. For the copolymer in solid-state the fluorescence quantum yield drops to 33 % at room temperature compared to 94 % in solution. Assuming that at low temperature this efficiency reaches 50 % and an inter-system-crossing rate of 4 % then under present experimental conditions one estimates 2 % for the triplet generation yield. Employing this value one arrives at a triplet generation rate flux of $1 \times 10^{19} s^{-1} m^{-2}$. Combining this rate with the corresponding slope at time zero, 10.3 Vs^{-1}, a value for the constant of proportionality of $\varepsilon = 1 \times 10^{-18} Vm^2$ is obtained. Using the latter value, c for optical excitation, i.e. the red dataset of Figure 5-20, is replotted versus the absolute triplet generation rate, I_0. Then a least square fit yields:

$$c(I_0) = 2.13 \times 10^{-13} I_0^{0.88} s^{-1} = \sqrt{I_0 \lambda^{opt} \gamma_{TT}(I_0)}$$

From this relation one finally obtains an estimate for the triplet-triplet-annihilation constant as $\gamma_{TT}(I_0) = 3 \times 10^{-13} I_0^{0.76} cm^3 s^{-1}$. This value is calculated for I_{norm} = 1 $m^{-2} s^{-1}$ (compare Equation 5-13), therefore also I_0 needs to be in the same units. To the authors best knowledge there is no consistent value for the annihilation constant of any conjugated polymers so far. In this context the recently derived intermolecular annihilation constant in polyspirobifluorene seems to be unrealistically high.[31] The triplet-triplet-annihilation in organic crystals does not depend on the exciton density, because here, triplet migration is non-dispersive as a consequence of a nearly isoenergetic site distribution. Pyrene and naphthalene as typical representatives exhibit $\gamma_{TT} = 2 \times 10^{-12}$ and $\gamma_{TT} = 3 \times 10^{-12} cm^3 s^{-1}$, respectively, and as such are of similar order compared to the value derived here for the copolymer.[20] No attempt has been made to repeat the above procedure for the homopolymer, on account of the corresponding noisy datasets.

5.4.8. Photo luminescence under applied electric field

Within this chapter several electric field effects that were additionally observed within this study are shown and analyzed.

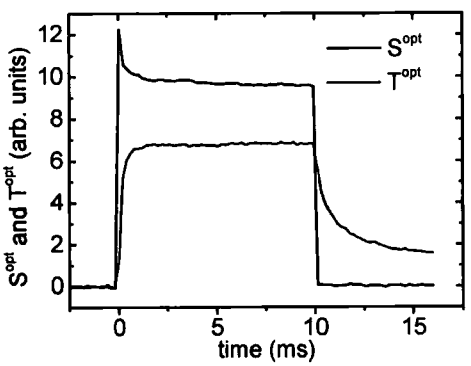

Figure 5-23 Comparison of the fluorescence and the induced absorption after optical excitation for ten milliseconds.

First of all is considered an unexpected behavior of the optical fluorescence signal (black curve) seen in Figure 5-10. This dataset, which is shown

again in Figure 5-23 on a linear scale, reveals a ~ 30 % drop of the fluorescence intensity compared to the initial value that occurs on the time scale of one millisecond. This observation suggests the existence of a photo generated transient singlet quencher. In view of bimolecular singlet-triplet-annihilation the quencher could potentially be the triplet exciton. Hereby, the photo generated triplet density increases within the first millisecond and afterwards approaches a constant value due to bimolecular triplet annihilation. At first glance the mirror symmetric build-in of the triplet density and the drop of the fluorescence intensity as shown in Figure 5-23 seem to be consistent with this assumption. However, contradictory are the electrical curves since here no comparable drop of the fluorescence intensity during the triplet accumulation is observed. Therefore, the triplet exciton itself is not the singlet quencher. More likely appears exciton-ion quenching due to photo generated charge carriers. In such a situation no comparable drop in the electrical signals is expected as here the singlet generation always happens in an environment with a time-independent charge carrier density that is determined by the current flow through the device. Note, the time dependence of the charge carrier density in the active polymer layer would be very similar compared to the triplet density as in both cases the continuation of the accumulation is limited by bimolecular annihilation. This would explain the qualitatively mirror symmetric behavior of the photo generated singlet and triplet signals, shown in Figure 5-23.

The charge carrier migration through the polymer layer occurs on a microsecond time scale, which is evident from the corresponding RC time constants, compare Figure 5-13. Considering a polaron density that builds up on a millisecond time scale, using an applied bias it should be possible to continuously sweep the generated charge carriers out of the polymer layer and thereby achieve a higher photoluminescence yield. Corresponding experimental data that confirm this notion are shown in Figure 5-24.

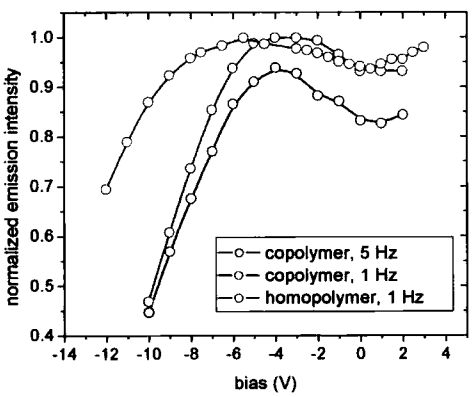

Figure 5-24 Dependencies of the photoluminescence on applied reverse bias. The optical pulse length was 10 ms and the repetition frequency either 1 or 5 Hz as indicated. During the normalization for the copolymer datasets the relative order was preserved.

Here the photoluminescence efficiency reaches a local minimum for zero internal fields around +1V. At this point

the photo generated charge carrier population does not sense any potential and as such the highest densities are achieved. For increasing reverse bias up to about -4 V the storage time of the charge carriers will continuously decrease, which is observed as an increase in the photo luminescence efficiency. The observed drop in photoluminescence efficiency for even higher applied fields corresponds to the onset of singlet exciton dissociation. The repetition frequency of the 10 ms optical excitation pulse also influences the results. This is shown in the same figure for the copolymer fluorescence after excitation with either 1 or 5 Hz, with both normalized curves being in the correct relative order. Apparently, in the absence of any internal field (~ +1V) there is still a significant difference whether the excitation is repeated every 200 or every 1000 ms. From this one concludes that the depletion of the charge carrier reservoir, which probably proceeds via bimolecular annihilation, is a rather slow process at these temperatures. Finally, a comparison of the relative homo- and copolymer datasets shall be undertaken. For the homopolymer, higher fields are required to sweep the charge carriers out of the device but also to dissociate the singlet exciton. For example at -10 V the copolymer fluorescence is quenched by 55 % but the homopolymer only by 13 %. This observation can be explained in terms of the dissimilar hole mobilities in both materials.

5.4.9. The triplet exciton under applied electric field

Unlike with fluorescence, for the triplet exciton the influences of a negative applied bias field on the triplet generation rate can only be obtained indirectly upon fitting the corresponding curves. Here the photo induced triplet absorption curves were usually measured with and without applied electric field in the same measurement run, in order to have a reference.

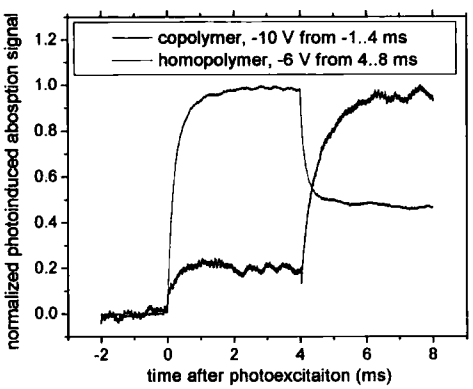

Figure 5-25 Typical normalized photoinduced triplet absorption signals under partly overlapping reverse bias as indicated.

In Figure 5-25 two typical original datasets are shown. For the red homopolymer dataset optical excitation was provided from 0 to 8 ms and at 4 ms an electrical bias of -6 V was additionally applied. Apparently, this modest bias field causes a significant decrease of the steady-state triplet density of about 50 %. Remember from Figure 5-24 at the same reverse field the fluorescence is even enhanced when compared to zero bias.

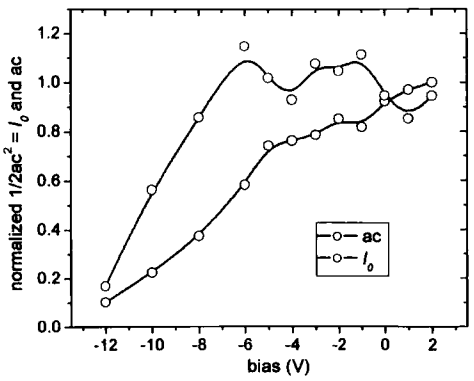

Figure 5-26 Normalized steady state value and the initial slope of the photo induced absorption signal of the copolymer under an applied reverse bias.

However, apparent from Figure 5-26, the strong influence of the electric field only affects the steady state value (*ac*) but not the initial triplet generation rate. Here, I_0, closely resembles the fluorescence quenching shown in Figure 5-24 as the rate is within experimental error constant up to -6 V and subsequently simply follows the descending singlet exciton dissociation. This suggests that there is *no* effect of the bias field on the triplet exciton itself within the bias range investigated here. Furthermore, the triplet dissociation at these fields is not expected considering the fluorescence quenching. Here, the singlet exciton is about 0.5 eV lower in energy compared to a polaron pair and from Figure 5-24 electric fields in excess of the equivalent of -7 V are required in order to initiate the singlet dissociation. The singlet exciton energy is ~ 0.7 eV above that of the triplet. Thus, one would expect the onset of direct triplet dissociation at bias voltages of order -17 V, which exceeds the investigated voltage range used here. However, on the other hand the steady state triplet density clearly is quenched even at these comparably small bias fields.

If one accepts that the triplet itself is not quenched then it must be the triplet-triplet annihilation, which is more efficient under applied field. Subsequently, it will be shown that the latter assumption indeed has a scientific basis and agrees well with many other observations. Following the classical treatment of bimolecular triplet annihilation by Suna *et al.* as a consequence of the spin addition of two spin-one excitations, initially nine intermediate states are formed with equal probability.[8, 20, 63] Each three of these states have spin zero, spin 1 and spin 2. Then the spin-1 and the spin-0 intermediates form triplet and singlet excitons, respectively, with the latter being potentially observed as delayed fluorescence. Although the nature of the intermediate spin-2 state (quadruple) corresponds to a pair of charge carriers, its decay is usually considered to yield excitons as well.[8, 20] On the other hand for the materials investigated here the energy of two triplets (~4.6 eV) significantly exceeds the sum of singlet and exciton binding energy (~3.5 eV), therefore from energetic reasons a dissociated pair of free charge carriers would also be possible. Importantly, the intermediate might also dissociate into two triplets

again and this is believed to be the most likely possibility.[8, 20, 63] The whole scenario is illustrated with the schematic drawing below.

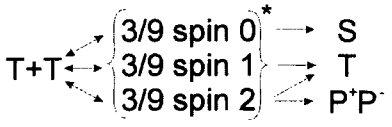

Equation 5-14

If one accepts the quadruple state as a source of free charge carriers then the effect of an applied electric field is immediately clear as then the charge carrier generation rate increases at the expense of the back transfer rate, which is equivalent to an annihilation constant that increases with electrical field. Consistent with the present findings, such a field dependent enhancement of the triplet-triplet annihilation rate resulting in charge carrier formation has been observed by Scher *et al.* for a molecularly doped polymer.[64] Furthermore, the whole scenario explains the field independent triplet generation rate and the simultaneously quenched steady state triplet density, as shown in Figure 5-26.

From both the time dependence under continuous excitation and the bias dependence on the photo-luminescence, in 5.4.8 it was concluded that photo generated charge carriers quench some of the singlet excitons. It was not yet considered how these charge carriers are photo generated. Commonly assumed is monomolecular singlet dissociation even in the absence of any bias field. However, given the large exciton binding energy in chapter **6** it is shown in detail that this process is highly unlikely to occur. On the other hand, there is nothing, neither energetically nor from the experimentally observed fluorescence data shown in Figure 5-23 and Figure 5-24 that opposes the above framework of triplet annihilation as a source of charge carriers. In this picture the photo generation of free charge carriers is a sequential process that involves the initial excitation of singlet excitons, which then partly convert into their triplet counterparts.[64] For continuous excitation the latter accumulate within the polymer layer until bimolecular annihilation, among others, causes the generation of free charge carriers, which appear in the experiments as singlet quenchers. This is a scientifically sound framework that consistently explains the rather slow build-up of the fluorescence quenching in optical excitation mode and the simultaneous absence of such a quenching for electric excitation.

Finally, the implementations of the above findings on the determination of the singlet-to-triplet generation ratio shall shortly be discussed. For these experiments the relative triplet and singlet rate under identical optical excitation conditions is needed. As the triplet generation rate is measured at time zero, this means there are no charge carriers yet generated. Thus, for the calculations the initial, unquenched

fluorescence level was used. No such considerations are necessary for electrical excitation, because here the permanently present polaron density acts like an impurity and as such linearly, i.e. independent of time, quenches a certain small fraction of the singlet and triplet exciton generation rate.

5.4.10. Charge carrier pairs versus triplet pairs as origin of the spin-resonance signals

In applying the spin-resonance method to conjugated polymers, singlet-to-triplet branching ratios, which clearly exceeded the quantum statistical limit, were repeatedly claimed in the recent past. Hereby the authors consider a framework that is very similar to the above introduced charge carrier generation due to triplet-triplet annihilation. Therefore, it is convenient to discuss these experiments now, rather than in the introduction. Corresponding photo excitation experiments that apply the above method to several conjugated polymers were mainly conducted by Vardeny, Wohlgenannt, and co workers. Their results, at least at first glance, provide a consistent and sound but at the same time surprising picture, which explains the numerous publications in prestigious journals. However, since all of these publications more or less contain similar data and conclusions, for the present intention it is enough to refer to and cite only one, Ref. [59].

This technique studies the change of the photo excited polaron, triplet or singlet density in a material as an applied microwave magnetic field is tuned to resonance. Here polaron and triplet densities are probed by their induced absorption (PADMR), the change in singlet density is optically detected (PLDMR). After photo excitation a certain density of polaron pairs is assumed to exist that is equally composed of pairs with parallel (S_0, T_0) and antiparallel (T_{+1}, T_{-1}) total spin. This equal probability implies a non geminate pair mechanism for the formation of these pairs. A magnetic field causes Zeeman splitting of the triplet states and an additionally applied alternating magnetic microwave field tuned to the Zeeman splitting induces spin flips and thereby equally populates the two kinds of antiparallel spin combinations. Both the singlet and triplet polaron pairs recombine with certain fixed rates into their corresponding excitons i.e.

$$S \leftarrow \left(P^{+}P^{-}\right) \rightarrow T$$

Equation 5-15

During resonance a reduced charge carrier and triplet density and an increase of the singlet emission is observed, which is interpreted as a higher cross-section for the singlet as compared to the triplet exciton formation.

However, now the possibility is discussed that all the potentially correctly observed phenomena by Wohlgenannt *et al.* are actually caused by triplet-triplet-annihilation (TTA) rather than non-geminate charge carrier recombination. To start with, the above magnetic resonance is *only* observed under experimental conditions that also enable the existence of long-lived triplets that decay by bimolecular annihilation (temperature below 100 K, large excitation dose up to 1000 (!) $mWcm^{-2}$, solid state).

Likewise the polaron pair, initially created by the annihilation of two triplets causes the formation of an intermediate.[64] According to the spin addition rules of two spin-1 particles, there are nine possible spin states for this intermediate: 3 triplets, 3 doublet and 3 mixed singlet/doublet states.[8, 20, 63] Given the above findings and the work of Scher *et al.*,[64] there will be a certain rate for the doublets to form geminate or non-geminate charge carriers, i.e. TTA is, like singlet-singlet-annihilation,[19] a source of charge carriers. The corresponding polaron signal might be observed by polaron induced absorption. If a magnetic field is applied then certain off-diagonal matrix elements mix the spin character of the above nine states resulting in more states with singlet character.[20] On the other hand the decay of this intermediate is unaffected by the field. Therefore, during resonance the relative singlet formation increases at the expense of both the triplet density and the polaron density. Consistently, Wohlgenannt and co authors observe an increase in the delayed fluorescence intensity that is accompanied by a proportional decrease of both the polaron and the triplet signal. The whole theory for triplet-triplet-annihilation under applied magnetic field, which is very similar to the above electron paramagnetic resonance, has been developed by Suna.[8, 20, 63] If the TTA picture is true then the actually observed magnetic resonance in the induced polaron signal is not caused by enhanced charge carrier recombination, but by their reduced production.

But is it possible to distinguish between both models? In this context Wohlgenannt *et al.* cannot answer the question where the proposed pair wise photo generated polaron density that subsequently recombines comes from. Considering monomolecular singlet dissociation, for MEHPPV the authors observed relative delayed luminescence intensities between 10^{-3} to 10^{-2}, which would require singlet exciton dissociation rates of order 3 %. However, recently an upper limit for singlet dissociation at zero field of 10^{-3} has been found by time-correlated-delayed-collection-field experiments.[45] On the other hand the observed delayed fluorescence intensities are consistent with triplet-triplet-annihilation.[12, 16, 17] For example in

Figure 4-5 the ratio between integrated delayed and prompt fluorescence is ~$2x10^{-4}$. The latter value is still lower than the above stated one, which, however, can be explained by the much lower inter-system-crossing rates in polyfluorenes as compared to MEHPPV[9] but also by the 20 times higher excitation dose applied by Wohlgenannt. Thus, on a qualitative level only the TTA model is able to account for both the existence of charge carriers and the experimental findings described by Wohlgenannt *et al.*[65]

Furthermore, the dependencies of the polaron and the delayed fluorescence signal on the laser dose have been measured. Consistent with both the TTA and the non geminate charge carrier recombination picture a square root dependence for the polaron signals at high excitation doses was observed. However, at low doses the increase is linear. Such an observation is consistent only with the TTA picture: at low doses monomolecular decay prevails for higher doses the bimolecular decay dominates. On the other hand by their very nature, charge carriers can only decay bimolecularly, so where does the linear rise come from? What is meant by Wohlgenannt and co authors with their proposed monomolecular decay path for (single) charge carriers?

To summarize the above comments the results by Vardeny and Wohlgenannt should be treated with great care as the alternative, triplet-triplet-annihilation, is at least an equally likely possibility. Noteworthy, similar experiments on electrically rather than optically excited polymer films by Greenham *et al.* find no difference between singlet and triplet exciton formation cross section and in such a way also contradict the above photo excitation work.[66]

5.4.11. Geminate pair formation and recombination due to triplet-triplet-annihilation

In Figure 5-27 the influence of the electric field on the triplet induced absorption has been probed in the absence of any triplet generation, i.e. 1 ms after a 2 ms optical excitation pulse. In doing so any sequential influence of the electric field on the prior formed singlet exciton can be excluded and as such one only observes triplet phenomena. Already without electric field (black dataset) the relative fast decay of the curve is exclusively caused by triplet-triplet-annihilation. Otherwise in this time frame the triplet density should be almost constant considering the monomolecular triplet lifetime of 500 ms, compare Figure 5-8. A significant drop of the triplet density is observed as soon as an electric field is applied. As expected higher fields have a stronger effect. From the figure one infers a quenching of the remaining triplet density by 5.5 and 30 % for -10 and -20 V, respectively. This modest

triplet quenching at -10 V might be compared with the fluorescence quenching at the same field observed in Figure 5-24, 55 %.

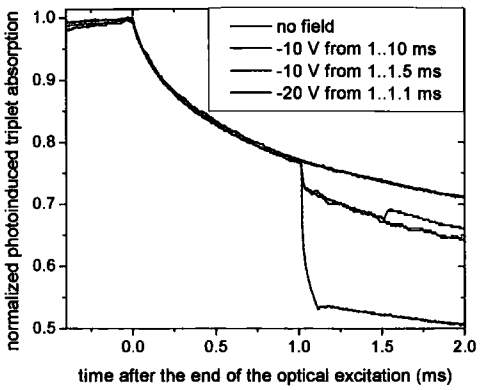

Figure 5-27 Normalized triplet induced absorption signals of the copolymer after 2 ms optical excitation with different reverse electrical bias as indicated.

However, the most striking feature is a certain recovery of the induced triplet absorption signal after the switch-off of the bias field. For the -10 V dataset this effect amounts to more than 50 % of the initially, at the switch-on of the field, quenched triplets. This recovery is a clear evidence for the sequential charge carrier generation, i.e. the first step is the field dependent geminate pair formation and the second, rate limiting step is the final dissociation of this pair into free charge carriers and this is completely consistent with recent time-resolved delayed collection field experiments by Hertel *et al.* on singlet exciton dissociation.[45] Note, any direct triplet quenching mechanisms, for example mirror charge quenching at the cathode, one would not expect any recovery of the signal. The effect is more pronounced for intermediate bias fields around -8 V. Again the field dependent charge carrier mobility is the key to understand this observation: At intermediate fields the triplet-triplet-annihilation already favors the charge carrier generation. However, most of these charge carriers are still coulombically bound and a higher electric field is required to sweep these charges out of the polymer film. On the whole this recovery effect is both qualitatively and quantitatively very closely linked to the fluorescence quenching shown in Figure 5-24. The overall picture is completed by another experimental observation. If a certain electrical field pulse is switched on later then relatively fewer triplets are quenched compared to the triplet density that is present at the time of the application of the field. If the electrical field directly acts on the triplet excitons, one would expect to have always the same proportion of triplets to be quenched. This again confirms that the electric field mainly acts on the triplet annihilation and much less on the triplet itself. These findings also shine some new light on recent triplet quenching experiments by Sinha *et al.*[11] Here, triplet exciton-ion quenching, with the polarons being mobilized by the electric field, was invoked to explain the phosphorescence quenching under applied electric field. In view of the present findings, at least part of the observed phosphorescence quenching might also be explained by the field

dependent bimolecular triplet annihilation efficiency.

Furthermore, the triplet recovery after the switch-off of the field is very similar to the classical experiments by Deussen, Schweitzer, and coauthors.[4, 67, 68] In these early experiments the polymer sample was optical excited with a simultaneously applied reverse bias field. Then, a spike in fluorescence, which is observed once the electric field was turned off, was explained by the recombination of field–stabilized geminate pairs, which were formed by singlet exciton dissociation. In this context the recovery of the triplet signal observed here should also be accompanied by a similar spike, because in principle one quarter of the geminate pairs should have a sum spin of zero and as such enable the observation of fluorescence after recombination. Thus, it would be very interesting to repeat the experiments of the above authors and investigate the influence on the fluorescence spike on whether the electric field is applied during or after optical excitation.

Already from the field dependent triplet-triplet annihilation quite a significant effect would be expected, which shall briefly be quantified next. For the green curve shown in Figure 5-27 the electric field pulse causes a 2 % recovery of the signal relative to the steady state triplet density. Assuming the equivalence of the four charge carrier pairs with different sum-spin, an estimated ~0.7 % of the steady state triplet concentration converts into singlet excitons at the turn-off of the field. By simply considering the triplet generation rate without any bimolecular annihilation then the level of the steady state triplet concentration would be reached after ~ 500 µs. This means that the integrated fluorescence area of this potential spike is identical to the integrated fluorescence after excitation with a 3.5 µs long optical pulse. Such fluorescence signals should easily be observed, but unfortunately the corresponding experiments have not been performed so far.

5.5. Conclusions

Given that potential consumer applications are driven in pulse mode, it appears that the microsecond time scale with moderate excitation doses contains the most useful information about working devices with regard to the design and driving rules. In this time domain one can study the build-up of triplet excitons and polaron density as well as the mutual interactions of the latter with the singlet exciton as they will occur in real applications. This knowledge is considered critical in order to optimize conjugated polymer based devices.

In the present study, using somewhat standard experimental techniques the time-dependent triplet accumulation during both optical and electrical excitation has been measured as a

function of the corresponding fluorescence level. Given the simplicity of the experimental set-up, which features neither a particularly high time-resolution nor an exceptional sensitivity, the obtained results are still comprehensive and give unique insights into working devices.

During the whole investigation especial emphasis was laid on the determination of the singlet-to-triplet generation ratio. In contrast to recent findings,[47, 59] the latter ratio is obtained as a universal constant and as such neither depends on the investigated material nor on the applied field. Albeit the accuracy of the absolute value is limited by the high error margins of the inter-system-crossing rates, it is safe to conclude that the true singlet generation rate will be at least close to the quantum statistical limit of 25 %, which clearly does not include previous outcomes of 50 or even 90 %.[42, 43, 46, 47, 53, 58, 59, 65] In this context the present study also gives a rather complete overview of the manifold problems that one needs to carefully account for, even for simple relative measurements, and as such unveils why many previous studies generated only arbitrary values.

Furthermore, evidence is provided about the dispersive nature of triplet migration, which is rate limiting for bimolecular triplet annihilation. Here the corresponding annihilation rate is dependent on the actual triplet exciton density, because the average time it takes for a triplet to encounter its nearest neighbor decreases non-linear with the intersite separation.

Furthermore, the occurrence of singlet exciton-polaron quenching has been confirmed by fluorescence measurements both as a function of time and applied electric field. In the absence of any stimulating electric field, several experimental observations suggest a generation mechanism for polarons predominantly via triplet-triplet-annihilation rather than direct singlet exciton dissociation. Hereby considered is a sequential process, which involves the initial formation of geminate pairs. These pairs then either recombine into singlet or triplet excitons, or fully dissociate, with the latter rate being dependent on the applied electric field.

Also a model has been developed in detail that describes the triplet accumulation under constant excitation in the framework of bimolecular annihilation. The successful application of this model to the experimental data confirms the existence of a relatively small charge carrier recombination zone, which exhibits a layer thickness of only 6 nm for polyspirobifluorene.

The development as well as the results of the latter model takes a prominent part of the chapter. At this point the reader might be left with the feeling that a significant part of the conclusion of the whole chapter depends on whether or not this model exactly describes the

underlying physics. However, in all cases apart from the recombination layer, the model was only a tool to quantify the observed triplet induced absorption curves. In a way the situation is similar to the data analysis in ellipsomety. Here if a suitable model is lacking, then one can always simulate the measured data with a set of harmonic oscillators, which have no physical meaning. In such a way the simulation parameters in the present study can always be considered as nothing else than an exact description of the measured curves. In conclusion the main findings are not linked to the model. For example, consider the triplet density dependent triplet annihilation rate. If simply the steady state values are plotted as a function of optical excitation dose then one still observes an algebraic dependence with exponent 0.88 rather then the classically expected square root slope, which still means that the annihilation constant is density dependent.

6. Nanosecond delayed emission of indirect intrachain excitons

6.1. Introduction

The photo excitation of small light emitting molecules leads to the formation of a tightly bound metastable singlet exciton with a well defined energy level.[8] After a long debate the primarily excited state in polymeric systems is now also generally considered as a molecular singlet exciton,[3, 68] rather than a free charge carrier according to a one dimensional band picture.[2, 69] For highly luminescent systems, such as considered in this study, the main deactivation channel for most of these primary excitons is the radiative decay, which gives rise to the widely studied prompt fluorescence.[70] Characteristic for dilute systems are mono exponential decays featuring lifetimes of the order of one nanosecond. Furthermore, a few percent of the singlet excitons convert into triplet excitons via inter-system-crossing. In the absence of bimolecular and impurity quenching, gated spectroscopy enables the observation of the corresponding emission, phosphorescence, with typical lifetimes of the order of one second.[12, 13, 15-17] Besides these direct mono exponentially decaying emissions, conjugated oligomers and polymers generally feature delayed luminescence that is isoenergetic to the prompt fluorescence.[15, 17, 38] The occurrence of such delayed emission in a time domain long after the typical prompt emission as well as its non exponential decay kinetics enables one to distinguish the corresponding delayed singlet excitons from their directly decaying counterparts. Unlike many organic crystals, the delayed luminescence in the conjugated polymers and oligomers considered here cannot originate from so-called E-type delayed fluorescence, i.e. inter-system-crossing from the triplet back to the singlet manifold.[8] Here a strong electron-electron correlation causes the triplet exciton energy level to be about 0.7 eV below its singlet counterpart,[71, 72] which prevents any thermally assisted back-transfer. The most frequent source of delayed fluorescence is bimolecular triplet-triplet-annihilation (TTA), which has been observed in thin film and frozen solution.[16, 37, 73] The assignment of TTA as the origin of the delayed fluorescence is usually (see for example chapter 4) based on laser dose experiments, where the delayed fluorescence depends quadratically but the triplet density, measured via the phosphorescence signal, only linearly on the excitation power. The examination of frozen solutions has attracted much attention as here many researchers generally base there conclusions upon the assumption that, unlike in thin solid films, isolated polymer chains are probed.[16, 18, 37] This however is clearly not the case as in these frozen solutions the polymer chains form extended clusters, which

was shown in chapter 4 and in Ref [73]. Within this context the disappearance of the observed delayed luminescence as soon as the solutions start to melt, i.e. the solid-state aggregates dissolve, is further unambiguous proof to confirm the interchain nature of the observed triplet-triplet-annihilation delayed fluorescence in such frozen solutions.[16, 37] In conclusion, in those experiments one probes the bulk and unlike that claimed by the authors, the observed phenomena are *inter*chain as opposed to *intra*chain in nature. Actually, in most common polymers this cluster formation only enables one to observe delayed fluorescence due to triplet-triplet-annihilation, which on truly isolated systems is prevented as a consequence of an average triplet generation density of less than one triplet per chain. Nevertheless, very recently King *et al.* succeeded to observe true intrachain triplet-triplet-annihilation delayed fluorescence in a dilute polymer solution by using a combination of extremely high excitation doses (~ 1 mJ/cm^2) accompanied with the highest available molecular weight polymer (more than 1000 repeat units).[31]

Besides triplet-triplet-annihilation delayed fluorescence, another source of delayed fluorescence that is frequently discussed in literature mainly by the Bässler group is delayed charge carrier recombination.[4, 13, 18, 38, 45, 67, 74-76] The numerous reports and interpretations of experimental findings within the framework of the geminate charge carrier recombination were triggered by a single observation by Schweitzer *et al.* that the optically excited delayed fluorescence can be quenched by an electric field.[4, 67, 68] The authors finally based their conclusions on the assumption that the triplet is not affected by an electric field but also on the experimental observation that the delayed fluorescence rises linearly with excitation dose, which rules out any bimolecular processes. However, Sinha *et al.* disproved the first assumption in our own laboratories when they showed that the triplet exciton is actually strongly quenched by an electric field most likely due to exciton polaron interactions.[11] Also the second point does not withstand a closer examination as the linear laser dose dependency of the delayed fluorescence was accompanied by a square root dependence for the prompt fluorescence. In fact this observation is fully consistent with the high excitation doses (> 100 μJ/cm^2) used in the above-mentioned but also in subsequent studies as it is the fingerprint of singlet-singlet-annihilation. Thus the observed delayed fluorescence was actually quadratically dependent on the singlet exciton density in line with the triplet-triplet-annihilation picture but contrary to geminate pair recombination. In this context singlet-singlet-annihilation is a

fast process compared to inter-system-crossing, i.e. the triplet density is proportional to the density of the surviving singlet excitons, which is observed as fluorescence, rather than to the applied excitation dose. For a long time, researchers related to the Bässler group ignored both these facts, which contradict the geminate pair picture and it was not until recently that Romanovskii *et al.* clarified this point when they showed that the delayed fluorescence has a bimolecular origin as compared to the prompt fluorescence.[19] Note, all the above said does not exclude the existence of geminate pairs. However, they cannot directly be formed from the singlet exciton. Instead either high electric fields or bimolecular exciton annihilation is required for the geminate pair formation. This is also consistent with the observation of geminate pair recombination following triplet-triplet-annihilation at the end of chapter **5**.

To summarize, in contrast to the claims of numerous published experimental work, there hasn't been a single observation of true *mono*molecular (i.e. depending linearly on excitation dose) delayed fluorescence. Furthermore, such a delayed luminescence is not expected within the common excitonic picture. Under optical excitation one directly excites a bound state that is approximately 400 meV lower in energy than a corresponding pair of free charge carriers.[68] Monomolecular delayed fluorescence due to charge carrier recombination now implies that this tightly bound singlet exciton dissociates, i.e. gathers about 400 meV, and forms a pair of charge carriers which can then again recycle to the singlet exciton! For energetic reasons the whole process should be highly unlikely if not impossible. Nevertheless, there has been extensive theoretical work directed on this issue. Bässler *et al.* initially believed that the necessary dissociation energy can simply be gained by thermally assisted jumps of the excitation within the DOS.[77] In a more recent model Arkhipov *et al.* describes the singlet dissociation as an intrachain, hot process where the initial excess energy from the optical excitation is retained in a local heat bath for a certain time and as such causes the geminate pair formation.[78]

As a consequence of the plain existence of these theoretical models, any novel kind of delayed fluorescence that cannot be explained by triplet-triplet-annihilation has also to be discussed in terms of the monomolecular geminate pair picture, even though so far there hasn't been any experimental evidence for such pairs in conjugated systems and it appears very unlikely that they will ever be observed.

In the present chapter, time-resolved spectroscopy has been applied in the

nanosecond time regime, mainly on isolated conjugated systems. Unexpectedly, here a novel kind of non exponentially decaying long lived fluorescence is observed with the interesting characteristics of being isoenergetic to the prompt fluorescence and intrachain in nature. Furthermore, this delayed emission is generically observed in all kinds of conjugated systems including laser dyes, oligomeric and polymeric systems. This long-lived, generic fluorescence can neither be attributed to the normal singlet exciton nor to delayed, regenerated singlet excitons either due to bimolecular triplet annihilation or due to geminate pair recombination. Thus, one infers the existence of a further directly excited singlet state in conjugated systems that so far has neither theoretically been predicted nor experimentally been observed.

Considering the abundant number of publications on many kinds of conjugated systems, at first glance it seems highly unlikely that such a generic feature has been completely overlooked so far. However, the signal under examination is both very weak (typically 10^{-5} of the prompt fluorescence intensity) and fast decaying (within 100 ns after excitation). Thus, the observation of these signals really requires the time-resolved detection system employed here, which is unique in its combination of a very sensitive light detection with superb time resolution. In fact the presented data for the first time scan the fluorescence decay, in one measurement, through the tail of the prompt fluorescence directly into the delayed emission regime, thereby detecting signal drops in excess of eleven (!) orders of magnitude in only two orders of time. In all previous gated spectroscopy studies only the micro- and millisecond time domain could be examined, because the time resolution of the employed ICCD cameras was of order 30 to 100 ns only.[12, 16, 79] Similarly, any very fast time-resolved fluorescence detection such as femto second or single-photon-counting fluorescence studies are nowhere near sensitive enough to observe weak delayed fluorescence signals. Therefore, the fact that this delayed fluorescence has not been reported in the literature so far is not at all astonishing as the time domain required, the nanosecond time scale, cannot be investigated with common light detection systems.

6.2. Sample Preparation

In order to verify the generic nature of the observed delayed emission, many kinds of organic materials from various sources have been investigated. These include commercially available laser dyes (Exciton); small molecules such as anthracene (Aldrich); several fluorene oligomers that were either synthesised in the Durham University

Chemistry department or provided by the group of Prof. Ulli Scherf; polyspirobifluorene (Covion); and several co-polymers that have been synthesized by TNO Industrial Technologies and which were obtained via Philips Research Eindhoven. The majority of the experiments were done on dilute systems employing various "ultra pure" solvents including methylcyclohexane (MCH), ethanol, methanol, decaline or toluene (Romil). Typically the weight fractions of the investigated systems were chosen between 10^{-4} and 10^{-5}, which roughly corresponds to optical densities at the excitation wavelength between 0.1 and 0.6. The influence of molecular oxygen on the delayed fluorescence was investigated by removing the dissolved air for several of the solutions by four freezing-thaw-cycles. However, if not explicitly stated otherwise then non-degassed solutions were used.

For reasons described below, only a few out of the whole range of the pristine conjugated systems, namely some meta-coupled copolymers, are suitable for solid-state measurements. Thin films made of some of these copolymers have been prepared by spin coating a 2 % by weight polymer solution onto previously cleaned sapphire substrates. For one of these co-polymers the influence of an applied electric field on the delayed fluorescence has been investigated using sealed, high-quality devices that were fabricated by Philips Research Eindhoven, compare Figure 5-4.

For the spectrally- and time-resolved luminescence detection, set-up and procedures as described in chapter 3 were employed. In order to suppress bimolecular annihilation processes the excitation pulse dose, if not stated otherwise, was kept below 10 $\mu J/cm^2$.

Also, a time-correlated single photon counting system (TCSPC, fixed excitation at 390 nm, pulse width 75 ps, detection channel width 5 ps) was used as an alternative, accurate measure of the fluorescence decays in the initial time region. Here the fluorescence lifetimes are obtained after a deconvolution of the laser scatter pulse with the measured signal, which is assumed to be multiple exponential. However, all the results of this experiment that are presented here are well described by a single exponential lifetime. This combination of experiments enables one to gain full excited state decays and to simultaneously verify the time-resolution of the ICCD spectrometer.

With the time resolved luminescence set-up it is very difficult to find an absolute relation between the applied excitation dose and the corresponding luminescence signal. If one is interested in absolute emission yields only relative measurements are possible using a standard reference, which relates the measured intensities

to a known quantum yield. Therefore in the emission intensity versus time plots, i.e. in the decay graphs, the y-axis for each data set is arbitrarily chosen. It follows that the absolute emission intensities of different data sets, even of the same material, cannot be compared with each other. Within this context decay graphs within the same plot are frequently and without stating it explicitly, arbitrarily offset for clarity.

6.3. Results

6.3.1. Small molecules

Within this first part of the results the fluorescence decays of common small molecules anthracene, BBO, Coumarin 450, Coumarin 500, and Rhodamine 6G in dilute solutions are investigated. The chemical structures of the substances as well as the solvents used are given in Table 6-1 at the end of 6.3.3. With the exception of anthracene these materials are all laser dyes and as such possess high emission quantum yields of order 90 % in dilute solutions. In such a situation, classical mono exponential fluorescence decays are expected, because neither bimolecular annihilation nor non-radiative quenching mechanisms play a major role.

In Figure 6-1 the corresponding fluorescence intensities versus time are shown on a double logarithmical scale. Indeed in the initial time period strictly mono-exponential decay kinetics are observed, which is evident by the linear behavior after re plotting in a semi logarithmical fashion such as shown for a representative data set in Figure 6-2.

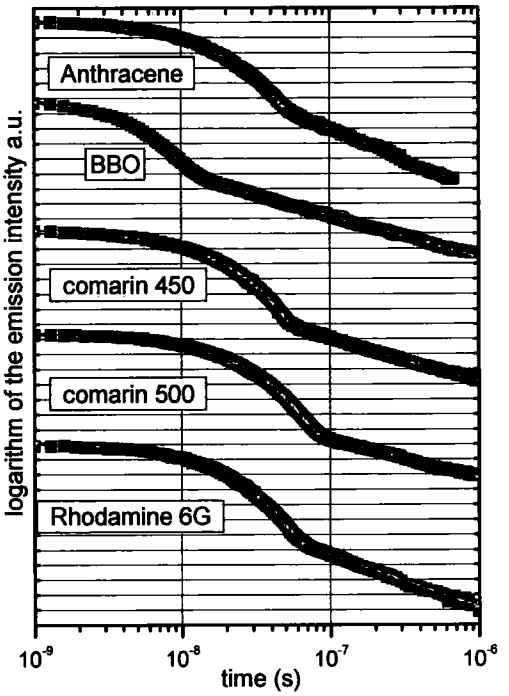

Figure 6-1 Compendium of double logarithmical decay curves of several small molecules in dilute solution, solvent is given in Table 6-1. The green solid lines are least square fits according to Equation 6-1 with fitting parameters given in Table 6-1.

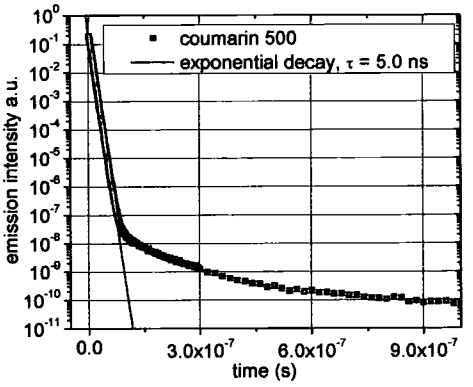

Figure 6-2 A representative data set from Figure 6-1, Coumarin 500, replotted in a semi-logarithmical fashion. The solid green line refers to a single exponential fit to the prompt fluorescence.

In this figure the mono exponential decay is observed over a region of seven orders in intensity, which already corresponds to an impressive 16 times the characteristic lifetime of the observed emission! However, exponential kinetics describe the measured data sets only up to a certain point in time, subsequently a clearly different decay law is obeyed. It is this additional contribution to the fluorescence (consistent with chapter 4 hereafter called DF1) to which the present chapter is dedicated.

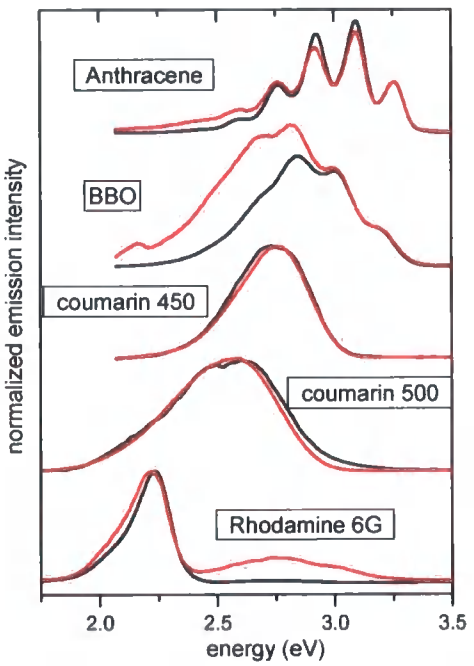

Figure 6-3 Compendium of normalized fluorescence spectra of the materials shown in Figure 6-1 that represent the prompt, exponential decay regime (black) and the algebraic delayed fluorescence component (red). (In detail, all times nanoseconds: Anthracene PF 5..15, DF 100..500; BBO PF 1..8, DF 20..100; Coumarin 450 PF 5..30, DF 85..500; Coumarin 500 PF 5..15, DF 150..500; Rhodamine 6G PF 5..15, DF 100..500.)

First in making use of the full decays, one is able to compare the corresponding emission spectra of the two fluorescence contributions, which are shown for the above five molecules in Figure 6-3 on a common energy scale. Here gate times are each chosen such that either the prompt (PF) or the delayed fluorescence (DF) is selectively detected.

Evidently PF and DF are isoenergetic, i.e. the high energy portions of both spectra coincide which each other and there is no spectral shift. However, the spectra are not exactly identical. For well-resolved vibronic spectra, such as anthracene, a redistribution of the emission intensity within the different modes is generally observed. For anthracene the leading vibronic mode is relatively enhanced for the DF1 spectrum, which - if it can be observed - seems to be a general trend. Worth noting, these redistributions occur immediately at the turning point into DF1 (for anthracene ~ 60 ns). Subsequently, no further spectral alterations or energy shifts of the DF1 are observed (see also Figure 6-14). Some of the laser dyes, namely BBO and Rhodamine 6G, exhibit pronounced different spectral features in addition to their fluorescence spectra. Most likely these stem from weakly emissive impurities and consequently these long-lived emission contributions were omitted by means of selective integration for the decay curves shown

in Figure 6-1. As an example for BBO only the high energy portion of the fluorescence spectrum, starting from 3.0 eV was used for the decay kinetics. Asymptotically, the DF1 decay kinetics generally obey algebraic laws, which is evident by the linear behavior in the double logarithmical plot in Figure 6-1. For anthracene a least square fit yields an exponent of –4.07, which is the highest value observed for all materials. The slopes of the other materials that are shown in Figure 6-1 range between – 2.5 and – 3.5. As shall be shown, the slope of a certain material hardly ever changes under different experimental conditions. Therefore, the exponent should be considered a material constant similar to the fluorescence decay constant.

Bearing in mind the observation that both fluorescence contributions within their corresponding time domains obey very elementary decay kinetics, it appears reasonable to simulate the whole fluorescence decay with only one model, which should give an improved fit also in the turn over region from PF to DF1. Obviously, a summation of single-exponential plus an algebraic expression should describe the observed decays:

$$F(t) = A_1 e^{-\frac{t}{\tau}} + A_2 t^{-b}$$

Equation 6-1

Simulations according to Equation 6-1 are included in Figure 6-1 as green solid lines and are in markedly excellent agreement with the experimental data. The two important fitting parameters, i.e. the mono exponential lifetime τ and the algebraic decay exponent b are given in Table 6-1 at the end of 6.3.3. However, Equation 6-1 certainly cannot fully account for the observed experimental situation as a lower cut-off frequency needs to be included within the algebraic component for scaling reasons. Without doing so the emission intensity would approach infinite high values for short delay times. Details will be discussed within 6.3.7.

6.3.2. Fluorene-type oligomers and polymers

To gain a deeper insight into the nature of the DF1 emission, a whole series of chemically similar polyfluorene-type materials have been probed. Tested within this study were the mono disperse oligomers para-difluorene (2-fluorene), para-trisfluorene (3-fluorene) as well as the polymer derivatives poly(9,9diethyl-hexyl)para-fluorene with two different average molecular weights corresponding to 10 (10-fluorene) and approximately 100 (100-fluorene) repeat units and a very high molecular weight polyspirobifluorene with about 1000 repeat units (1000-fluorene). All chemical structures are shown in Table 6-1 at the end of 6.3.3. One might find it strange that the simplest member of the fluorene family, fluorene itself, is not included in the list of tested systems. With the time-resolved set-up described

in chapter 3 one is limited to excitation energies no higher than 3.5 eV. This energy is just about enough to excite four ring molecules, such as para-difluorene (absorption spectrum shown in Figure 6-10). Compared to these molecules the absorption of fluorene on its own is shifted too far into the blue spectral region and cannot be excited with the system used here. Nevertheless, already the above range of conjugated systems offers the unique opportunity to study the DF1 of chemically similar molecules as a function of the molecular weight and the length of the molecules, respectively.

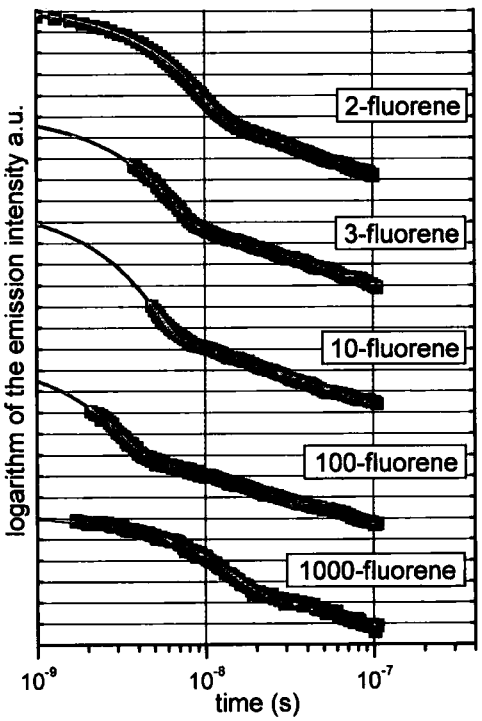

Figure 6-4 Compendium of fluorescence decays of fluorene derivatives in a double logarithmic scale with the number of repeat units as indicated.

For the ease of comparison all materials have been dissolved in the same solvent, toluene. The fluorescence decay curves of the five materials are shown in a double logarithmical scale in Figure 6-4. Again, for each of the fluorene derivatives an algebraically decaying delayed fluorescence component, subsequently to the mono-exponential decaying prompt fluorescence, is observed.

For the polymers and oligomers shown in Figure 6-4 the DF1 regime is already achieved after an intensity drop of the PF of about five orders as compared to seven orders in case of the laser dyes in Figure 6-1. Since for all investigated systems (fluorenes and laser dyes) the emission quantum yield in dilute solutions is roughly close to 100 %, it immediately follows that the DF1 in fluorene derivatives is about 100 times stronger than in the above small molecules. In consequence it is much easier to study the DF1 emission using the fluorene derivates as opposed to the laser dyes.

Likewise for Figure 6-1, green solid lines according to Equation 6-1 are also included in Figure 6-4. However, as a consequence of the short PF lifetimes and unlike for the laser dyes, τ was not simulated as a free parameter but fixed to the exact values that were obtained with the time-correlated-single-photon-counting method (TCSPC). In such only the PF amplitude A_1 was adjusted to fit the experimental data. All obtained fitting parameters are given in Table 6-1. The decay exponents of the two small fluorene oligomers fall into the same range (between -2.5 and -3.5)

like the laser dyes from Figure 6-1. Interestingly, within the fluorene family longer molecules seem to correspond to generally smaller slopes, i.e. both polyfluorenes exhibit slopes close to -2. As further confirmed by the polymer results shown in 6.3.3 below, this dependency of the slope of the delayed fluorescence on the length of the conjugated system is not restricted to the fluorene family, but is a generic characteristic of the DF1. As an empiric rule of thumb: the DF1 decay exponent decreases when the molecular weight, respectively the length of the molecule, increases.

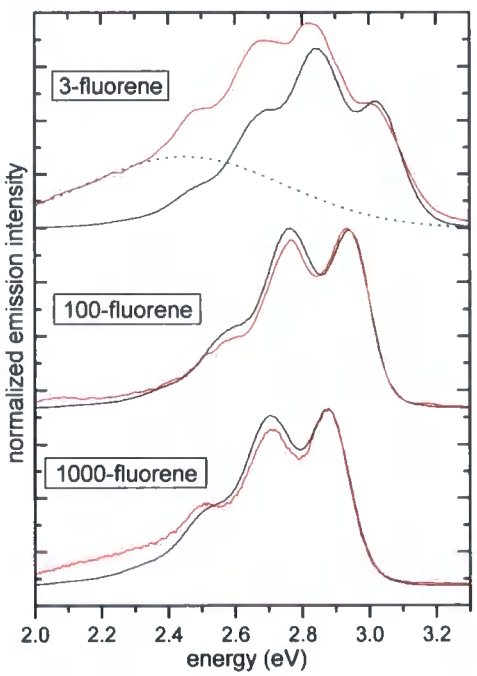

Figure 6-5 Comparison of the normalized PF (black) and DF1 (red) of three fluorene derivatives as indicated. The green dotted line is a Gaussian simulation according to the keto emission centered at 2.45 eV. (all times in nanoseconds: 3-fluorene: PF 0..2, DF1 20..200; 100-fluorene: PF 0..2, DF1 10..100; 1000-fluorene: PF 0..2, DF1 50..200ns.

In Figure 6-5, spectra, which selectively monitor the PF and DF1, are shown on a common energy scale for three of the fluorene derivatives. As for the well-resolved anthracene spectrum of Figure 6-3, for both polyfluorenes the leading vibronic mode (i.e. the 0-0 transition) of the delayed fluorescence spectrum gains intensity relatively to the other satellite modes when compared to the prompt fluorescence. The same effect might also be present in the oligomers, but an additional delayed emission contribution impedes an accurate comparison of the prompt with the delayed fluorescence. After a long debate, in which excimer, aggregates and the like were extensively put forward, the origin of this emission has by now evidently be assigned to weakly emissive, oxidized fluorene units, i.e. fluorenone.[33] For the time-resolved luminescence studies these "keto" defect sites often pose a substantial problem, because with 6 ns[33] its mono-exponential lifetime falls exactly into the investigated time-domain. The small oligomers with two and three repeat units and the 10-fluorene suffer a lot from this unwanted emission. For this reason the spectra of 2-fluorene and 10-fluorene are not included in Figure 6-5 as these look similar to those of 3-fluorene and as such are not very meaningful. Nevertheless, the spectrum of the defect emission is known to closely resemble a Gaussian function centered around 2.45 eV, such as the

green dashed line that is included in the 3-fluorene part of Figure 6-5. Therefore, for the DF1 decay kinetics, it is still possible to selectively integrate over spectral areas that are not affected by the keto emission. For example only the blue energy portion of the 3-fluorene fluorescence spectrum, starting from 3.0 eV has been used for the corresponding decay graph shown in Figure 6-4. Compared to the fluorenes, the laser dyes of 6.3.1 are much more resistant against oxidation as these materials are designed to work in harsh conditions.

To summarize the above: if the vibronic spectrum of the fluorescence is well resolved and if any keto emission is sufficiently weak then it appears a generic trend that the leading vibronic mode relatively increases for the DF1. This spectral redistribution occurs immediately at the turning point, i.e. the spectra shown in Figure 6-3 and Figure 6-5 represent the relevant fluorescence contribution. Based on the unequal emission spectra, a slightly dissimilar energy conformation for the prompt and delayed singlet exciton can be inferred. Following the Franck-Condon-Principle, the observed differences in the vibronic spectra suggest that the DF1 singlet excited state is more similar (less excited state relaxation) to the singlet ground state as compared to its prompt counterpart.

6.3.3. Further polymeric systems

In the recent past, meta-coupled conjugated copolymers that contain carbazole, fluorene and oxadiazole moieties have attracted considerable research interest due to their potentially superior properties as active materials in electroluminescence applications when compared to common para-coupled homo polymers.[80-84] In this last part of the general results a representative of this uncommon class of materials is introduced, an alternating copolymer consisting of carbazole and fluorene. For the present study of uttermost importance is that some of these copolymers, including the above one, are the only conjugated systems so far known that allow the observation of the DF1 emission in the solid state.

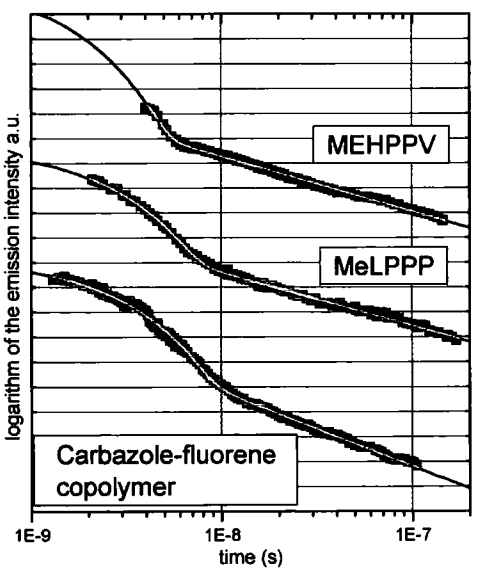

Figure 6-6 Comparison of the fluorescence decay of three polymeric systems in a double logarithmic scale. Green lines are least square fits according to Equation 6-1 with parameters given in Table 6-1.

However, to start with, all the decay graphs shown in Figure 6-6 are obtained from dilute solutions. For the purpose of completeness this graph also contains the fluorescence decays of the two archetypical and widely-studied polymers methyl-poly(para-phenylene) (MeLPPP) and 5-(2'ethyl-hexyloxy)-*p*-phenylene vinylene) (MEHPPV). However, both of these polymers are not well suitable for advanced delayed luminescence studies as they suffer from backbone oxidation, i.e. keto defects. For MeLPPP this is already born out of the complicated synthesis whereas for MEHPPV the vinyl linkage is susceptible to oxidation. For these two polymers the fitting procedure according to Equation 6-1 was again backed up with TCSPC lifetimes. Consistent with the empirical rule for high molecular weight systems both polymers feature DF1 gradients close to -2.0 whereas for the copolymer an unusually large exponent of -2.86 is found. All chemical structures and the fitting parameters are given in Table 6-1 below.

name	chemical structure	solvent	PF τ (ns)	DF1 b
anthracene	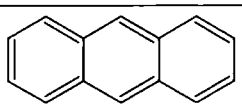	MCH	3.6	4.07
BBO	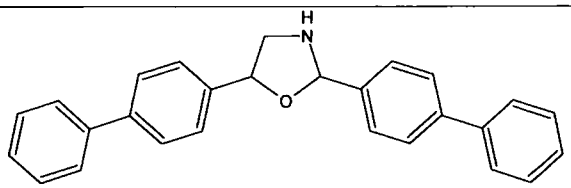	toluene	0.96	2.77
Coumarin 450	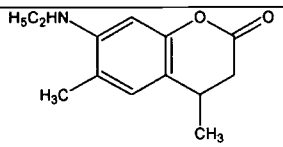	metha-nol	3.6	2.87
Coumarin 500	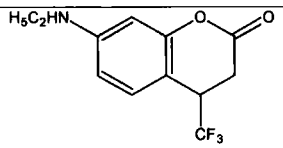	ethanol	5.0	2.51
Rhodamine 6G	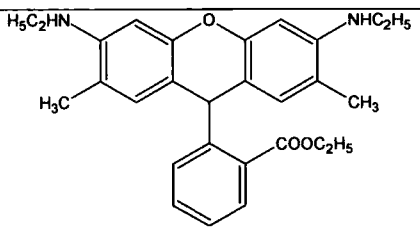	ethanol	3.9	3.48

2-fluorene	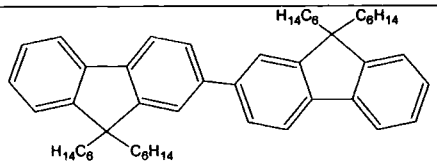	toluene	~0.78	3.51
3-fluorene	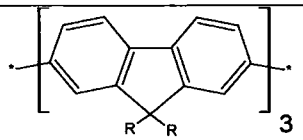	toluene	0.64	2.98
10-fluorene	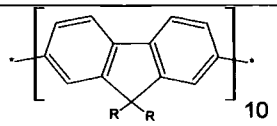	toluene	0.43	2.68
100-fluorene	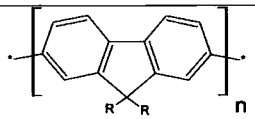 n~100	toluene	0.35	2.26
1000-fluorene	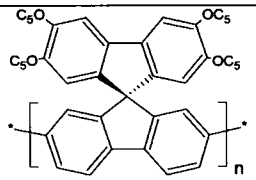 n~1000	toluene	2.1	2.08
MEHPPV *	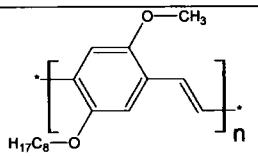	toluene	0.35	2.21
MeLPPP *	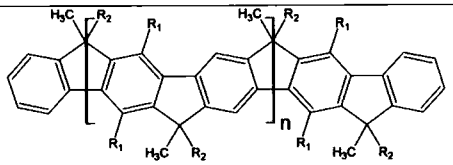	toluene	0.67	2.13
carbazole-fluorene copolymer	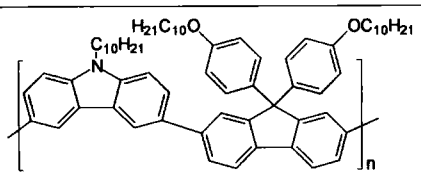	toluene	~0.73 **	2.86

*Table 6-1 Compendium of chemical structures of all the above described materials as well as the used solvents. Also given are fitting parameters, fluorescence lifetime τ and the exponent b, as obtained with Equation 6-1. * Unlike for all other experiments where 355 nm was used, MEHPPV and MeLPPP were excited at 500 and 420 nm, respectively. ** the PF decay is not strictly mono-exponential.*

6.3.4. The DF1 in the framework of bimolecular processes

So far any experimental observation of isoenergetic delayed fluorescence in organic systems could consistently be attributed to either triplet-triplet-annihilation or delayed charge carrier recombination.[8] In the present and the

following section, experimental evidence is shown and discussed, which unambiguously proves that the DF1 emission eludes any such assignment within either of the above stated, archetypical mechanisms for the delayed generation of singlet excitons.

The most common origin of delayed fluorescence is the pair wise annihilation (TTA) of a certain triplet exciton density (n_T) following the rate equation:

$$DF = \frac{dn_T}{dt} = -\gamma_{TT} {n_T}^2$$

Equation 6-2

For the dilute systems considered in the present study, γ_{TT} takes the form of a diffusion time constant, i.e. rate limiting for any potential delayed fluorescence emission is the encounter of two molecules that each carry a triplet exciton, compare also chapter **4**. For the laser doses used throughout, multiple triplet excitations on a single molecule can safely be ruled out. This is immediately clear for the laser dyes and small oligomers, but also holds true for polymeric systems as shown in chapter **4**. Following Equation 6-2 any delayed fluorescence that originates from triplet-triplet-annihilation will have a quadratic dependence on the excitation dose. However, after optical excitation the triplet exciton forms in a sequential process from the initially excited singlet exciton. Therefore the quadratic laser dose dependency for the delayed fluorescence is only observed if the singlet density, for example measured as fluorescence, simultaneously depends linearly on excitation dose, i.e. any non-linear quenching mechanism such as singlet-singlet-annihilation plays no major role. Nevertheless, even in the presence of singlet-singlet-annihilation the delayed fluorescence following triplet-triplet-annihilation would still be quadratic when compared to the fluorescence.

The DF1 emission is in general *not* caused by TTA. This has already been demonstrated in great detail within chapter **4** using a representative polyfluorene derivative, which is very similar to the here considered 100-fluorene. The two main experimental observations that contradict the bimolecular triplet annihilation picture are first the linear dependency of the DF1 (with simultaneously linear PF) on the excitation dose, shown in Figure 4-6, and secondly the fast decay of the DF1, which is not accompanied by a corresponding drop in the triplet density as measured using time-resolved transient absorption, Figure 4-8. Instead, the triplet density remains almost constant in the nanosecond time domain in dilute solutions.

In the following a few complementary experimental results of two other systems are presented that in the light of the other experimental results beyond doubt allow excluding TTA as the origin of the DF1 emission.

In Figure 6-7 the fluorescence decay of the same 2-fluorene dilute solution has been measured under identical experimental conditions with the only difference that for the red data set the air dissolved in the solvent was removed. Accompanied by a slight increase of the PF a significant increase of the delayed fluorescence is observed for the degassed solution. For both kinds of solution the delayed fluorescence (DF) is isoenergetic to the prompt one. However, as a consequence of the absence of the triplet quencher, oxygen, the increase in the DF is caused by diffusion limited triplet-triplet-annihilation.

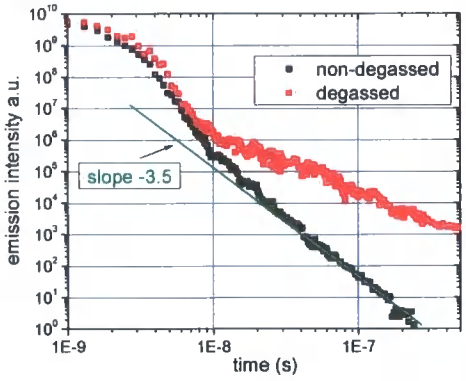

Figure 6-7 Comparison of the fluorescence decay under identical conditions of 2-fluorene dissolved in toluene (OD<0.1) both, degassed and non-degassed.

This notion is supported by the direct comparison of the laser excitation dose dependencies for the above solution with and without oxygen, which is shown in Figure 6-8 on a double

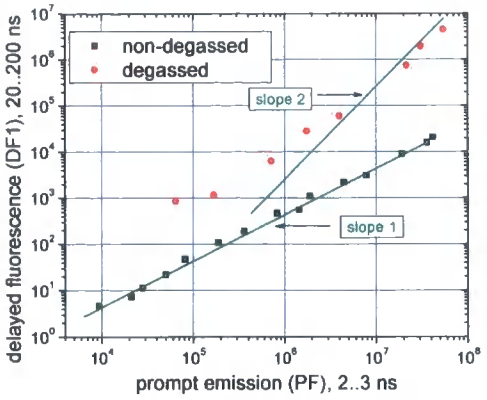

Figure 6-8 Laser excitation dose dependency of the delayed versus the prompt fluorescence for both degassed and non-degassed 2-fluorene toluene solutions.

logarithmic scale. Unlike the absolute measurements of Figure 4-6, this graph only shows the DF relative to the PF without explicitly measuring the laser dose. The delayed fluorescence of the non-degassed solution, i.e. the DF1, rises strictly linearly compared to the PF, which means both kinds of fluorescence have the same laser dose dependency. This is in clear contrast to the DF that is observed for the degassed solution which for higher excitation doses asymptotically approaches a quadratic behavior relative to the PF, consistent with the TTA picture.

Unlike for the above 2-fluorene but similar to polyfluorene (Figure 4-7, chapter 4), for MEHPPV even in the degassed solution the DF1 emission with its characteristic rapid decay can be observed up to about 100 ns, compare Figure 6-9. But again, for longer times the DF1 fluorescence of the degassed solution is buried underneath the TTA delayed

fluorescence. Additionally to the emission decay, the time-resolved transient absorption of the degassed solution has been probed at 780 nm, close to the peak of the corresponding transient triplet spectrum, compare Figure 4-8.[31] Any such long-lived transient absorption signal could only be observed for the degassed solution. Consistent with the TTA framework, the decay of the delayed fluorescence is proportional to the first derivative of the triplet decay and as soon as the triplets are quenched at about 100 µs the DF signals simultaneously also vanishes.

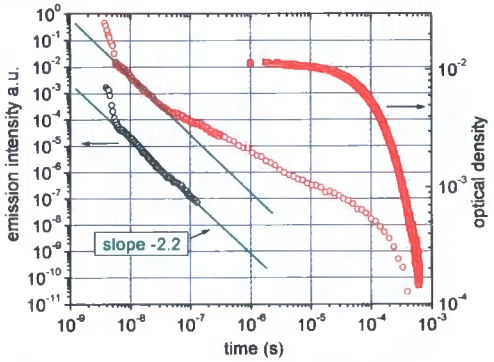

Figure 6-9 Fluorescence decays of MEHPPV in toluene non-degassed (black open cycle) and degassed (red open cycle). The red closed cycles correspond to the time-resolved transient triplet absorption signal for the degassed solution.

At this point it is safe to disregard TTA as origin of the DF1 emission. Additionally, the observed linear laser dose dependencies, but also the small molecule results, rule out any potential contribution from singlet-singlet-annihilation as origin for the DF1 emission. Such a mechanism - geminate pairs that generate with the aid of the excess energy after bimolecular singlet annihilation - was recently discussed by Romanovskii *et. al* in order to explain the delayed fluorescence observed in photo excited MeLPPP films.[19] Consistently but in contrast to the results found here, the authors observed a square root dependence of the PF on laser excitation dose and simultaneously a linear one for the DF, i.e. relative to the PF the DF is quadratically dependent on the excitation dose.

For very similar reasons non-geminate delayed charge carrier recombination can also be discarded, since this again would require quadratic dose dependencies.

6.3.5. The DF1 in the framework of geminate pair recombination

A reader who is not intimately familiar with the abundant number of publications about geminate pairs in the literature might find the following discussion too long and complicated, as the small molecule and oligomer experimental results counter the basis of any delayed charge carrier recombination anyway as there is simply no space for two of them to be individually localized. However, in order to really prove that the here observed DF1 has on the one hand not been observed so far and on the other hand eludes a consistent description within all common theoretical frameworks about delayed fluorescence one also

has to discuss the geminate pair picture.

There is only one phenomenological model for the description of the delayed isoenergetic fluorescence that implies a linear excitation dose dependency – the delayed recombination of geminate pairs. Though there has never been a consistent experimental observation for any conjugated system, the potential existence of these geminate pairs was lively debated by Bässler, Arkhipov and coworkers.[18, 38, 45, 67, 74, 77, 85, 86] In their framework the long-lived excitations are considered as correlated (coulombically bound) electron-hole pairs, i.e. two independent charges that are far enough away from each other so they do not act as a single excitation (no electron exchange). In such, the overall energy of a geminate pair is clearly higher (by about 0.4 eV the exciton binding energy) as compared to the corresponding singlet exciton. The formation of such pairs is discussed either as a direct excitation or via sequential dissociation from the initially excited singlet exciton. The direct excitation of electron hole pairs implies an exciton binding energy of order k_BT only, which contradicts the standard model, but nevertheless has been repeatedly concluded from so-called "ultrafast" studies mainly by Heeger, Moses and others.[87-91] All seriously discussed geminate pair models start from the initially excited singlet exciton, which then dissociates into a geminate pair. In doing so, they mainly try to answer the key question where the necessary exciton dissociation energy of 0.4 eV comes from. Favored at the moment is a theory by Arkhipov *et al.* that rests on the notion that thermal excess energy after photo excitation is temporally retained in a local heat bath, which then promotes the singlet dissociation into a charge carrier pair.[74] In this context dissociation is only possible if the excess energy is at least as large as the exciton binding energy, which Arkhipov assumes at around 0.35 eV for MeLPPP. This model is further relevant for the present study as it implies an intrachain dissociation mechanism, the only one that will anyway be possible for isolated molecules. Following Arkhipov's approach, the yield for geminate pair formation, which would be directly linked to any potential delayed fluorescence emission, is related to the provided excess energy. Therefore, studying the delayed fluorescence intensity as a function of excitation energy will show whether or not Arkhipov's model is suited to account for the origin of the DF1 emission.

Two absorption spectra of the fluorene series, 2- and 1000-fluorene are shown in Figure 6-10. For the oligomer 2-fluorene, excitation at 355 nm results in an excess energy of ~ 0.1 eV, which is much smaller than the generally assumed exciton binding energy,

0.4 eV. However, in contrast to Arkhipov's model, DF1 is still observed with typical intensity, compare Figure 6-4.

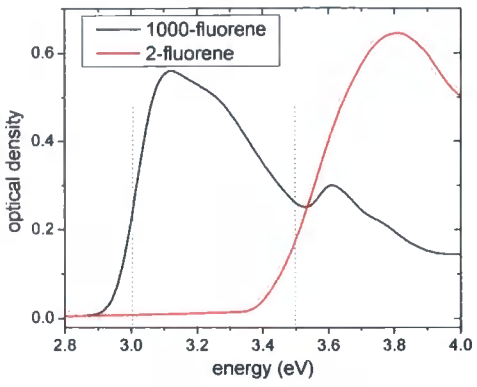

Figure 6-10 Absorption spectra of 2-fluorene and 1000-fluorene dissolved in toluene. The green dotted lines indicate the laser excitation energies for Figure 6-11, 412 and 355 nm.

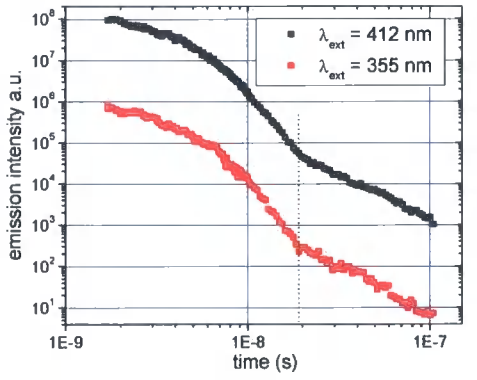

Figure 6-11 Double logarithmic fluorescence decay of 1000-fluorene solution after excitation with two different energies. The graphs are offset for clarity and the dashed line denotes the turning point between PF and DF1.

In Figure 6-11 the fluorescence decays of 1000-fluorene are compared after exciting both right on the absorption edge at 412 nm and at higher energies at 355 nm; both energies are indicated as dashed lines in Figure 6-10. Apparently, neither the fluorescence lifetime nor the delayed fluorescence decay exponent change upon changing the excitation energy. Concomitantly, no alterations of the prompt nor of the delayed fluorescence spectrum are observed (not shown). Most importantly, the relative emission intensities, respectively the position of the turning point between PF and DF1 (indicated by a dashed line in Figure 6-11) is unaltered as well. Therefore, the higher excess excitation energy (0.6 as compared to 0.1 eV) does not yield more delayed fluorescence. Respectively, the DF1 has the same excitation energy dependence as the singlet exciton and the on-chain dissociation model by Arkhipov is unsuitable to explain the origin of the DF1 fluorescence. At this point it is safe to disregard geminate pairs as the origin of the observed delayed fluorescence.

6.3.6. The DF1 in the solid-state: the temperature dependence

To summarize the above, neither triplet-triplet-annihilation nor geminate pair recombination cause the observed DF1. Furthermore, independent of the experimental conditions in dilute solutions, prompt and delayed fluorescence appear with fixed relative emission contributions.

After characterizing the delayed fluorescence observed on isolated molecules the DF1 is analyzed in the solid-state, i.e. in thin films. Here it is much harder to suppress bimolecular annihilation of both kinds of excitons,

which potentially leads to delayed fluorescence either via TTA[73] or due to geminate pair recombination following SSA.[19]

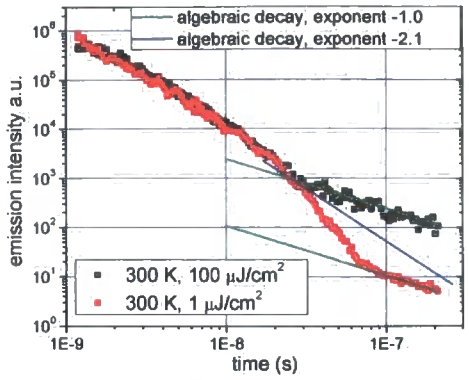

Figure 6-12 Normalized fluorescence decays of a 1000-fluorene thin film excited at two different doses as indicated.

A typical decay data set, obtained for a solid 1000-fluorene film at room temperature and moderate excitation dose, is shown in Figure 6-12 (black). For this particular material, in solid state the quantum yield drops to 30 % (solution 94 %), concomitantly the prompt fluorescence decays faster as compared to dilute solution and is non-exponential. A delayed fluorescence contribution is indeed observed, but the emission obeys an algebraic decay law with slope close to –1 instead of –2.1 and has a bimolecular origin. In chapter 4 this delayed fluorescence was beyond doubt assigned to TTA. Thus, under typical experimental conditions in thin films any potential DF1 emission would be buried underneath the TTA delayed fluorescence. To illustrate this point, the expected (from solution data, see Figure 6-4) DF1 decay is drawn in Figure 6-12 as a blue line. Next in order to suppress the TTA a very low excitation dose has been used (red data set of Figure 6-12). Indeed, the contribution of the bimolecular delayed fluorescence relative to its prompt counterpart is reduced by a factor of 30. However, the expected (blue solid line) monomolecular DF1 contribution is still not observed. This either means the state that causes the DF1 is not excited in the solid state or the state is present but has more non-radiative decay channels compared to the prompt fluorescence. Reduced temperature (20 K) in addition to low excitation does not enable the observation of DF1 emission in solid state either.

Following the theory outlined in chapter 4, in order to suppress migration activated triplet-triplet-annihilation, the diffusivity, or more precisely, the jump frequency ν_{ij} of the triplet excitons needs to be reduced. According to Equation 4-6 of chapter 4, an obvious possibility is to increase the average inter site separation, R_{ij}, which is directly related to the site density, *N*. This is to the extreme realized in dilute solutions but to a certain extent can also be applied to solid state by using low concentrations of polymers imbedded into an inert matrix polymer. However as shown in chapter 4, cluster formation occurs and in such the organic material is not isolated.[73] Another straight forward way to lower

ν_{ij} would be to decrease the temperature. But again, for the present purpose this alone is not sufficient. The jump frequency ν_{ij} also depends on the "extension" of the triplet exciton, which in Equation 4-6 is described by the parameter α - the inverse localisation length. Apparently α cannot simply be influenced by the experimental conditions as it is a material parameter. Nevertheless, within recent progress in advanced material design for polymer light emitting diode applications, a series of novel *meta*-coupled copolymers and oligomers has been synthesized, which features very high triplet energy levels accompanied by greatly reduced triplet mobility's.[81, 83, 84, 92] An important finding within the study of these materials is that the longest *para* coupled chain segment within the polymer backbone determines the triplet wave function delocalization and in such the triplet energy of the system. Thus in terms of Equation 4-6, deliberately introduced conjugation breaks by *meta* coupled co-monomers result in a substantial increase in the parameter α as compared to common *para* coupled polymers. Indeed, for some of these copolymers the TTA activity is sufficiently suppressed that one is able to observe the DF1 emission even in solid state. Subsequently, solid-state results of one representative of this family of *meta* coupled copolymers, the alternating carbazole-fluorene copolymer described in 6.3.3 shall be discussed.

First two general remarks: these copolymers are rather complicated systems to understand, which is for example demonstrated by the typically non-exponentially decaying prompt fluorescence even in dilute solution. Furthermore, the solid-state data of the copolymers are subject to quite large fluctuations between different samples with respect to the triplet-triplet-annihilation delayed fluorescence intensity. It appears that high-quality samples (made by Philips Research) exhibit stronger DF2 emission than those made at Durham, which again is not well understood so far.

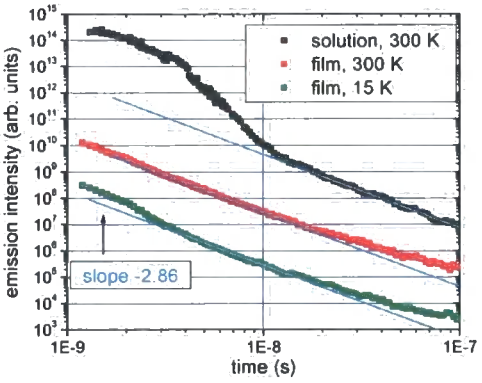

Figure 6-13 Fluorescence decay kinetics of the copolymer including toluene solution, film at 300 and 20 K. As usual the data are arbitrarily offset.

Nevertheless, in Figure 6-13 the fluorescence decay curves of the copolymer measured for dilute solution as well as thin solid film at two temperatures are shown. On first glance a comparison between solid state and solution data appears to be rather difficult, if not arbitrary. Nonetheless, the common features that

can be relocated in all data sets comprise a monomolecular DF1 as well as a prompt fluorescence contribution, though the latter is strongly quenched in solid state especially at ambient temperature. Additionally, for the thin film data a bimolecular triplet-triplet-annihilation contribution is visible already at delay times exceeding ~ 20 ns, which decays with the typical algebraic decay law with slope -1.

Several interesting conclusions can be drawn from Figure 6-13. Firstly, within experimental error the exponent of the algebraic decay law of the DF1 emission is independent of the experimental environment, i.e. bulk as compared to isolated molecule. Especially the DF1 decay is not accelerated, which suggests an intra chain state that neither interacts with neighboring chain segments nor does it get quenched by impurities. Secondly, the substantial relative change in the emission intensity between solid-state and dilute solution data can be interpreted in two ways: either there is more DF1 in solid state or there is less prompt fluorescence. On account of the results shown in Figure 6-12, the latter is the much more likely option. Furthermore, experimental observations indicate that the overall emission strength is considerably reduced in solid-state as compared to dilute solutions, though no absolute measurements (quantum yield) have been made. The prompt fluorescence is most likely quenched by thermally activated hopping, i.e. by singlet exciton *migration* to impurity sites, because firstly the prompt emission intensity increases by a factor of three going from ambient to low temperature and secondly compared to the solution data in solid state the lifetime of the PF is quenched rather than the amplitude. At the same time there is no thermally activated "lifetime" quenching on the DF1 decay, i.e. the decay slope is independent of both the thermal activation energy and the site density. Considering that the PF is strongly quenched by (thermally activated) migration to impurity sites but under the same conditions the DF1 is not, suggests that the state that causes the DF1 emission is much less mobile, or maybe immobile, as compared to the singlet exciton.

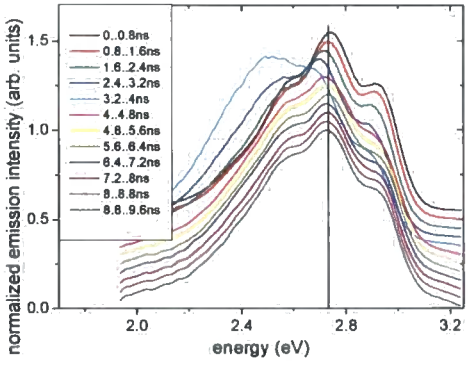

Figure 6-14 Compendium of time-resolved, normalized fluorescence spectra of the copolymer taken at 20 K and taken with 800 ps detection window. The black solid line is a guide to the eye and the spectra are offset for clarity.

As outlined above, the singlet exciton migration within the DOS is much more efficient in solid state as compared to dilute solutions, because of the higher

site density in the former case. Similar to the triplet exciton findings described in 4.4.7, this migration process is accompanied by energy relaxation within the DOS, which, due to the higher number of sampled sites, is more pronounced in the solid-state.

In Figure 6-14 a range of time resolved fluorescence spectra covering both the PF and DF1 region of the green, low temperature data set of Figure 6-13 is shown on a common energy scale. In this plot the continuous red shift of the prompt fluorescence due to energy relaxation is clearly observed, which reaches its highest extent at about three to four nanoseconds. In this time period the luminescence of the longest lived singlet exciton is observed, which already shows some additional low energy features of unknown origin. Subsequently and coincident with the beginning of the DF1 emission (compare Figure 6-13), the emission shifts back to the blue spectral region and now takes an averaged energetic position of the prompt fluorescence. During the DF1 time domain no further alternations of the emission spectrum are observed. This is further proof for the migration of the prompt singlet exciton and the immobility of the DF1 state. Also visible in Figure 6-14 is the change of the vibronic spectrum at the turning point from prompt to delayed fluorescence, i.e. at about 4 ns. Immediately at this point in time the leading vibronic mode is relatively reduced as compared to the PF spectrum, but no subsequent alternations of the spectrum are observed.

Note again, a similar PF energy shift as compared to Figure 6-14 does not occur in dilute solutions due to the suppressed singlet exciton migration. Therefore PF and DF1 appear nearly isoenergetic independent of the chosen time-resolved PF spectrum.

6.3.7. The DF1 in solid-state: Energy transfer studies

With the similarity of polymer and oligomer results in mind as well as the above copolymer findings it was already concluded that migration is neither decisive for the population nor for the decay of the DF1 state. Assuming a fully immobile excited state for the DF1 emission, it should be possible to employ a migration activated fluorescence quenching channel and in such uncover the otherwise buried DF1 contribution in the solid state fluorescence. This approach of selectively quenching the prompt fluorescence indeed works, which is shown in the present section by two examples. These involve migration activated singlet energy transfer to an emissive guest molecule and to an impurity site.

As a first example singlet energy transfer to keto defect sites in 3-fluorene imbedded into zeonex is presented. The abundant occurrence of

these keto quenching sites in the oligomers of the fluorene family has already been discussed. Furthermore, it has recently been shown that these defect sites can be excited either directly at around 2.8 eV or via thermally activated singlet exciton migration[10, 33, 73] and as such will most efficiently be populated at room temperature in solid samples.

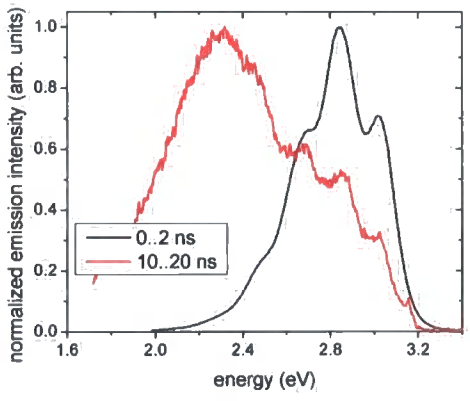

Figure 6-15 Normalized prompt and delayed fluorescence spectra of 3-fluorene imbedded in an inert matrix polymer.

In Figure 6-15 typical room temperature prompt and delayed fluorescence spectra of 3-fluorene imbedded into zeonex are shown. Such an environment is already close to the solid state, because phase segregation of the oligomer within the matrix polymer occurs. Although absent in the prompt fluorescence, strong keto defect emission is observed in the delayed luminescence spectrum. Note, the inert matrix polymer is needed, because unlike the high-molecular weight polymers, the small oligomers cannot be processed into films via spin-coating. For the fluorescence decays shown below only the blue spectral region, starting at 3.0 eV, was integrated to avoid the keto defect emission.

In Figure 6-16 a compendium of fluorescence decays of 3-fluorene in different solvents and temperatures is shown. The graphs are normalized to the delayed fluorescence component, so only relative statements about PF and DF intensity can be made. The series toluene, decalin and zeonex at 300 K corresponds to increasing phase segregation of the 3-fluorene within its solvent, which is accompanied by an increase of the migration activated singlet energy transfer to the keto defect sites causing a quenching of the prompt fluorescence. On the other hand, decreasing the thermal activation energy of the same sample (zeonex film) reduces singlet energy migration towards the keto quenching sites and more prompt fluorescence is observed as compared to room temperature.

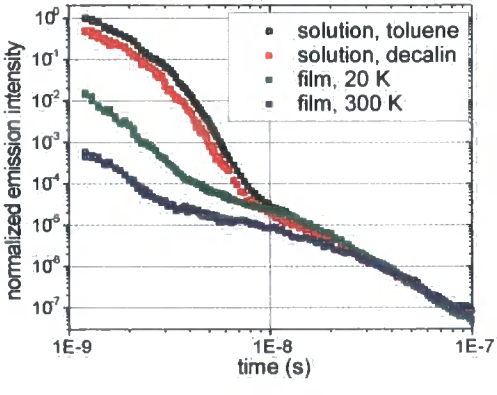

Figure 6-16 Fluorescence decays of 3-fluorene in two different solvents as well as imbedded into the inert matrix polymer zeonex at room and low temperature. The graphs are normalized to the DF1 emission.

For all decays shown in Figure 6-16 no triplet-triplet-annihilation delayed fluorescence is observed. This is not at all astonishing considering the high keto defect content of this oligomer. The latter reduces the DF2 delayed fluorescence component in two ways: firstly the competing singlet transfer to the keto defects causes the ISC rate to decrease and secondly the delayed, bimolecularly formed singlet excitons might again transfer to the quenching sites. As a consequence the DF1 component is visible even in this quasi solid state. Likewise for the copolymer data, the DF1 slope is not affected by the surrounding environment.

The uncovered DF1 decay kinetics of the initial 15 ns of the zeonex film as presented in Figure 6-16 do not follow the asymptotic slope of –3.0. Qualitatively, such a behavior is expected for any algebraic decay law with an exponent ≤ -1, which must have a higher cut off frequency for scaling reasons. A re-examination of the solution decay curves of Figure 6-16 already shows that the mono exponential decay does not directly turn into the slope of –3.0, but develops a little hump. Making use of the uncovered decay kinetics of the solid state data of Figure 6-16, one is now able to determine the higher frequency cut off and subsequently obtain a realistic value of the overall DF1 emission quantum yield in solution. In practice the whole fluorescence decay ($F(t)$) was simulated as a sum of a mono exponential and an algebraic contribution, albeit for solid state mono exponential kinetics are a simplification:

$$F(t) = A_1 e^{-\frac{t}{\tau}} + \frac{A_2}{1+\left(\frac{t}{t_1}\right)^b}$$

Equation 6-3

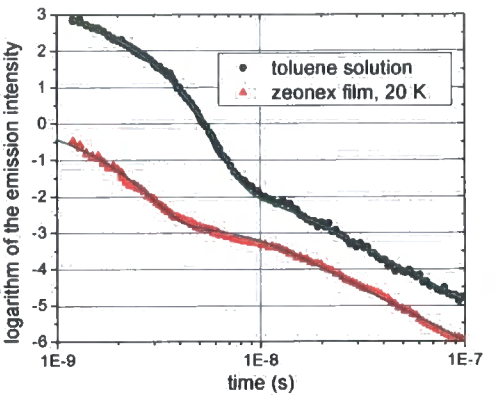

Figure 6-17 Two fluorescence decays from Figure 6-16 that are fitted using Equation 6-3.

Least square fits are shown as solid green lines in Figure 6-17. First, from the zeonex film (red dataset) the inverse cut off frequency was obtained as t_1 = 8.5±0.3 ns. Next, the decay curve of the dilute solution was fitted with fixed t_1 and τ, with the latter taken from the TCSPC experiment (b was anyway fixed to –3.0). Apparently, both simulations describe the decay curves well. Integrating over the two fluorescence contributions of Equation 6-3 and scaling the sum to the quantum yield of 3-fluorene in dilute solution, 0.90, one is able to work out the selective quantum yield of the DF1 for 3-fluorene in solution, QY_{DF1} = 0.0002±0.0001.

Following the same strategy as outlined for 3-fluorene above, now 1000-fluorene is examined. As a consequence of the spiro-bridge, this polymer is virtually inert against backbone oxidation, and consequently does not exhibit any keto defect emission. For this material the prompt fluorescence can be quenched by migration activated singlet energy transfer to an emissive guest molecule, the heavy metal dopant platinum octaethylporphyrin, PtOEP.

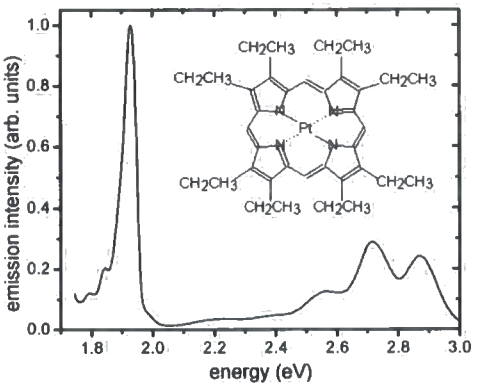

Figure 6-18 First millisecond normalized luminescence spectrum of 100-fluorene doped with ~ 10 % by wt PtOEP. The chemical structure of the dopant is shown in the inset.

In Figure 6-18 the chemical structure as well as the luminescence of a very similar guest/host system are shown. Due to a large spectral separation of guest and host emission it is very easy to selectively only integrate over the host fluorescence emission. Furthermore, the dopant is known as an efficient singlet scavenger with simultaneously long emission lifetime of around 100 µs.[93] Both these features allow for a selective study of the remaining host fluorescence in the initial 100 ns undisturbed by any dopant emission. Besides, cw temperature dependent studies on polyfluorene doped films confirmed that the host guest energy transfer is a migration activated process rather than a direct Förster-type transfer. The latter process is inefficient due to a vanishing small spectral overlap between host emission and guest absorption spectrum in this guest host system, which has been measured in our laboratories.

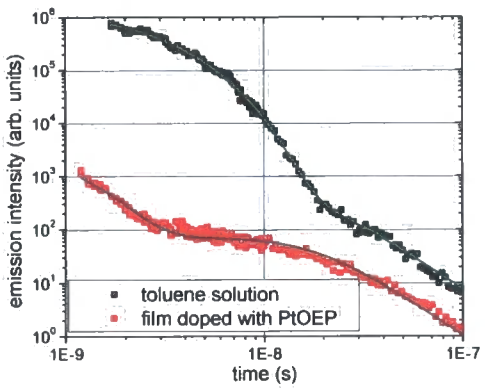

Figure 6-19 : Fluorescence decay curves of 1000-fluorene in a dilute solution and of a thin film doped with 10 % PtOEP. The green lines are least square fits according to Equation 6-3.

The decay of the selectively integrated fluorescence (excluding any dopant emission) of a 1000-fluorene film doped with 10 % by wt PtOEP is shown in Figure 6-19 (red dataset). The fluorescence emission intensity (i.e. the host emission) is reduced by approximately 10^5 compared to the fluorescence emission in dilute solution, which is included in the same figure for comparison (black dataset). This is a clear indication of the efficient singlet quenching by the guest dopant. A welcome side effect is the absence of

any delayed fluorescence due to TTA, since this bimolecular process scales with the square of the singlet density. For this heavily doped film the remaining prompt fluorescence is visible only in the initial 2 ns. At this time the same spectral redistribution as described above for dilute solution occurs as the prompt fluorescence turns into isoenergetic, monomolecular DF1. Consistent with both the copolymer and the 3-fluorene findings, the observation of DF1 in this quenching experiment means that the corresponding DF1 excitation is not transferred to the guest molecule, and therefore is much less mobile as compared to the common singlet exciton.

Note, the solid state decay curves of Figure 6-12 (red) and Figure 6-19 (red) are not in contradiction to each other, because the doped curve is much lower in intensity than any data point of Figure 6-12. Therefore, DF1 (more exactly its excited state) exists in solid state as well but the absolute emission intensity is lower as compared to dilute solution.

Following the same procedures as applied for 3-fluorene, from the doped film (red dataset in Figure 6-19) for 1000-fluorene the inverse cut off frequency was obtained as t_1 = 18.5±0.2 ns. Finally, very good agreement to the experimental data was obtained by fitting the dilute solution fluorescence decay (black data set of Figure 6-19) to Equation 6-3 with fixed parameters t_1, τ = 2.1 ns (from TCSPC) and b = 2.5. Again, after scaling the overall emission of Equation 6-3 to the quantum yield of 1000-fluorene in dilute solution, 0.94, it is possible to work out the selective DF1 emission quantum yield in solution, QY_{DF1} = 0.004.

	τ (ns)	t_1 (ns)	-b	DF1*
3-fluorene	0.64	8.5	2.96	2E-4
1000-fluorene	2.1	18.5	2.5	4E-3
copolymer	~0.73	< 3.5	2.86	>2E-4

*Table 6-2 Fitting parameters according to Equation 6-3, which yield the green solid lines shown in Figure 6-17 and Figure 6-19, respectively.*In this column the overall quantum yield of the DF1 emission in solution is given in absolute numbers.*

Table 6-2 shows the fitting parameters according to Equation 6-3 for the two fluorenes. The same procedures cannot be applied for the copolymer, because for the plateau time only a higher limit can be discerned from the corresponding solid state data of Figure 6-13, t_1 < 3.5 ns. Nevertheless, assuming an overall emission quantum yield in solution of 50 %, a lower limit for the copolymer DF1 quantum yield in solution would be QY_{DF1} > 0.0002.

To summarize the above experimental results, the DF1 state is most likely an intra chain and immobile excitation and as such is neither affected by the surrounding media such as the solvent nor by neighboring chain segments. Furthermore, thermal activation energy

does neither influence the population nor the decay of the DF1 excited state. The higher DF1 quantum yield for the 1000-fluorene as compared to the 3-fluorene supports the previous empirical observation that conjugated systems with higher average molecular weight generally exhibit stronger DF1 emission.

6.3.8. The DF1 in solid-state: applied electric field

Unfortunately, the above keto or PtOEP containing films are not suitable for electric field quenching experiments, as both the impurity and the dopant act as a charge trap. For example, keto emission is easily observed in electro luminescence devices, because fluorenone is an electron trap and thus acts as a recombination centre in a working device.[11] Furthermore, doped electroluminescence devices generally exhibit higher turn-on voltages as compared to their undoped counterparts, which again is a direct consequence of the counter potential that forms inside the active polymer layer by the trapped electrons.[52, 94] As a result electric field quenching experiments are only possible using the meta coupled copolymers, as exclusively these materials are known to show the DF1 emission in pristine solid state. Therefore, for the present field dependence investigation, sealed high-quality electro luminescence devices with a low work function barium-aluminium cathode, similar to those used in section 5.3.1, of the above copolymer have been used.

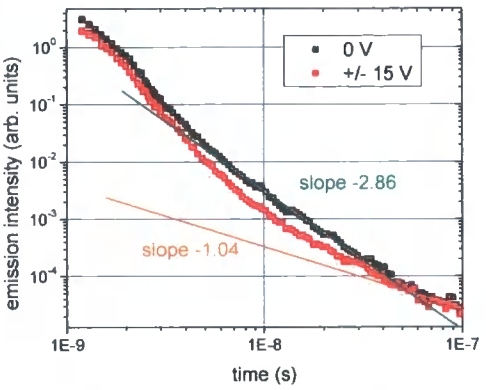

Figure 6-20 Fluorescence decay kinetics taken at 20 K of the copolymer with and without an applied bias voltage as indicated. The green solid line indicates the DF1, the orange the TTA component. These graphs are taken under identical conditions and thus can absolutely be compared with each other.

In Figure 6-20 low temperature fluorescence decays of the copolymer after photo excitation with and without an applied electric field are shown. In order to sufficiently suppress the TTA (DF2) fluorescence component a very low excitation dose (~ 1µJ/cm^2) has been used. However, there is still a bimolecular fluorescence component visible for delay times exceeding ~ 40 ns for the zero bias curve. Therefore the DF1 component, with its typical decay slope of -2.86, is squeezed on a relatively short time domain in between the prompt and the bimolecular delayed fluorescence. Once an electric field is applied the prompt fluorescence drops by about 30 %, which is a typical value for such experiments.[4, 67, 68] In this context, the graphs in Figure 6-20 were taken under identical experimental

conditions (apart from the bias), i.e. they are not normalized. Along with this drop in the PF, the DF1 component is quenched as well by about 50 %. The interesting observation now is that the DF1 is more strongly quenched than the PF. This suggests a higher dipole moment of the corresponding excited state of the DF1 as compared to the common singlet exciton. For the whole study this is the first time that experimental conditions could actually influence the DF1 emission independent of the PF. However, due to the close proximity of the PF and the DF2 signal it is not clear if amplitude or lifetime quenching of the DF1 signal occurred. On account of the above experimental findings the latter is the more likely possibility and should cause an accelerated decay slope.

It remains to clarify whether the experimentally observed bias effect is a pure electric field effect or if maybe exciton polaron interactions, i.e. charge carrier quenching, needs to be invoked. To clarify this point, the decay kinetics under forward and reverse applied bias, i.e. with and without charge carriers present in the active polymer layer, were compared. In this context, within the investigated 100 ns time frame the emitted electro luminescence for + 15 V is negligible as compared to the photo luminescence. However, for negative and positive applied bias virtually identical decay kinetics were obtained and thus averaged to the single data set shown in Figure 6-20. Consequently, a true electric field rather than a charge carrier quenching effect has been observed.

6.4. Conclusions

To summarize, a new kind of generic mono molecular fluorescence has been observed in conjugated organic systems that is distinct from the common singlet emission by its non-exponential, longer decay kinetics that obey algebraic laws. In general the decay exponents range between -1.5 and -4.1 while higher molecular weight systems tend to exhibit more slowly decaying delayed emission, which is accompanied by higher delayed emission quantum yields. However, even for the latter materials the emission quantum yields of the delayed fluorescence are a fraction of a percent only.

The corresponding excitation is an immobile intrachain state and its absorption directly matches that of the normal singlet exciton, in other words increasing the excess excitation energy does not result in more delayed emission relative to the prompt emission. The delayed emission spectrum is isoenergetic to the prompt fluorescence, which for energetic reasons excludes the singlet exciton as a potential precursor state. Consistent with a directly excited and immobile excitation, population and decay of this state are independent of the provided

thermal activation energy. A higher dipole moment as compared to the common singlet state is inferred from electric field quenching experiments.

From these experimental observations one concludes the existence of a new type of singlet excited state that has neither been experimentally described nor theoretically been predicted so far. What is the nature of this state on a microscopic level? In view of the large number of different materials, which all showed the DF1 emission in solution, it has to be something generic that is intrinsically linked to the conjugation itself. Ring torsions between neighboring repeat units can be excluded, mainly on account of the observed DF1 in the ladder-type polymer MeLPPP, but also because changes in the solution viscosity do not affect the DF1 emission intensity or the decay exponent. One might speculate about a rare metastable generic distortion of conjugated systems in the first excited singlet configuration as a result of the optical excitation. The associated change of the overlap integral between first excited and ground state will then lead to the observed distribution of longer singlet lifetimes. In the style of the inorganic semiconductor field such an excited state could appositely be called an indirect exciton.

Currently the potential existence of such distorted excited singlet wave functions is being tested for very simple molecules, such as anthracene, by means of quantum mechanical calculations. In common with similar treatments, first the complete set of wave functions is calculated with the molecule in the energetically lowest conformation. These energy levels should be able to predict absorption and fluorescence spectra but also the triplet level. Given that this complete set is correct, it would be easy to calculate the wave function overlap of the conformational relaxed excited state with the ground state and in such predict the excited state mono exponential fluorescence lifetime. The final step, which is different from all previous treatments, is then to involve some conformation perturbation of the ground state Hamiltonian, i.e. a bend or torsion and redo the calculations. In this way it might be possible to find some distribution (perhaps parameterized in a tilt or bend angle) of longer fluorescence lifetimes.

7. General Conclusions

Devices based on light emitting small organic molecules or conjugated polymers have great potential to replace in the very near future all current display technologies owing to their superior emission properties combined with the unmatched versatility of organic materials. From the current point of view, it is much more difficult to foresee which of the two competing organic technologies, namely small organic molecules (OLEDs) versus long polymers (polyLEDs), will finally be employed for large scale display applications. In this context, the development of OLEDs is approximately ten years ahead of the polyLED technologies, with OLEDs currently already entering the consumer markets. On the other hand, large area polymer devices shall be based on the very cost effective ink-jet printing technology. Furthermore, cross linked conjugated polymers may potentially be used to engineer flexible displays that really withstand everyday use. It is also conceivable that applications, which require only low quality devices such as disposable electronic newspapers or large area lighting applications, may employ the cheap polymer technology whereas high quality applications such as computer screens would be fabricated using OLEDs.

However, several issues need to be solved before full-color polymer displays will really be able to enter the consumer markets. One of them concerns the more than 75 % triplet exciton fraction, which needs to be harvested in order to achieve sufficient device efficiency. The currently employed strategy is based on phosphorescent dopants; thus the population and depopulation mechanisms of such dopant-host systems need to be studied and optimized. This, however, requires in the first place a thorough knowledge of the triplet properties of the undoped host polymer. Here, the present work provides a fundamental framework, which in detail characterizes the behavior of the triplet excitons in thin solid films made of conjugated host materials. This then greatly helps to put other work on the triplet exciton into the right perspective.

As a direct consequence of the naturally large energetic variance of conjugated polymers, the triplet diffusion at early times after its formation and/or low temperature is highly dispersive that is dependent on time. This initial time regime is accompanied by a rapid loss of energy as the triplet exciton relaxes towards the low states of the density of states distribution (DOS), which implies that the average triplet energy is time dependent as well. All observed phosphorescence stems from energetically relaxed triplet excitons, with the true centre of the DOS being about 100 meV higher in energy than the observed

spectra. It is, however, the centre of the triplet DOS which determines whether or not triplet energy transfer to phosphorescent dopants is exothermic or endothermic. Recently, Baldo *et al.* have observed an efficient population of a certain phosphorescent guest molecule albeit the host polymer phosphorescence level was slightly below that of the guest triplet level.[95] This was then interpreted as proof for endothermic triplet energy transfer – which it is in fact not considering the true, energetically higher, centre of the DOS rather than the phosphorescence energy.

Subsequent to the dispersive regime, classical, non dispersive triplet diffusion is established, being characterized by a true diffusion constant and a time-independent average triplet energy. During this classical diffusion the triplet excitons are efficiently quenched by migration activated triplet-triplet annihilation, which also accounts for the lack of any phosphorescence emission at room temperature. This has rather drastic implications on the correct interpretation of many experimental situations that study the triplet exciton. For example, there is no need to propose temperature dependent inter-system crossing rates, which some authors do in order to explain the lack of long-lived triplet excitons at room temperature. Also, the majority of researchers invoke mono-exponential triplet lifetimes in order to interpret the triplet dynamics or the absolute triplet densities from quasi steady-state transient triplet absorption experiments. In fact, there is no meaning for such unimolecular decay constant for the triplet exciton for temperatures above 100 K. Here the triplet decay is generally dose and temperature dependent following algebraic instead of exponential kinetics. Only true time resolved experiments will unveil the triplet exciton dynamics.

The turnover times from dispersive to non dispersive diffusion are strongly temperature dependent, ranging from typically a few hundred nanoseconds at room temperature to about one second at 100 K. In consequence, the triplet energy transfer to the phosphorescent dopant in an electroluminescent device should take no longer than approximately 100 ns in order to avoid triplet exciton quenching by bimolecular annihilation. Otherwise, there will be a competition between triplet energy transfer to the guest and bimolecular annihilation leading to a loss of device efficiency.

Future work should now study triplet energy transfer in guest-host systems, with the focus of population of the guest from the host and depopulation of the host to the guest. The latter process, which has become known as triplet energy back transfer, will be of uttermost importance when investigating blue phosphorescent guest host systems. Most likely the goal, a highly efficient blue emitter, cannot be achieved without new materials

possessing significantly lower singlet-triplet splittings than the currently studied polymers.

Following several experimental attempts over the last years, the 25 % limit for the singlet generation yield in electroluminescent devices has become questionable. However, it follows from the present work that all measurements so far did not at all account for triplet-triplet annihilation. In consequence, the triplet exciton density has been drastically underestimated relative to the singlet density, leading to almost any possible value between 50 and 95 % singlet yield. Compared to this previous work the present method is improved twofold: firstly, the triplet density is measured *relative* to that of the singlet and the electrical excitation experiments were measured *relative* to the optical one. No absolute quantities except for the inter-system crossing rate are needed. Secondly, bimolecular triplet annihilation has carefully been accounted for. To do so, the time dependent triplet accumulation after continuous excitation limited by annihilation has been simulated under the premise that the inhomogeneous excitation profile is preserved during the experiment. Here, for the first time, one naturally gains a direct measurement of the charge carrier recombination layer in working electroluminescent devices. Regarding the singlet generation yield, the results clearly show that the quantum statistical 1:3 limit is not violated at all. It is noteworthy that these results stem from working electroluminescent devices based on pristine, undoped polymers that are free of keto defect sites to the highest chemically possible level.

In conclusion, there is no fundamental advantage of using conjugated polymers for device applications compared to small organic molecules, as both simply obey the quantum statistical singlet generation limit. Thus, simple singlet emitters will not yield sufficient quantum efficiency. Instead, one must harvest the triplet excitons as well and guest-host systems are most likely the only way to achieve this.

Within this work, evidence is provided for a new kind of delayed fluorescence, which has not been described in the literature so far. This luminescence has virtually identical characteristics compared to the prompt fluorescence except for obeying algebraic decay kinetics with material dependent exponents ranging from – 1.5 to -4.1. Beyond doubt, common sources of delayed fluorescence such as bimolecular triplet annihilation or delayed geminate or non-geminate pair recombination cannot explain the experimental observation. Compared to the prompt fluorescence, this new emission is extraordinarily weak and one needs to sample at least 15 exponential lifetimes before the fluorescence

decay turns into this slower decaying, algebraic regime. This is why it has escaped any previous detection. The highly sensitive time resolved system employed here is essential for the observation of such weak signals.

So far, this new kind of luminescence has been detected in a wide range of organic materials including dye molecules, fluorene oligomers and several different conjugated polymers. Future work should also look into luminescent inorganic semiconductor thin films and quantum dots. At first glance, it seems too far-fetched to assume such a universal nature of the non-exponential emission decay. However, there are indeed theoretical predictions that, if applicable, would provide a conclusive explanation of the experimental observations. Based on a rigorous quantum mechanical treatment of the decay of metastable ensembles from first principles, as early as 1958 the Russian physicist Khalfin proved mathematically that any luminescence decay, whose excited state distribution is energetically bound from below, must asymptotically decay slower than exponential, thereby featuring algebraic kinetics.[96] Interestingly, this prediction implies a memory effect for the excited state decay as an old ensemble of states decays slower than a fresh one. Though this work has been theoretically confirmed numerous times, up to now it has withstood any experimental verification. For organic materials the excited state distribution is the DOS and the low energy boundary simply is the ground state, zero energy. The turn over time from the exponential into the algebraic mode is expected to occur earlier for systems with small energy release and wide excited state distribution. Both these presumptions are naturally fulfilled for the organic materials investigated here. Thus, there are strong indications that the observed algebraic luminescence decay is indeed the long sought-after unimolecular non exponential excited state decay.

List of publications

Feller, F., C. Rothe, et al. (2002). "Temperature dependence of the space-charge distribution in injection limited conjugated polymer structures." Journal of Applied Physics **91**(11): 9225-9231.

Hintschich, S., C. Rothe, et al. (2003). "Population and decay of keto states in conjugated polymers." Journal of Chemical Physics **119**(22): 519346.

Hintschich, S. I., C. Rothe, et al. (2003). "Temperature dependence of long-lived photoexcitations in a polythiophene." Synthetic Metals **135**(1-3): 365-366.

King, S., C. Rothe, et al. (2004). "Triplet build in and decay of isolated polyspirobifluorene chains in dilute solution." The Journal of Chemical Physics **121**(21): 10803-10808.

King, S., C. Rothe, et al. (submitted). "Measurements of the absolute inter-system-crossing rates of polyspirobifluorene derivatives." Chemical Physics Letters.

Rothe, C., H. Al Attar, et al. (submitted). "Absolute measurements of the triplet-triplet-annihilation rate and the charge carrier recombination layer thickness in working polymer light-emitting diodes based on polyspirobifluorene." Physical Review B.

Rothe, C., K. Brunner, et al. (2005). "Effects of triplet exciton confinement induced by reduced conjugation length in polyspirobifluorene copolymers." Journal of Chemical Physics **122**(8): 084706.

Rothe, C., R. Guentner, et al. (2001). "Trap influenced properties of the delayed luminescence in thin solid films of the conjugated polymer poly(9,9-di(ethylhexyl)fluorene)." Journal of Chemical Physics **115**(20): 9557-9562.

Rothe, C., S. Hintschich, et al. (submitted). "Experimental evidence for non-exponential, unimolecular luminescence decay at long times in organic materials." Nature.

Rothe, C., S. Hintschich, et al. (2002). "Spectroscopic investigation of the different long-lived photoexcitations in a polythiophene." Journal of Chemical Physics **116**(23): 10503-10507.

Rothe, C., S. I. Hintschich, et al. (2002). "Pressure dependent radiative quantum yields of the prompt and delayed luminescence of polyfluorene films." Chemical Physics Letters **360**(1-2): 111-116.

Rothe, C., S. King, et al. (submitted). "Direct measurement of the singlet generation yield of polymer light emitting diodes." Nature.

Rothe, C., S. King, et al. (submitted). "Electric field induced singlet and triplet exciton quenching in films of the conjugated polymer polyspirobifluorene." Physical Review B.

Rothe, C., S. King, et al. (submitted). "Resonatly enhanced remote heavy metal effect in doped conjugted polymers." Nature Materials.

Rothe, C., S. M. King, et al. (2004). "Triplet exciton state and related phenomena in the beta-phase of poly(9,9-dioctyl)fluorene." Physical Review B **70**(19): 195213.

Rothe, C. and A. P. Monkman (2002). "The dynamics and trap depth distribution of triplet excited states in thin films of the light-emitting polymer poly(9,9-di(ethylhexyl)fluorene)." Physical Review B **65**: 3201.

Rothe, C. and A. P. Monkman (2003). "Triplet exciton migration in a conjugated polyfluorene." Physical Review B **68**(7): 075208.

Rothe, C., L. O. Palsson, et al. (2002). "Singlet and triplet energy transfer in a benzil-doped, light emitting, solid-state conjugated polymer." Chemical Physics **285**(1): 95-101.

Sinha, S., C. Rothe, et al. (2002). "Detailed investigations on the photophysical properties of poly(2,5-pyridine diyl)." Journal of Chemical Physics **117**(5): 2332-2336.

Sinha, S., C. Rothe, et al. (2003). "Photophysics of poly(2,5-pyridine diyl)." Synthetic Metals **135**(1-3): 371-372.

Sinha, S., C. Rothe, et al. (2003). "Electrophosphorescence and delayed electroluminescence from pristine polyfluorene thin-film devices at low temperature." Physical Review Letters **90**(12): 127402.

van Dijken, A., J. J. A. M. Bastiaansen, et al. (2004). "Carbazole Compounds as Host Materials for Triplet Emitters in Organic Light-Emitting Diodes: Polymer Hosts for High-Efficiency Light-Emitting Diodes." J. AM. CHEM. SOC. **126**: 7718-7727.

References

1 M. Munowitz, *Principles of Chemistry*, London, (2000).

2 A. J. Heeger, S. Kivelson, J. R. Schrieffer, and W. P. Su, Reviews of Modern Physics **60**, 781 (1988).

3 H. Bassler, M. Gailberger, R. F. Mahrt, J. M. Oberski, and G. Weiser, Synthetic Metals **49**, 341 (1992).

4 M. Deussen, M. Scheidler, and H. Bassler, Synthetic Metals **73**, 123 (1995).

5 P. W. Atkins, *Molecular Quantum Mechanics*, 1983).

6 E. F. H. Brittain, W. O. George, and C. H. J. Wells, *Introduction to molecular spectroscopy; theory and experiment* (Academic Press, London, New York,, 1970).

7 T. H. Forster, in *10th Spiers Memorial Lecture*, 1959), p. 7.

8 M. Pope and C. E. Swenberg, *Electronic Processes in Organic Crystals and Polymers* (Oxford University Press, Oxford, 1999).

9 H. D. Burrows, J. S. de Melo, C. Serpa, L. G. Arnaut, A. P. Monkman, I. Hamblett, and S. Navaratnam, Journal of Chemical Physics **115**, 9601 (2001).

10 C. Rothe and A. P. Monkman, Physical Review B **65**, 3201 (2002).

11 S. Sinha, C. Rothe, R. Guentner, U. Scherf, and A. P. Monkman, Physical Review Letters **90**, 127402 (2003).

12 Y. V. Romanovskii, A. Gerhard, B. Schweitzer, U. Scherf, R. I. Personov, and H. Bassler, Physical Review Letters **84**, 1027 (2000).

13 D. Hertel, S. Setayesh, H. G. Nothofer, U. Scherf, K. Mullen, and H. Bassler, Advanced Materials **13**, 65 (2001).

14 A. Kadashchuk, A. Vakhnin, Y. Skryshevski, V. I. Arkhipov, E. V. Emelianova, and H. Bassler, (submitted).

15 C. Rothe, S. Hintschich, A. P. Monkman, M. Svensson, and M. R. Anderson, Journal of Chemical Physics **116**, 10503 (2002).

16 D. Hertel, H. Bassler, R. Guentner, and U. Scherf, Journal of Chemical Physics **115**, 10007 (2001).

17 C. Rothe, R. Guentner, U. Scherf, and A. P. Monkman, Journal of Chemical Physics **115**, 9557 (2001).

18 D. Hertel, Y. V. Romanovskii, B. Schweitzer, U. Scherf, and H. Bassler, Synthetic Metals **116**, 139 (2001).

[19] Y. V. Romanovskii, V. I. Arkhipov, and H. Bassler, Physical Review B **6403**, 033104 (2001).

[20] J. B. Birks, *Organic molecular photophysics* (J. Wiley, London, New York,, 1973).

[21] M. Smoluchowski, Zeitschrift fuer Physikalische Chemie **92**, 129 (1917).

[22] R. Richert, H. Bassler, B. Ries, B. Movaghar, and M. Grunewald, Philosophical Magazine Letters **59**, 95 (1989).

[23] B. Movaghar, B. Ries, and M. Grunewald, Physical Review B **34**, 5574 (1986).

[24] B. Movaghar, M. Grunewald, B. Ries, H. Bassler, and D. Wurtz, Physical Review B **33**, 5545 (1986).

[25] M. Scheidler, B. Cleve, H. Bassler, and P. Thomas, Chemical Physics Letters **225**, 431 (1994).

[26] B. Ries and H. Bassler, Journal of Molecular Electronics **3**, 15 (1987).

[27] B. Ries, H. Bassler, M. Grunewald, and B. Movaghar, Physical Review B **37**, 5508 (1988).

[28] M. Grunewald, B. Pohlmann, B. Movaghar, and D. Wurtz, Philosophical Magazine B-Physics of Condensed Matter Statistical Mechanics Electronic Optical and Magnetic Properties **49**, 341 (1984).

[29] H. Cordes, S. D. Baranovskii, K. Kohary, P. Thomas, S. Yamasaki, F. Hensel, and J. H. Wendorff, Physical Review B **63**, 094201 (2001).

[30] T. Miteva, A. Meisel, W. Knoll, H. G. Nothofer, U. Scherf, D. C. Muller, K. Meerholz, A. Yasuda, and D. Neher, Advanced Materials **13**, 565 (2001).

[31] S. King, C. Rothe, and A. Monkman, The Journal of Chemical Physics **121**, 10803 (2004).

[32] J. Lange, B. Ries, and H. Bassler, Chemical Physics **128**, 47 (1988).

[33] S. Hintschich, C. Rothe, S. Sinha, and A. P. Monkman, Journal of Chemical Physics **119**, 519346 (2003).

[34] G. Schonherr, H. Bassler, and M. Silver, Philosophical Magazine B-Physics of Condensed Matter Statistical Mechanics Electronic Optical and Magnetic Properties **44**, 369 (1981).

[35] G. Fytas, H. G. Nothofer, U. Scherf, D. Vlassopoulos, and G. Meier, Macromolecules **35**, 481 (2002).

[36] A. P. Monkman, H. D. Burrows, I. Hamblett, and S. Navaratnam, Chemical Physics Letters **340**, 467 (2001).

[37] Y. V. Romanovskii and H. Bassler, Chemical Physics Letters **326**, 51 (2000).

[38] Y. V. Romanovskii, A. Gerhard, B. Schweitzer, R. I. Personov, and H. Bassler, Chemical Physics **249**, 29 (1999).

[39] A. I. Rudenko and H. Bassler, Chemical Physics Letters **182**, 581 (1991).

[40] L. Pautmeier, U. Rauscher, and H. Bassler, Chemical Physics **146**, 291 (1990).

[41] A. P. Monkman, H. D. Burrows, L. J. Hartwell, L. E. Horsburgh, I. Hamblett, and S. Navaratnam, Physical Review Letters **86**, 1358 (2001).

[42] Y. Cao, I. D. Parker, G. Yu, C. Zhang, and A. J. Heeger, Nature **397**, 414 (1999).

[43] J. S. Kim, P. K. H. Ho, N. C. Greenham, and R. H. Friend, Journal of Applied Physics **88**, 1073 (2000).

[44] M. Segal, M. A. Baldo, R. J. Holmes, S. R. Forrest, and Z. G. Soos, Physical Review B **68**, art. no. (2003).

[45] D. Hertel, E. V. Soh, H. Bassler, and L. J. Rothberg, Chemical Physics Letters **361**, 99 (2002).

[46] A. S. Dhoot, D. S. Ginger, D. Beljonne, Z. Shuai, and N. C. Greenham, Chemical Physics Letters **360**, 195 (2002).

[47] L. C. Lin, H. F. Meng, J. T. Shy, S. F. Horng, L. S. Yu, C. H. Chen, H. H. Liaw, C. C. Huang, K. Y. Peng, and S. A. Chen, Physical Review Letters **90**, art. no. (2003).

[48] A. S. Dhoot and N. C. Greenham, Physical Review Letters **91**, art. no. (2003).

[49] L. C. Lin, H. F. Meng, J. T. Shy, S. F. Horng, L. S. Yu, C. H. Chen, H. H. Liaw, C. C. Huang, K. Y. Peng, and S. A. Chen, Physical Review Letters **91**, art. no. (2003).

[50] M. A. Baldo, D. F. O'Brien, M. E. Thompson, and S. R. Forrest, Physical Review B **60**, 14422 (1999).

[51] I. N. Hulea, R. F. J. van der Scheer, H. B. Brom, B. M. W. Langeveld-Voss, A. van Dijken, and K. Brunner, Applied Physics Letters **83**, 1246 (2003).

[52] A. van Dijken, A. Perro, E. A. Meulenkamp, and K. Brunner, Organic Electronics **4**, 131 (2003).

[53] J. S. Wilson, A. S. Dhoot, A. Seeley, M. S. Khan, A. Kohler, and R. H. Friend, Nature **413**, 828 (2001).

[54] A. P. Monkman, S. King, and C. Rothe, Nature (submitted).

[55] A. J. Campbell, D. D. C. Bradley, H. Antoniadis, M. Inbasekaran, W. S. W. Wu, and E. P. Woo, Applied Physics Letters **76**, 1734 (2000).

[56] S. I. Hintschich, C. Rothe, and A. P. Monkman, Synthetic Metals **135**, 365 (2003).

[57] personal communication with Dr. Klemens Brunner.

[58] Z. Shuai, D. Beljonne, R. J. Silbey, and J. L. Bredas, Physical Review Letters **84**, 131 (2000).

[59] M. Wohlgenannt, C. Yang, and Z. V. Vardeny, Physical Review B **66**, art. no. (2002).

[60] R. Richert and H. Bassler, Chemical Physics Letters **118**, 235 (1985).

[61] R. Richert and H. Bassler, Journal of Chemical Physics **84**, 3567 (1986).

[62] B. P. Lyons and A. P. Monkman, Journal of Applied Physics **96**, 4735 (2004).

[63] A. Suna, Physical Review B **1**, 1716 (1970).

[64] H. Scher and T. E. Orlowski, Physical Review Letters **50**, 775 (1983).

[65] M. Wohlgenannt, K. Tandon, S. Mazumdar, S. Ramasesha, and Z. V. Vardeny, Nature **409**, 494 (2001).

[66] N. C. Greenham, J. Shinar, J. Partee, P. A. Lane, O. Amir, F. Lu, and R. H. Friend, Physical Review B **53**, 13528 (1996).

[67] B. Schweitzer, V. I. Arkhipov, U. Scherf, and H. Bassler, Chemical Physics Letters **313**, 57 (1999).

[68] B. Schweitzer and H. Bassler, Synthetic Metals **109**, 1 (2000).

[69] A. J. Heeger, Solid State Communications **107**, 673 (1998).

[70] S. C. J. Meskers, J. Hubner, M. Oestreich, and H. Bassler, Chemical Physics Letters **339**, 223 (2001).

[71] A. Kohler and D. Beljonne, Advanced Functional Materials **14**, 11 (2004).

[72] A. Kohler, J. S. Wilson, R. H. Friend, M. K. Al-Suti, M. S. Khan, A. Gerhard, and H. Bassler, Journal of Chemical Physics **116**, 9457 (2002).

[73] C. Rothe and A. P. Monkman, Physical Review B **68**, 075208 (2003).

[74] V. I. Arkhipov, E. V. Emelianova, S. Barth, and H. Bassler, Physical Review B **61**, 8207 (2000).

[75] V. I. Arkhipov, E. V. Emelianova, and H. Bassler, Chemical Physics Letters **340**, 517 (2001).

[76] R. Kersting, U. Lemmer, M. Deussen, H. J. Bakker, R. F. Mahrt, H. Kurz, V. I. Arkhipov, H. Bassler, and E. O. Gobel, Physical Review Letters **73**, 1440 (1994).

[77] V. R. Nikitenko, D. Hertel, and H. Bassler, Chemical Physics Letters **348**, 89 (2001).

78 H. Bassler, V. I. Arkhipov, E. V. Emelianova, A. Gerhard, A. Hayer, C. Im, and J. Rissler, Synthetic Metals **135**, 377 (2003).

79 C. M. Cuppoletti and L. J. Rothberg, Synthetic Metals **139**, 867 (2003).

80 A. van Dijken, J. J. A. M. Bastiaansen, N. M. M. Kiggen, B. M. W. Langeveld-Voss, C. Rothe, A. P. Monkman, I. Bach, P. Stößel, and K. Brunner, J. AM. CHEM. SOC. **126**, 7718 (2004).

81 C. Rothe, K. Brunner, I. Bach, S. Heun, and A. P. Monkman, Journal of Chemical Physics (accepted).

82 I. Avilov, P. Marsal, J. L. Bredas, and D. Beljonne, Advanced Materials **16**, 1624 (2004).

83 P. Marsal, I. Avilov, D. A. da Silva, J. L. Bredas, and D. Beljonne, Chemical Physics Letters **392**, 521 (2004).

84 K. Brunner, A. van Dijken, H. Borner, J. Bastiaansen, N. M. M. Kiggen, and B. M. W. Langeveld, Journal of the American Chemical Society **126**, 6035 (2004).

85 B. Schweitzer, V. I. Arkhipov, and H. Bassler, Chemical Physics Letters **304**, 365 (1999).

86 V. Gulbinas, Y. Zaushitsyn, V. Sundstrom, D. Hertel, H. Bassler, and A. Yartsev, Physical Review Letters **89**, art. no. (2002).

87 C. Zenz, G. Lanzani, G. Cerullo, W. Graupner, G. Leising, and S. DeSilvestri, Chemical Physics Letters **341**, 63 (2001).

88 D. Moses, A. Dogariu, and A. J. Heeger, Chemical Physics Letters **316**, 356 (2000).

89 P. B. Miranda, D. Moses, and A. J. Heeger, Physical Review B **70**, art. no. (2004).

90 P. B. Miranda, D. Moses, and A. J. Heeger, Physical Review B **6408**, art. no. (2001).

91 W. Graupner, G. Cerullo, G. Lanzani, M. Nisoli, E. J. W. List, G. Leising, and S. De Silvestri, Physical Review Letters **81**, 3259 (1998).

92 A. van Dijken, J. Bastiaansen, N. M. M. Kiggen, B. M. W. Langeveld, C. Rothe, A. Monkman, I. Bach, P. Stossel, and K. Brunner, Journal of the American Chemical Society **126**, 7718 (2004).

93 C. Rothe, L. O. Palsson, and A. P. Monkman, Chemical Physics **285**, 95 (2002).

[94] A. J. Cadby, P. A. Lane, H. Mellor, S. J. Martin, M. Grell, C. Giebeler, D. D. C. Bradley, M. Wohlgenannt, C. An, and Z. V. Vardeny, Physical Review B **62**, 15604 (2000).

[95] C. Adachi, R. C. Kwong, P. Djurovich, V. Adamovich, M. A. Baldo, M. E. Thompson, and S. R. Forrest, Applied Physics Letters **79**, 2082 (2001).

[96] L. A. Khalfin, Soviet Physics Jetp-Ussr **6**, 1053 (1958).